Investigation of High Frequency Switching Transients on Wind Turbine Step Up Transformers

by

Mantosh Devgan

A thesis
presented to the University of Waterloo
in fulfillment of the
thesis requirement for the degree of
Master of Applied Science
in
Electrical and Computer Engineering

Waterloo, Ontario, Canada, 2015

AUTHOR'S DECLARATION

I hereby declare that I am the sole author of this thesis. This is a true copy of the thesis, including any required final revisions, as accepted by my examiners.

I understand that my thesis may be made electronically available to the public.

Abstract

Pre-mature failures of wind turbine step up (WTSU) transformers have been reported in the wind farms although, the failed transformers had previously passed all quality assurance tests and had assembled all standard requirements. Vacuum circuit breaker (VCB) initiated steep front transient impact is one of the potential causes of such insulation failures. The use of VCB as switching devices and intense cable network increases the likelihood for high frequency transient overvoltages (TOVs) in wind farms. Multiple prestrikes and restrikes of VCB in conjunction with cable capacitance and inductance of transformer give rise to fast steep front voltage transients, which eventually cause insulation failures in WTSU transformer. This emphasizes the need to conduct switching transient analysis studies for wind power plants, to investigate the severe switching overvoltages experienced by WTSU transformers. In this work, high frequency modeling in a broad frequency range for major components of the wind farms and an investigation of switching transients on WTSU transformer are presented. An adaptive model of VCB capable of simulating statistical phenomena and overvoltages on circuit breaker and the components that it interacts with is developed in PSCAD/EMTDC. A high frequency phase model of single core cable, taking into account the high frequency effect of cable, i.e., electromagnetic transient propagation, skin effect and reflections is simulated in PSCAD/EMTDC. A linear wideband frequency-dependent black box model of an actual WTSU transformer based on the experimental determination of admittance matrix in a wide frequency range and subjecting the measured admittance matrix to an approximation by means of a rational function through vector fitting is used to simulate WTSU transformer. The rational function obtained for WTSU transformer can then be realized into an RLC network for time domain simulations in PSCAD/EMTDC. A test bench is simulated using the above mentioned high frequency models and replicating Type-IV wind turbine generator synchronized with the grid. Transient scenarios are investigated to understand the most severe switching transients experienced by WTSU transformers, considering the worst repeated switching transient overvoltages and the steep rate of voltage rise experienced by the WTSU transformer. Six different attributes of voltage waveforms across the WTSU transformer are used to investigate the transient behavior in the cases carried out on the proposed test bench.

Acknowledgements

I am deeply in debt to my supervisor, Dr. Shesha Jayaram, without whose support and guidance the completion of this thesis would not have been possible.

My deepest gratitude goes to all the members of my family, for the wonderful support they provided; especially my mother, Mrs. Rama Kanta Sharma, my father Mr. Vijay Sharma and my sister Swati Devgan.

I would like to thank Dr. Magdy Salama and Dr. Kankar Bhattacharya for being the readers of my thesis.

Many thanks are due to my friends at HVEL, including Mahdi Khanali, Mohammad Saleh Moonesan and Mohana Krishnan, for the wonderful time we spent together. Special thanks to my great friend Shahryar Anjum, who supported me throughout this journey.

I dedicate this thesis to my parents, who are no less than GOD to me.

.

Table of Contents

List of Figures

List of Tables

Nomenclature

LTEP	Long Term Energy Planning
WTSU	Wind Turbine Step Up Transformer
VCB	Vacuum Circuit Breaker
DFIG	Doubly Fed Induction Generator
TOV	Transient Overvoltage
TRV	Transient recovery Voltage

Chapter 1
Introduction

Power systems have undergone profound changes over the past five decades. Energy producers are looking at alternatives of traditional thermal plants that use fossil fuels in renewal energy sources, such as wind and solar. In fact, a serious commitment to reduce carbon dioxide emissions, together with the desire to avoid fossil fuel, has resulted in tremendous growth of wind energy around the world. In Canada, every province is adopting wind power as a potential source of energy to supplement its energy grid. The current wind power generation capacity in Canada is about 8517 MW, which accounts for 3.17% of the country's total electricity demand [1]. Further, a strategy has been outlined by Canada's association on wind energy that anticipates this form of energy reaching a capacity of 56,000 MW by 2025 [1]. This will feed 20.5% of Canada's total electricity demand.

Some of the nuclear plants in Canada are in the process of being refurbished. As elsewhere in the world, the inclination in Ontario is now towards the construction of wind energy systems as being cost-competitive, stronger, and affordable. Ontario has invested $1.73 billion within the past five years alone to install new wind farms with a capacity of 1,040 MW [2]. In 2013, a LTEP was released in Ontario. The LTEP proposes the procurement of 300 MW of wind energy in 2015, while identifying similar opportunities for 2016 [3]. As of December 2014, there were 69 wind farms installed in the province of Ontario, with a total number of 1852 wind turbines. The province plans to build 6,736 new wind turbines over the next 20 years, with a predicted contribution of 25% of Ontario's total generation capacity by 2035 [4].

Electrical utilities across North America are predicting a high dependability on wind power in the near future [5]. However, these utilities have encountered serious challenges from the perspective of power system transient studies when incorporating wind power into existing transmission and distribution systems [6], [7]. A WTSU is installed with every turbine in a wind farm. The function of this transformer is to 'step up' the output voltage level of the turbine generator from the generation system rated voltage to the voltage level of the collector system, which is generally medium voltage. Failures in these wind turbine step-up transformers have occurred at an alarming rate, leaving wind farm operators and transformer manufacturers to identify the plausible causes of such failures.

Vacuum circuit breaker initiated high frequency steep front switching transients is expected to be one of the reasons behind the wind turbine transformer failures. Wind turbines are typically switched

off several times a day due to extensive variations in wind speed, thus resulting in vast fluctuations in power generated by the turbine unit. In such conditions, circuit breakers (commonly vacuum circuit breakers) are used to isolate the unit from the collector grid. During the procedure of isolating the wind turbine unit from the grid by VCB, transient overvoltages are produced due to switching operation of VCB. These overvoltages are generated by 'chopping' the current, giving rise to transient recovery voltage. The current chopping in synchronization with the transformer's inductance and capacitance of the cable produces high di/dt and dV/dt. In the wind farms, each wind turbine is equipped with WTSU transformer that is directly connected to vacuum circuit breaker through a cable. Electrical systems with both long and short cables have shown the ability to produce transient voltages at the transformer terminals containing high frequency oscillating waveforms. Despite the fact that the magnitude of these transient overvoltages is less than the BIL rating of the transformer, such an event can prompt high oscillatory voltages inside the transformer windings, resulting in resonance thus causing transformer failures [8].

Standard power system deployment studies usually include reactive power requirement studies, load flow, fault level, short circuit analysis, voltage ride-through capability, etc., but fail to provide information about vacuum circuit breaker initiated steep front transient overvoltages experienced by wind turbine step-up transformers [9]. This emphasizes the need to conduct switching transient analysis studies for wind farms.

1.1 Background

1.1.1 Renewable energy systems: An overview

Renewable sources of energy have been an alternative for non-renewable sources of energy for the past six decades. The benefits of renewable energy are that it is sustainable, pervasive, and generally non-polluting. Moreover, solar cells and wind turbines do not utilize water to produce electricity, giving these energy sources crucial advantages in dry areas such as the western and south western portions of the United States [10]. In contrast, nuclear power plants and thermal electric plants use huge quantities of water.

Despite their advantages, there are also some disadvantages associated with renewable energy. The main ones are high initial cost, variability, and low density, as there is a need for a large captured area and back-up power. Other disadvantages associated with renewable energy are brine from geothermal energy, odor from biomass, avian and visual pollution issues related to wind farms, etc. [10].

Additionally, building a large facility for renewable energy often creates problems for local residents due to odor problems, noise, and lowered property values.

1.1.2 Evolution of wind energy

Wind power generation is an evolving process. In pre-industrial eras, wind was used mainly as a source of energy for grinding grain, pumping water, and enabling transportation. Prior to the invention of the steam engine, wind and water mills were the largest source of power generation [1].

The 11th century saw people from the Middle East using windmills for production of food. In the centuries that followed, the Netherlands polished and redefined the windmill, using it for marshes and draining lakes at the Rhine River Delta. By the late 19th century, windmills were being used to pump water for ranches and farms and for power generation of industry and homes [11]. Figure 1.1 shows Charles Brush's windmill, which is considered the first windmill used for energy generation purposes [12].

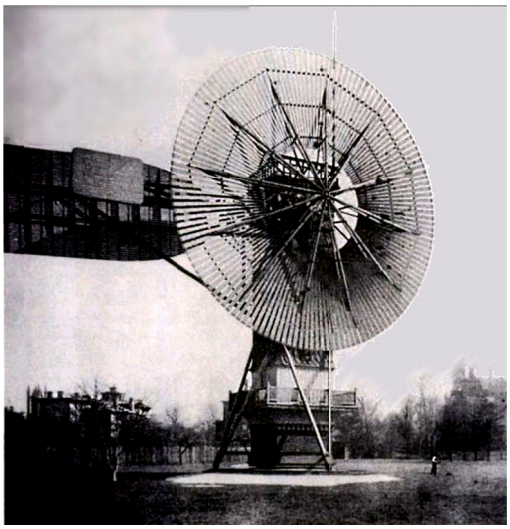

Figure 1.1: Charles Brush's windmill [1]

North American pioneers used windmills for grinding corn and wheat, pumping water and cutting wood at saw mills. The development of electric power saw new applications of wind power, especially for lighting buildings located at remote areas from the power generation station. The 20th century saw the development of small wind plants suitable for residences and large wind plants connected to the grid, but it was the oil crisis of the 1970s that altered the world's energy scope [11]. The crisis resulted in the creation of an interest in alternative energy sources and thus resulted in the appearance of adding wind power to existing generation system.

1.1.3 Wind energy today in Ontario

Wind energy has become a conventional power source in the Canadian electrical energy portfolios [12]. As shown in Figure 1.2 there is a gradual increase in wind energy contributions to Ontario's total electrical generation, from 3% in 2013 to 8% in 2015. Ontario has 3600 MW of power coming from wind energy. Long-term energy plan released by Ministry of Energy in Ontario declared that 1,100 MW of new wind energy will be delivered in 2016.

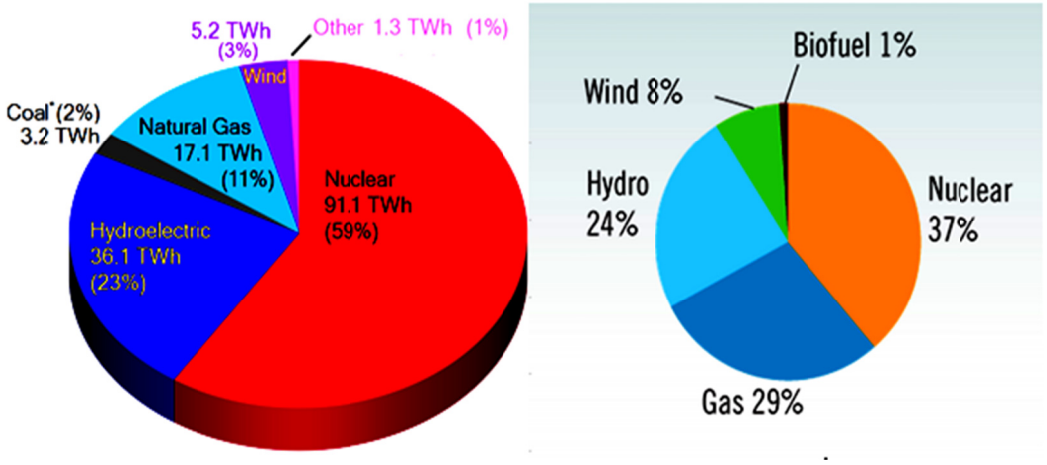

Figure 1.2: Ontario supply mix 2013 and 2015 [4]

An investigation of wind deployment and operating conditions in Ontario concludes that:

- The wind industry in the Ontario, including deployment activities and manufacturing associations, easily satisfied the surge in demand for increased wind power generation.
- Variations in wind energy have only a slight impact on grid reliability and economic concerns.
- Challenges around the deployment of wind power plants, such as land use, wildlife concerns, radar interconnection issues, etc., can be efficiently handled with proper planning.

1.2 Types and Typical Configurations of Wind Farm Generators

At present, there are many designs available in the market. These differ from each other in factors such as fixed speed and variable speed operations, type of connection with turbines, and type of interface with the grid.

Based on generator type, wind turbines can be broadly classified as [13]:

- Permanent Magnet Synchronous Generators (PMSG)
- Field Excited Synchronous Generators (FESG)
- Doubly-Fed Induction Generators (DIFG)

An alternative way of classifying wind generators is by type of connection with the turbine, whether gear connected or direct connected. Prior to 1990, manufacturers preferred gear connections, as they are light weight and can convert relatively low wind speeds to the high rotational speeds required by induction generators. Because of this ability, induction generators were quite small, and the total weight of such systems was less compared to direct drive systems. However, the main disadvantage of this approach is that it reduces the efficiency of the system. For this reason, manufacturers today are more interested in direct drive generator systems, of which only synchronous generators are currently available. Table 1-1 shows a comparison of the latest available wind generators.

Table 1-1: Latest Wind Generators [13]

No.	Generator type	Gearbox	Manufacturer	Power Rating	Turbine rotor speed	Generator voltage rating	Grid connection type	Nacelle weight	Generator weight
1	FESG	Yes	DeWind	2MW	20 rpm	13.8 kV	4	62000 kg	N/A
2	FESG	Direct drive	Enecron	4.5 MW	N/A	N/A	2	N/A	220000 kg
3	IG	Yes	Vestas	850 kW	26 rpm	690 V	2	38000 kg	N/A
4	IG	Yes	Vestas	2 MW	16.7 rpm	690 V	2	67000 kg	N/A
5	IG	Yes	Vestas	3 MW	N/A	1000 V	3	70000 kg	N/A
6	DFIG	Yes	Gamesa	850 kW	25 rpm	690 V	3	33000 kg	N/A
7	DFIG	Yes	DeWind	2 MW	20 rpm	690 V	3	62000 kg	N/A
8	DFIG	Yes	Gamesa	2 MW	16 rpm	690 V	4	107000 kg	N/A
9	PMSG	Direct drive	Zephyros	1.5 MW	18 rpm	3000 V	4	N/A	47200 kg
10	PMSG	Direct drive	Vestas	3 MW	N/A	N/A	4	70000 kg	N/A
11	PMSG	Direct drive	The Switch	3.8 MW	21 rpm	690 V	4	N/A	81000 kg
12	PMSG	Yes	The Switch	950 kW	N/A	690 V	4	N/A	3400 kg

Based on the type of grid integration interconnection, there are four classifications of wind generators:

Type I Wind Turbine Generator: These are fixed speed wind turbine generators that have limited control (2-3%) of slip [14]. The generators consume reactive power and the rotor blades are pitch-regulated to control power. In this type of wind turbine configuration, the wind turbine step-up transformer is directly connected to the squirrel cage induction generator (SCIG). The speed of the wind turbine remains fixed in conjunction with the frequency of the grid. Real power is generated in this system due to the creation of negative slip, which occurs when the shaft of the turbine rotates faster in comparison to the speed corresponding to the frequency of the electrical grid [15]. In contrast, positive slip refers to the motoring mode. Under steady state conditions, the operating speed of the turbine is almost linearly dependent on the torque. During spasmodic variations in the speed of wind, mechanical inertia of the system confines the rate of change of output power (dP/dt) [16].

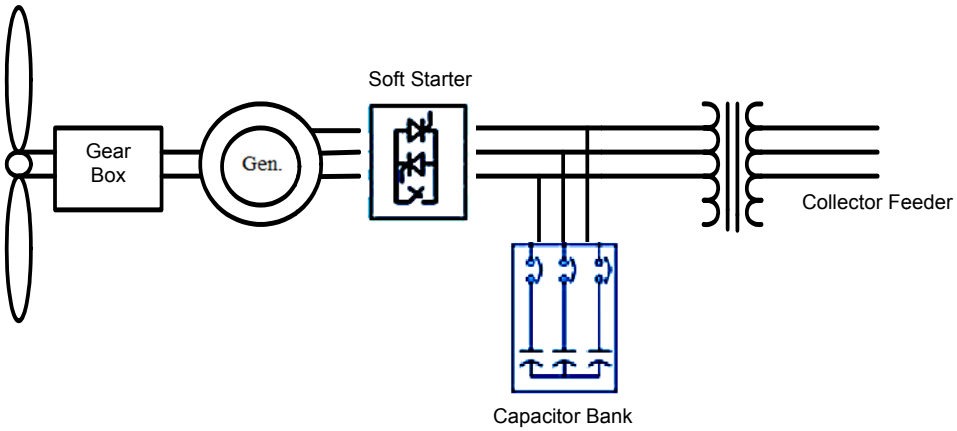

Figure 1.3: Schematic representation of Type I wind generator

Type II Wind Turbine Generator: These are variable speed wind turbine generators that have more control of slip (up to 10%) and can consume reactive power like type I wind turbine generators. Type II wind turbine generators have the turbine step-up transformer directly connected to the wound rotor induction generators in a fashion similar to type I turbines. The only difference is the presence of a variable resistor in the rotor circuit of the machine, which is not present in Type I. This can be achieved with the use of power electronics and a group of resistors exterior to the rotor and slip rings, providing a path for the current to flow between the resistors and the rotor [14]. To keep power constant during bursting conditions, the variable resistors provide rapid control of the rotor current.

Even during grid disturbances, the variable resistors [16] can influence the machine's dynamic response.

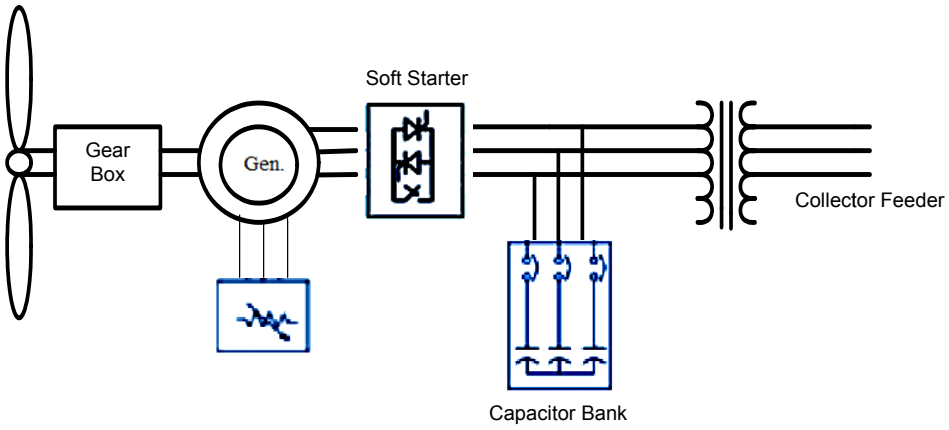

Figure 1.4: Schematic representation of Type II wind generator

Type III Wind Turbine Generator: Type III wind turbine generators are also variable speed turbines, but they have more control of slip (up to 50%) and can provide comprehensive reactive power control. Partial scale converters are needed for this type of wind turbine [17]. DFIGs are generally referred to as Type III turbines and are an upgrade to Type II turbines. Type III turbines are equipped with variable frequency AC excitation of the rotor circuit, whereas Type II turbines have only simple resistance. A current-controlled voltage source converter with adjustable control of the magnitude and phase of the rotor current serves as an external supply to the rotor [14]. Additionally, there is back-back connection between a grid side converter and a rotor side converter for exchanging power with the grid.

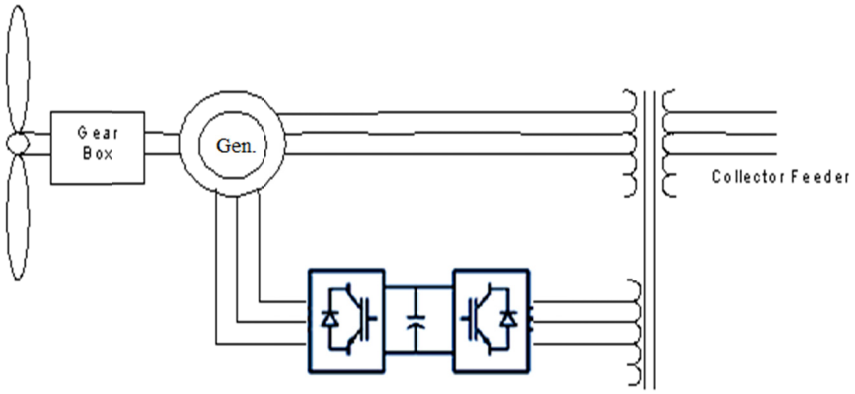

Figure 1.5 Schematic representation of Type III wind generator

Type IV Wind Turbine Generator: Now a day, this is the most widely used wind turbine. Like Types II and III, Type IV also provides variable voltage control, but provides 100% control over slip. Reactive power control is an additional feature of Type IV wind turbines [18]. Furthermore, these turbines provide an adjustable design and operation because the grid is connected to the output of the rotating machine via a back-back frequency converter. To obtain AC output from the machine, the turbine rotates at optimal speed. The machine runs at slow turbine speed as gearbox is removed, generating less frequency than the electrical frequency of the grid [19]. This type of rotating machine is similar to wound rotor synchronous machines as well as to conventional-type generators with field current control and high numbers of poles generally found in hydroelectric plants.

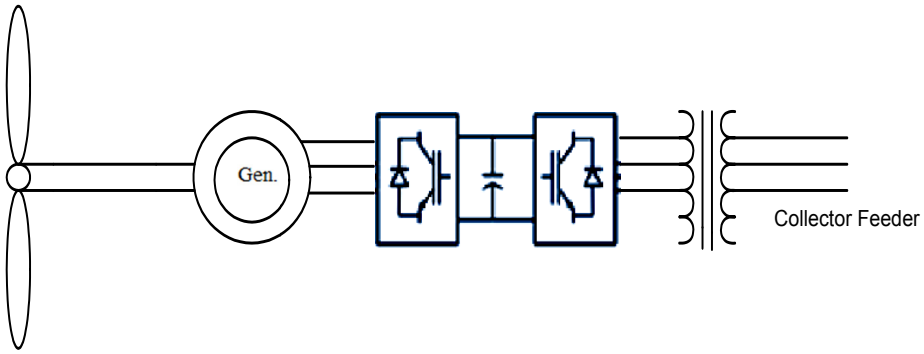

Figure 1.6: Schematic representation of Type IV wind generator

1.3 Wind Turbine Step-Up Transformers

Every wind turbine in a wind plant is usually equipped with a WTSU that raises the output voltage of generator turbines to the voltage of the collector system, which is typically set at a medium voltage level. These transformers are located at the base of the wind turbine (offshore wind farms) and are rated from 2 MVA - 5 MVA. For grounding purposes (i.e., mainly to provide neutral grounding), grounding transformers are located all across a wind farm. This system is connected to the step-up transformer located at the substation supplying power to the electrical grid [20]. Figure 1.7 shows the location of the WTSU transformer in a wind farm.

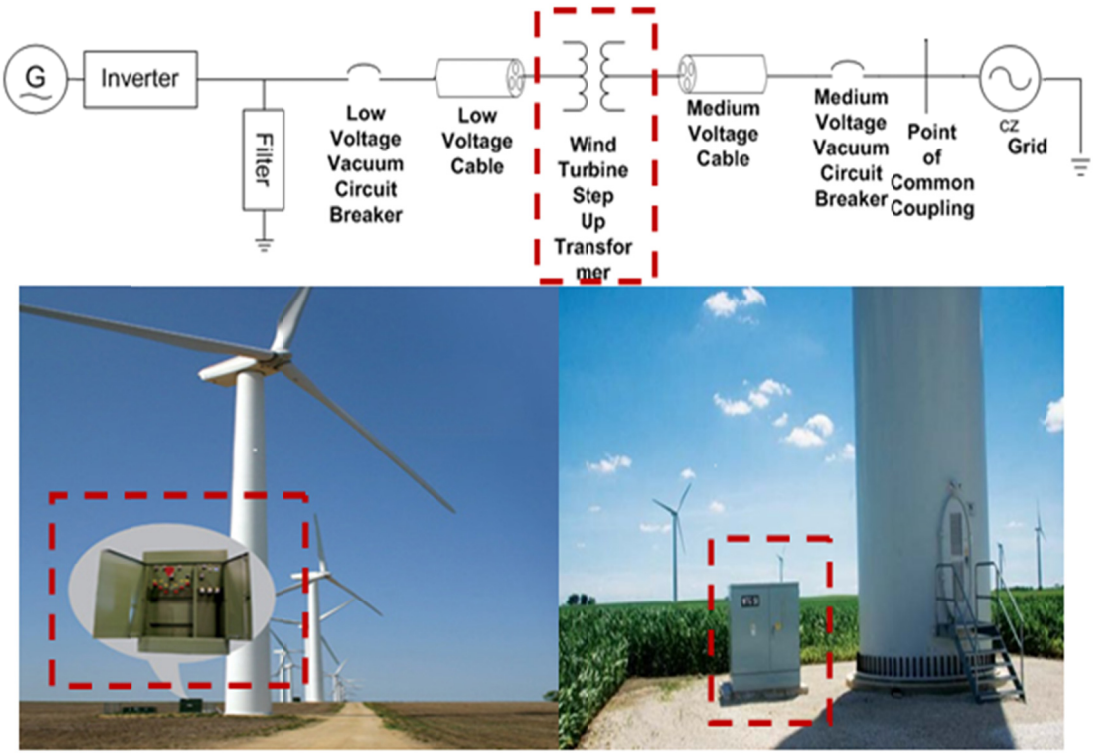

Figure 1.7: Location of WTSU transformer

Typically, conventional distribution transformers have been used as WTSU transformers. Owing to the substantial number of recent wind turbine transformer failures, there is a need for a more sturdy wind turbine transformer design [21], [22].

1.4 Problems Associated with Wind Turbine Step-Up Transformers

Despite the prevalence of WTSU transformer failures, identifying why they occur has been a tedious task for utility companies, wind farm operators, and developers of WTSU transformers [23]. Several reasons for the failures in WTSU transformers have been identified as follows:

a. **High frequency harmonics from converter side**: As mentioned earlier in this chapter, a distribution transformer cannot simply be used as a wind turbine step-up transformer, as the output of the inverter feeds the WTSU transformer [8]. Figure 1.8 shows the resonating frequencies caused by harmonics. One of these harmonic components can match the natural frequency of the grid and can create high voltage spikes.

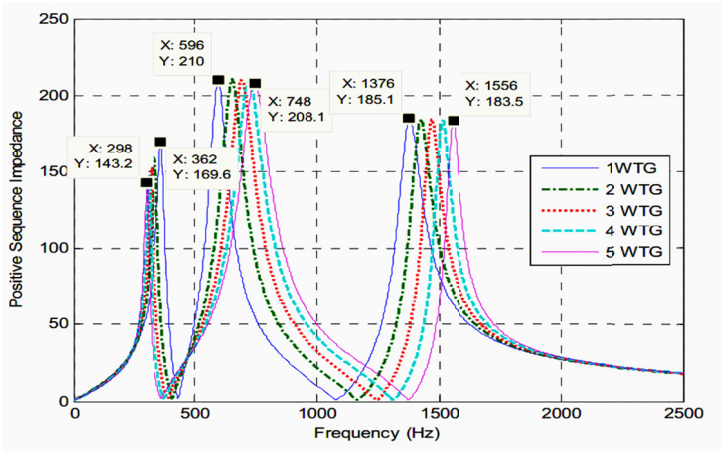

Figure 1.8: Resonating frequencies created by harmonics [34]

Given this scenario, WTSU transformers should be designed to withstand these high frequency harmonics. Secondly, due to the use of inverters, harmonics with frequencies of a multiple of 3^{rd}, 5^{th}, 7^{th}, 13^{th}, 17^{th}, and up to 23^{rd} are produced. Enhanced stray and eddy current losses within the windings and the other metallic structures of the transformer are caused by these harmonics [8]. Moreover, the harmonics produce burdens and temperatures that are almost three times higher than normal 60 Hz waveforms. Additional temperature increase can lead to problems of partial discharge, dissolved gasses, loss of life of a transformer, and eventually transformer failure. Therefore, WTSU transformers should be designed specifically to counter the severe effects of harmonics.

b. **Loading cycle of transformer:** Due to variations in wind speed, the loaded and unloaded conditions of WTSU transformers are totally different from conventional distribution transformers. Firstly, the core losses continue to occur because of the relatively long periods of light loading or when the transformer is sitting idle. Furthermore, from a long-term economical perspective, these core losses should be kept minimal [8]. A core construction that is specially designed with high-grade oriented electrical laminations and a choice of core flux density can reduce these losses.

The second problem concerns spasmodic changes in load, from full load to no load and again to full load. Due to variations in wind speed, a WTSU transformer can experience variations in load multiple times a day [8]. Sudden load variations result in variations in the current flowing through the transformer windings and can lead to thermal stresses within the transformer. Periodic variations in the loading phenomena can result in mechanical burdens on the

transformer windings. It also effects the insulation and clamping structures, and adds to loosening of the windings. Periodic temperature fluctuations are experienced by transformer cooling systems as well. Oil absorbs more gasses during heating, and when the oil cools, it releases the gasses, which results in the formation of bubbles. These bubbles create hot spots, giving rise to partial discharge and leading to the eventual deterioration of the insulation.

c. **Proper sizing of transformer**: To handle the unique conditions inherent in wind power, WTSU transformers should be properly sized. If they are not, the resulting dielectric burdens and overheating will eventually deteriorate the insulation system [23]. Hydrogen is predominantly generated within the transformer because of overheating and dielectric stresses. Increasing the kVA rating of the transformer has been potentially identified as a temporary solution to this problem, but it eventually adds to the losses.

d. **VCB initiated steep fronted transients**: Steep front transient overvoltages caused by switching are another major concern [24]. The wind turbine unit can be switched off multiple times a day due to extensive changes in wind speed and corresponding fluctuations in generated power. To isolate the wind turbine from the grid, circuit breakers are used. The switching operation of vacuum circuit breakers results in transient overvoltages because of the extensive cable network and transformers used in wind farms [25]. These transient overvoltages are produced by current chopping and result in high di/dt and dv/dt.

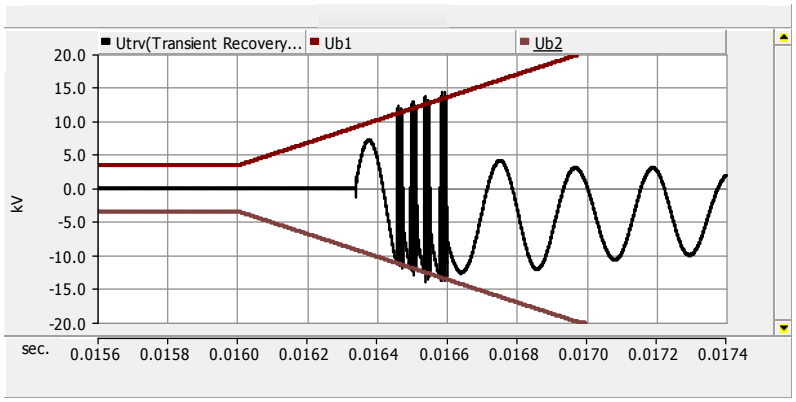

Figure 1.9: The phenomena of restriking and TRV across VCB

Although switching overvoltages caused by TRV have a magnitude lower than the basic impulse level of the transformer, such overvoltages can prompt a large oscillatory voltage within the windings and lead to failures [26]. IEEE standard C570.142 deals with this subject adequately.

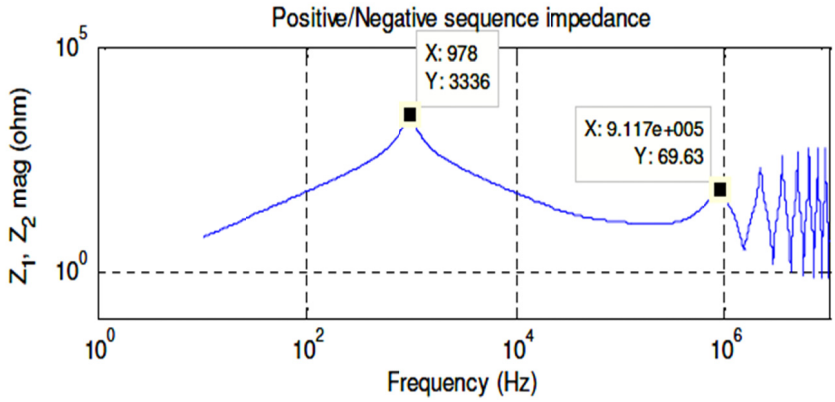

Figure 1.10: Resonating frequencies created by harmonics transients

Figure 1.9 shows transients alleviating because of switching VCB in electrical systems. Compared to harmonics, switching transients create high frequency oscillations with high dv/dt that deteriorate the insulation of transformer windings.

1.5 Thesis Organization

The thesis is organized as follows:

- *Chapter 1* provides a review of the evolution of wind power and explains the typical configuration of wind farms. As well, wind turbine step-up transformers and the problems associated with them are reviewed.
- *Chapter 2* provides a comprehensive overview of the literature and the prior work done in this area. Research that deals with the modeling of power system components, especially VCBs, cables, transformers and generation systems (for analyzing high frequency switching transients) is reviewed. Additionally, research done on the analysis of switching transients created by the interaction of switching devices and other power system components is also identified. Finally, a brief description of the potential problem is presented.
- *Chapter 3* deals with the modeling of VCBs, cables, and WTSU transformer in PSCAD/EMTDC. An adaptive high frequency model of a vacuum circuit breaker simulating statistical phenomena, the high frequency (phase) model of cables and a high frequency black box model of an actual WTSU transformer model are simulated in PSCAD/EMTDC to enable transient analysis of wind farm.

- *Chapter 4* presents a detailed analysis and propagation of switching transients in a wind turbine that is synchronized with the grid. Four different cases are defined, where switching transients generated due to the opening and closing operation of VCBs on lower and medium voltages are analyzed. The most severe and onerous conditions are observed, depending on various factors.
- *Chapter 5* provides a discussion on the results obtained at the end of chapter 4. In chapter 5, the comparison of the proposed transient study in wind farm with prior research work is presented.
- *Chapter 6* presents the thesis conclusion and suggests future work in the field of switching transient studies in offshore wind parks.

Chapter 2
Literature Review

In this chapter, details of the fundamental concepts of TOV, with special emphasis on switching transients, are provided in order to facilitate an understanding of the succeeding chapters. The transients presented here are the type caused by switching operations of vacuum circuit breakers (VCBs). A review of switching transients is followed by an evaluation of high-frequency transients due to switching of a three-phase transformer with a vacuum circuit breaker. A thorough literature review on transient overvoltage in cable systems and high frequency transients in large wind farms is presented in the latter part of this chapter. Finally, a discussion of "IEEE C57.142: Guide for the Occurrence and Mitigation of Switching Transients by Transformer, Switching Device and System Interaction" concludes this chapter.

In transmission and distribution systems, inevitable conditions like network switching operations generate transient overvoltages. A transient overvoltage results from the reaction of the electrical circuit to sudden variations in an electrical network, such as switching operations or a fault. A transient is a process in which a power system moves from a steady-state condition to a transient state [30]. It is generally very short-lived, ranging from microseconds to milliseconds [37, 38].

2.1 Classification of Transient Overvoltage

2.1.1 Impulse transients

Lightening is a cause of impulsive transients and is associated with the discharge of a current that can reach up to 200 kA. The impedance of the system seen by the lightening current limits the overvoltage developed in this case. Such, overvoltage situations often cause faults in power systems due to insulation failures, which in turn cause supply interruptions and voltage sags throughout the electrical network.

2.1.2 Oscillatory transients

Switching transients in power systems are a source of oscillatory transients. Circuit breakers are used to isolate a fault that generates such oscillatory transients. In order to carry out maintenance operation, the switching of distribution feeders and capacitor banks that are used to provide reactive power support, is also considered as additional source of oscillatory transients.

- **Circuit breaker initiated switching transients**

A switching overvoltage or switching surge is generated due to the interaction of the inherent elements (inductance, capacitance and resistance) associated with an electric network. When a current flows through an inductance, it produces magnetic flux. Any effort to change the magnetic flux (i.e., the current) will be opposed by the inductance, which is manifested by the generation of a counter EMF in the inductance in a direction that will keep the magnetic flux (and the current) constant. Therefore, when a circuit breaker tries to interrupt a current, a voltage is developed by the system inductance to oppose the change in current. The faster a switch tries to interrupt a current, the higher the resulting switching surge voltage is.

- **Shunt capacitor switching transients**

Shunt capacitors are used extensively in power transmission and distribution systems as a means of supplying reactive power for voltage support. These capacitors are implemented in the system to control the system voltage, increase the power transfer capability, reduce equipment loading, and lower energy costs by improving the power factor of the system. Depending on the level of reactive power support needed, switching of capacitor banks takes place. As the capacitor is defined by the instantaneous rate of change of voltage, the voltage at the bus bar collapses during the energization of a discharged capacitor. This results in oscillatory transient voltage, with a peak reaching up to 2 p.u.

A similar effect is observed during the switching off of a capacitor, which results in a restrike. A restrike occurs when the recovery voltage of a breaker causes the dielectric strength of switching contacts to break, re-establishing the current in the circuit. Under certain network conditions, the switching transients of a capacitor can be magnified to higher values. This often occurs when transients that originate from medium voltage move to a low-voltage electrical network, with power factor correction capacitors present. The overvoltage associated with this phenomenon can reach a peak value up to 4 times the corresponding power frequency voltage.

2.1.3 Travelling waves

The parameters of transmission lines and cables are distributed, as are of transformer and generator windings. The characteristic impedance of a circuit with distributed parameters is its ability to support traveling transient waves of voltage and current. The influence of the distributed parameters on the propagation of TOV depends on the frequency content of the waves.

Current and voltage waves travel in both directions from the point of excitation or disturbance. The ratio of the amplitudes of the voltage and the current waves on a transmission line or cable is called the characteristic impedance Z_0 of the line and for a lossless line is given by (2.1).

$$Z_0 = \sqrt{\left(\frac{L}{C}\right)}\Omega \tag{2.1}$$

where L and C are the distributed inductance and capacitance, respectively, of the line or cable. Typical values of characteristic impedance vary between 300Ω and 500Ω for overhead lines, and between 30Ω and 60Ω for cables.

The velocity of the propagation of the waves for a lossless line is given by (2.2) and depends on the medium of propagation. It is near the speed of light ($3*10^8$ m/sec) for overhead lines, and between one-half and two-thirds of this value for underground cables [2].

$$\nu = \sqrt{\frac{1}{LC}}\ \text{m/sec} \tag{2.2}$$

Like all other waves, travelling waves initiated by disturbances in power systems also have classic wave characteristics such as reflection and refraction.

- **Reflection and refraction of travelling waves**

When voltage and current waves propagate in power lines or cables, there exists proportionality between the two. The proportionality constant is the characteristic impedance of the line or the cable. When a wave arrives at a point of discontinuity (which could be an open end, an underground cable or transformer where the characteristic impedance changes), two new wave pairs are generated to keep this proportionality. One is reflected back and is superimposed on the incident wave, while the other is transmitted beyond the discontinuity. The amplitudes of the reflected and refracted waves are such that the voltage-to-current proportionalities are preserved for each.

$$V_2 = \left(\frac{Z_a - Z_b}{Z_a + Z_b}\right)V_1 \tag{2.3}$$

$$V_3 = \left(\frac{2Z_b}{Z_a + Z_b}\right)V_1 \tag{2.4}$$

The magnitudes of reflected and refracted voltage waves at a junction point with characteristic impedance waves Z_a and Z_b on the incident side and refractive side, respectively, can be quantified as:

Here, V_1 is the incident wave, V_2 is the reflected wave, and V_3 is the refracted (transmitted) wave. $\frac{Z_a - Z_b}{Z_a + Z_b}$ is called the reflection coefficient and $\frac{2Z_b}{Z_a + Z_b}$ is called the refracted coefficient.

The reflected current (I_2) and transmitted current (I_3) are given by:

$$I_2 = -\frac{V_2}{Z_a} \tag{2.5}$$

$$I_3 = -\frac{V_3}{Z_b} \tag{2.6}$$

These different types of transients discussed here are characterized by the following:

a. Rise time
b. Decay time
c. Peak values of overvoltage
d. Maximum current
e. Rate of rise of voltage

2.2 Vacuum Circuit Breaker initiated high frequency transients

About six decades ago, when the first generation of vacuum circuit breakers was still in use, research was mainly focused on high chopping current levels of circuit breakers. The chopping of a current in accordance with a transformer or motor circuit creates high frequency overvoltages in the form of reignition and restrikes [26], [52]. An investigation into current chopping behaviors of VCBs showed that the choice of contact material influences the interruption performance of a breaker around current zero [14], and that the chopping current was deduced to vary from 3A to 8A [27], [15]. Current chopping differs for a SF_6 circuit breaker or VCB [28], [33]. Moreover, the probability of reignition due to current chopping is statistically high and depends on the type of contact material [29]. Equation 2.7 [40] deduces the chopping current in VCB.

$$I_{ch} = (\omega \times i \times \alpha \times \beta)^{q} \tag{2.7}$$

Where, $\omega = 2 \times \pi \times 50$ Hz; $\alpha = 6.2 \times 10^{-16}$ sec; $\beta = 14.28$ and $q = (1 - \beta)^{-1}$ are the values as suggested in IEEE 57.142, and i refers to the magnitude of power frequency current.

In the late 1980s, after determining the working of VCBs, the interruption of transformers [51] as well as the switching off of motors [49], [55] were carried out in order to provide enough information for determining overvoltages and insulation co-ordination levels. This work was followed by the

creation of single-phase test circuits that could simulate the restrike and reignition phenomena in a vacuum circuit breaker [56].

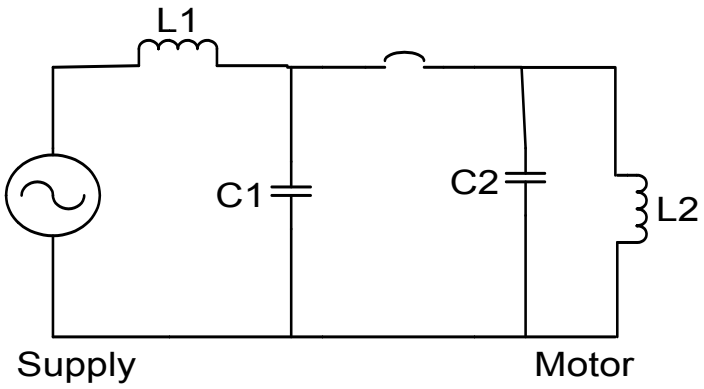

Figure 2.1: Test circuit showing switching off of a motor with a circuit breaker

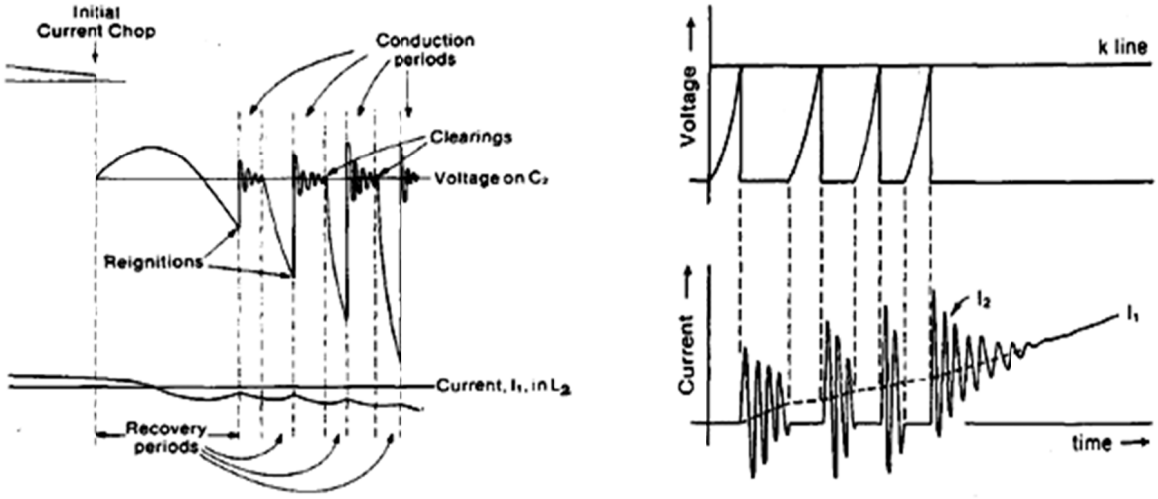

Figure 2.2: Reignition phenomenon in circuit breakers [33]

Figure 2.1 illustrates the test circuit under consideration, which shows the switching off of a motor. Figure 2.2 demonstrates the reigniting transients produced because of this phenomenon [33]. Under certain circumstances, results from a single-phase transformer can be applied to a delta star transformer connection, despite the fact that the delta-connected transformer phenomenon is more complicated because of mutual coupling [54], [57]. In determining the most severe conditions for switching transients' circuit parameters (e.g., length of cable), bus bars are varied in order to recognize most severe overvoltages [58].

The dynamic simulation of a vacuum circuit breaker in power system simulation software for transient studies was introduced in ATP/EMTP [35]. The model simulated characteristics of arc voltage, chopping current, voltage breakdown characteristics, high frequency current quenching ability. Estimation for expected transient overvoltage for a specific configuration of an electrical network was made. Two contact materials did the reignition and extinction of arcs. The contact materials used were Cr/Cu and Cr/Cu with additives of Zinc, Tin and Li_2O [36]. Cr/Cu and high Cr content showed a lower breaking capacity.

The arc voltage of the vacuum circuit breaker is independent of wide current range [37]. Ideally, the moment of current zero (during the extinction of the arc) gives rise to a TRV. In modern vacuum interrupters, the arc becomes unstable before zero during the switching of small currents at current levels in the range of 3-8 Amps [38].

The switching of inductive loads like motors and unloaded transformer circuits with VCBs has three potential sources of overvoltages: chopping overvoltage, multiple reignition overvoltage, and overvoltage caused by virtual current chopping [39].

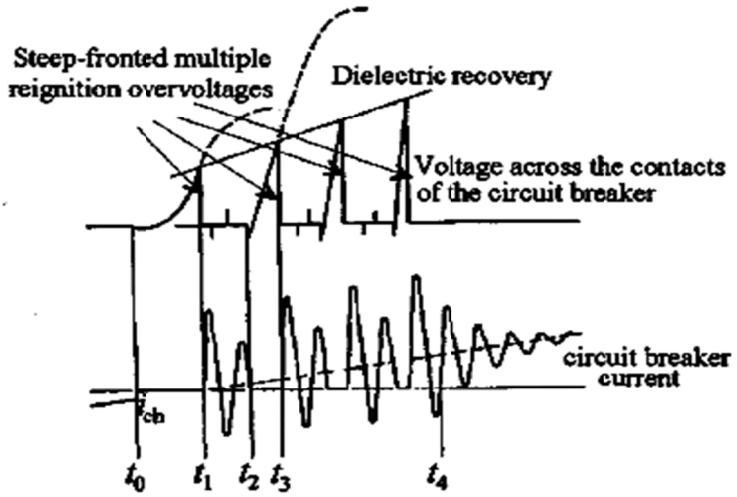

Figure 2.3: Description of multiple reignitions process [40]

As shown in Figure 2.3, overvoltages produced in VCBs are lower in magnitude but very steep. If the load in the form of a motor or a transformer is exposed to these transients, the insulation of loads can deteriorate or eventually fail. Table 2-1 shows the relationship between switching device performance with frequency interval.

Table 2-1: Relationship Between Switching Device Performance and Frequency Interval [41]

Circuit Breaker Performance	1 Hz - 3kHz	3 kHz - 20 kHz	10 kHz - 3 MHz	3 MHz - 20 MHz
Closing				
Mechanical Pole Spread	Important	Very important	Negligible	Negligible
Prestrike effect	Negligible	Important	Important	Very important
Opening				
High current interruption	Important for interruption capability studies	Important for interruption capability studies	Negligible	Negligible
Chopping current	Negligible	Important for interruption studies of small inductive currents	Very important	Negligible
Reignition effect	Negligible	Important for interruption studies of small inductive currents and capacitive currents	Very important	Very important
High frequency current interruption	Negligible	Negligible	Very important	Very important

As the transients observed occur in the high frequency range, the selection of the transformer is very important. Table 2-2 suggests different transformer models classified based on frequency range [41].

Table 2-2: Transformer Models for Different Frequency Intervals [41]

Transformers	1 Hz - 3kHz	3 kHz - 20 kHz	10 kHz - 3 MHz	3 MHz - 20 MHz
No Surge transfer	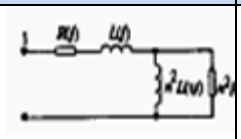	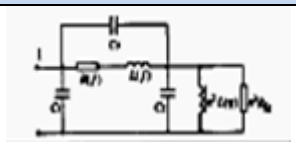	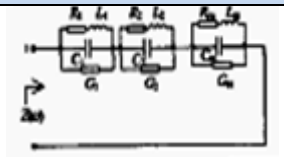	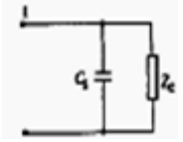
With surge transfer	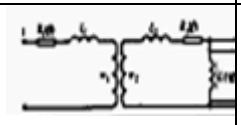	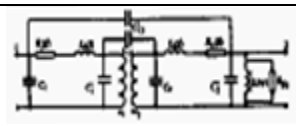	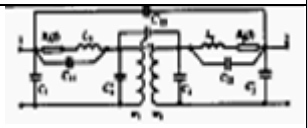	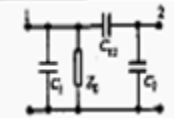
Short circuit impedance	Very important	Very important	Important for surge transfer	Negligible
Saturation	Very important	Very important	Negligible	Negligible
Frequency dependent series losses	Very important	Very important	Negligible	Negligible
Hysteresis and iron losses	Only for resonance studies	Very important	Negligible	Negligible
Capacitive coupling	Negligible	Very important	Important for surge transfer	Very important

2.3 Overvoltage Transients Experienced in Cable Systems

In an electrical system comprised of a switching device, cables and transformers, high frequency transients from the switching device are alleviated by the capacitance of the cable and the inductance of the transformer. Designers of power systems are mainly concerned with steady-state frequency design (or at least up to several orders of harmonics, as required by standards) rather than high frequency transients. To analyze the cable reflections, accurate modeling of cables is required to model the wave propagation, skin effect etc., in the cable.

Simply representing the cable as a π-model does not serve the purpose. For example, the semiconductor screens have a dominant role on the propagation characteristics at high frequencies [42]. To model the cable in PSCAD/EMTDC or any other power system transient analyzing software,

data is used from cable guides and in electrical system descriptions to create a model that closely resembles a cable in a real system. The idea is to be able to simulate both low frequency and high frequency effects, and to choose an approach for cable modelling that accurately reflects real conditions throughout a large frequency spectrum [33].

Due to the sheath that is present in an actual cable, the high frequency coupling phenomenon should also be included when modeling a cable. High frequency effects of power cables are important for modeling a cable in PSCAD/EMTDC. Some examples of the propagation of high frequency transients in a cable are given in [43] and [44], which, along with their respective references, provide a good overview of how transients travel in cables.

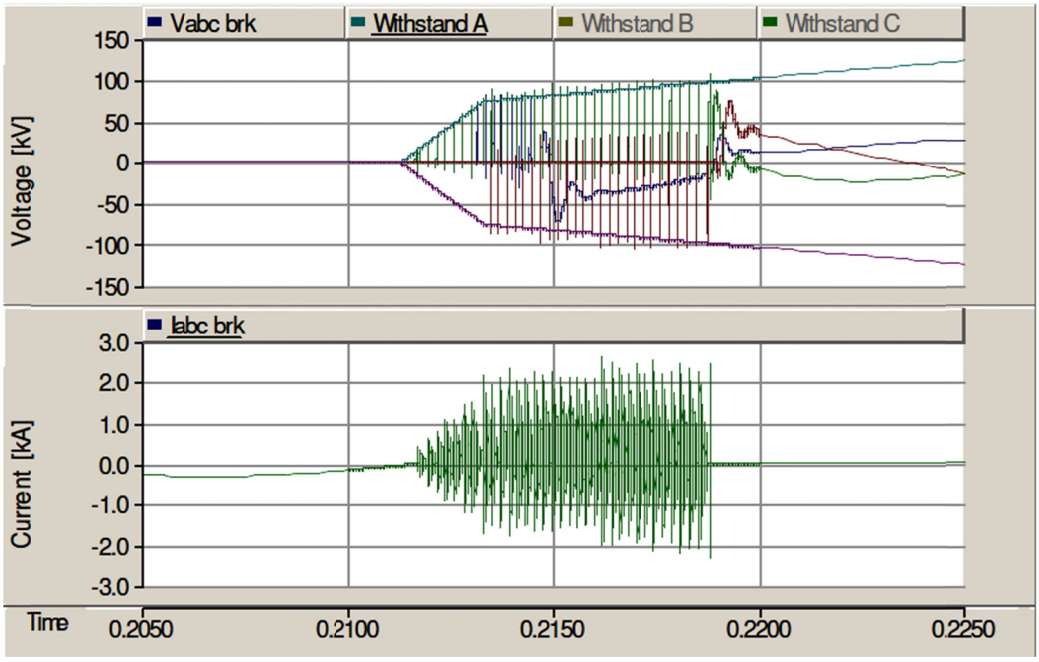

Figure 2.4: Voltage and current waveforms across a breaker [33]

Figure 2.4 shows the voltage and current across a breaker of an industrial system that makes use of extensive cable systems [33].

2.4 High Frequency Transients in Wind Farms

A wind farm has an extensive electrical network of cables, transformers, and switching devices (circuit breakers). Research has been carried out to analyze the generation, propagation and impact of high frequency transients in wind parks and to present an analysis as well as key results.

In cable networks, multiple prestrikes and reignitions are known to occur during switching operations, causing high frequency steep-fronted transient voltages and currents. Wind farm collector grids are composed of a vast amount of cables of different lengths and connecting points. These cable systems have low surge impedance compared to overhead lines in conventional transmission systems. Consequently, multiple prestrikes and reignitions of switching apparatuses with cables can cause transient overvoltages with larger time derivatives than overhead transmission lines. With the increase in cable grid (particularly wind parks), it has become important to characterize a collection grid cable system and the related transients during manoeuvres with different switching apparatuses [45].

The analysis of high frequency switching transients in wind parks starts with the creation of high frequency modeling of major components responsible for high frequency switching transients. The major power system components include cables, transformers, circuit breakers, and generation systems. The models need to be valid for high frequency (i.e., 60 Hz to 10 MHz) [46]. The influence of different wind farm topologies has also been investigated [47].

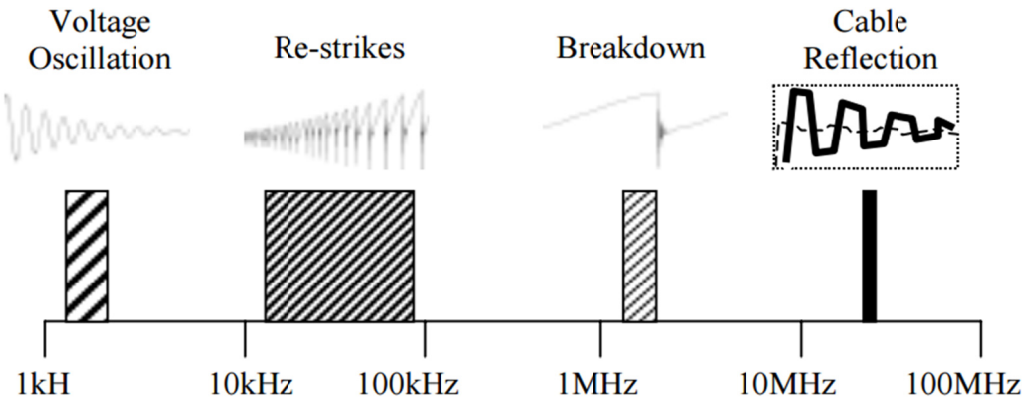

Figure 2.5: Frequency brackets and range in which transients propagate [43]

Figure 2.5 implies a relative ordering, whereby transient oscillations due to system components occur on the lower frequency spectrum (TRV oscillations), while cable reflections occur at relatively very high frequencies.

Transformers connected at the medium-voltage level in wind park collection grids are exposed to the stress of very fast transients generated during breaker switching operations. The rise time of the transient voltage in such systems is much shorter compared to the rise times of transients generated in transmission systems at a high-voltage level. The transformer excitation with VCBs shows the propagation of very fast transients with a 35-ns rise time and a 1-p.u magnitude. The inter turn

voltage among the windings exceeds the level obtained with a lightning impulse-shaped voltage waveform of 4.4 p.u. During a switching scenario with delta-connected transformers, where the winding is excited from both ends, the same 1-p.u./35-ns voltage step generates an inter turn voltage that exceeds the 1-p.u. level, which is more than 2.5 times higher voltage stress than during a lightning impulse test [45].

The voltage transients generated during breaker operations in cable systems in a wind park collection grid can reach very low-rise times. The rise times of these transients can be almost 50 times shorter than the rise time of a lightning pulse. Such transients can generate a very high voltage stress on the internal transformers insulation [46].

A critical switching scenario for estimating internal voltages using verified models of different types of transformers and wind turbine layouts (in order to account for typical wind turbine layouts found in modern wind farms) shows that the magnitude of the voltage transients is higher than the basic lightning impulse insulation level (BIL) [47]. Moreover, the rise time of the voltage surges is much shorter than the rise time of the lightning pulse. The shortest rise time of 40ns is obtained in a wind turbine layout where the wind turbine breaker is placed near the transformer. Due to very short rise times of the transients, very high internal overvoltages are estimated in dry-type transformer windings.

These internal overvoltages are much higher than overvoltages recorded for the basic lightning impulse level. For a wind turbine layout where a breaker is placed in the bottom of a tower and a dry-type transformer in a nacelle, the highest turn-to-turn voltage of about 1.5 pu is estimated. This is almost 4 times higher turn-to-turn voltage then the voltage obtained during the BIL test. In a wind turbine layout where a breaker is placed close to the transformer, the amplitude of the turn-to-turn voltages reached 1.8pu due to lower stray capacitances and thus a shorter rise time of voltage strikes [48].

2.5 Occurrence and mitigation of switching transients

The purpose of this IEEE guide (IEEE standard 57.142) is to provide a detailed description of the transformer's performance when impacted by oscillatory transients. These transients are typically produced upon interactions of the electrical system, switching device (not mechanical switching devices), transformer and load. The guide describes the operating conditions, which lead to the production of switching oscillatory transients, eventually resulting in damage to a transformer

insulation system. The nature of the interaction and electrical characteristics of the above-mentioned components is discussed in the guide, which also addresses several mitigation methods. The document provides a specific guide to the modeling technique of major power system components used to analyze switching transients in power systems.

The source and its corresponding transmission system is represented as a network of capacitances and inductances. Since the transient frequencies are significantly higher than the system power frequency, the dominant system parameters are the surge impedance or the capacitance of the cables and lines. The short circuit inductive impedance is not an important parameter. As far as generation systems are concerned, adaptive approximated models of different generators are used to simulate switching transients.

The loads of concern are mainly transformers that are unloaded, lightly loaded and inductively loaded. Non-linear loads (rectifier, variable speed motor drive, UPS system) may also be of concern, depending upon the impedance presented at the terminals of the transformer's natural frequencies. Severe voltages within the winding structure that produce stresses greater than the safety operation limit of the transformer’s insulation are produced within the transformer, if the transient voltage produced by system has a major oscillatory component at a frequency near to the natural frequency of the transformer.

Transformers possess a frequency-dependent impedance characteristic, as shown in Figure 2.6. Hence, the relationship between voltage across a transformer’s terminals and voltage produced within the windings of a transformer non-linearly depends on the frequency content of the voltage applied and the surge impedance of the transformer [49], [50]. Each individual transformer has a unique design that corresponds to its impedance v/s frequency curve. Hence, creating an equivalent frequency-dependent black box model of the original transformer is very important for the analysis of switching transients [50].

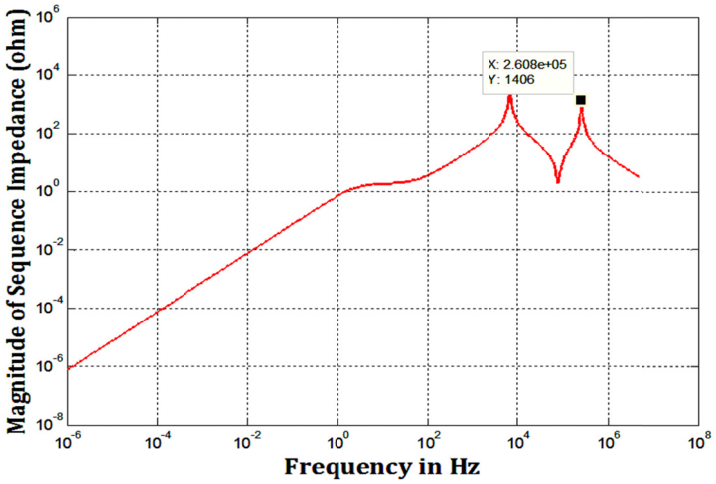

Figure 2.6: Example showing impedance vs frequency response

According to IEEE 57.142 standards, **a switching device** should be able to simulate the following characteristics:

- Dielectric strength between contacts during closing
- Contact gap at current zero during interruption
- Current chopping magnitude during interruption
- Breakdown voltage (reignition) after a current zero during interruption
- Interruption of high frequency inrush currents following reignitions
- Repetitive reignitions after interrupting high frequency inrush currents

2.6 Problem Identification

Literature review presented in this chapter concludes that switching devices like VCB, under certain network conditions cause switching overvoltages with fast rise times. Wind farms use VCBs as switching devices, which consist of intense cable networking. This increases the likelihood for high frequency TOV in wind farms. WTSU transformer insulation failures caused by switching transients have been reported [36], although the failed transformers had previously passed all quality assurance tests and had assembled all standard requirements [37]. The use of cable networks and VCBs in wind farms could be the source of insulation failures in WTSU transformer due to the fast steep front voltage transients caused by multiple prestrikes and restrikes of VCBs [39]. This emphasizes the need to conduct VCB initiated switching transient analysis studies for wind farms, to analyze the severe switching overvoltages experienced by WTSU Transformers.

2.7 Research Objectives

As the unpredictable problem of transient overvoltage and unavoidable switching action of VCBs, it is important to study fast switching transient overvoltage in wind farms. Despite the rising failure rate of WTSU transformers due to stresses from fast switching transient overvoltage, there is very little work done towards investigating and analyzing the switching transients experienced by WTSU. Due to this reason, following research objectives are set for this thesis:

- Developing a detailed user defined high frequency black box model of VCB in PSCAD/EMTDC, proficiently simulating overvoltages on all the system components, taking into account the statistical phenomena of VCB.
- Developing a single core cable model based on the geometry of cable, insulating material properties and incorporating a propagating wave frequency dependent phase model in PSCAD\EMTDC.
- Development of a sophisticated black box model of WTSU transformer using vector fitting algorithm and rational function approximation technique, in PSCAD\EMTDC. Presentation of an average model of DFIG concludes the simulation of power system components for switching steep front transient analysis.
- Simulating a test setup in PSCAD\EMTDC consisting of a Type-IV wind turbine synchronized with a grid to analyze the most onerous transient scenarios experienced by WTSU transformers.

Chapter 3
High Frequency Models of Wind Power Components

This chapter outlines the techniques of high frequency modeling of power system components that are responsible for propagation of switching initiated high frequency transients in a wind farm. These components are the switching device VCB, cables and wind turbine step up (WTSU) transformer. A detailed model of VCB that illustrates overvoltages not only on circuit VCB itself but also on the system components, considering all the statistical properties of VCB is outlined. The cable model based on the geometry, insulating material properties and type of connection with the electrical circuit incorporating a propagating wave frequency dependent phase model is presented. Elaboration of a sophisticated black box model using vector fitting algorithm and rational function approximation technique, in broad frequency range (20 Hz to 20 MHz) of WTSU transformer concludes the chapter.

3.1 Modeling of Vacuum Circuit Breaker in PSCAD/EMTDC

VCB is capable of quenching high frequency currents. The current quenching capability in synchronization with dialectic recovery characteristics result in high transient recovery voltage across VCB contacts. This statistical behavior of VCB's conducting arc causes interruption of high frequency current, eventually inducing numerous reignitions. Reignitions, depending on external circuit, may lead to critical overvoltages along the adjoining power system components. An accurate and complete model of a VCB in PSCAD is discussed in [31]. Following four criteria described in [59], should be taken into consideration for VCB model in PSCAD/EMTDC to show the statistical occurrence of reignitions:

- VCB contact opening can start before the natural current zero crossing
- First reignition occurs when high transient recovery voltage exceeds the withstand voltage of the VCB
- The phenomenon of reignition is followed by high frequency currents being superimposed on current zeros
- VCB model should have the ability to interrupt the high frequency current

For analyzing high frequency steep front transients in WTSU Transformer, a detailed high frequency model of VCB is developed in PSCAD/EMTDC. The model is able to simulate following statistical phenomena:

a. Arbitrary nature of arcing time, i.e. the time between arcing phenomena and current zero
b. Effective current interruption at high arcing times
c. Interruption debacles for lower arcing times
d. At high arcing times, no restrikes and reignitions occur
e. At low arcing times, single or multiple restrikes
f. Overvoltages due to current chopping
g. At lower closing times there are no pre-strikes.
h. At high closing times there are single or multiple restrikes
i. High frequency current quenching capability

3.1.1 Explanation of physical phenomena within a VCB

3.1.1.1 Current Chopping

During the opening operation of VCB, an arc is generated across the VCB contacts, as the current is yet to reach a natural zero crossing. At small magnitudes of current, the generated arc is unbalanced and terminates before the current zero crossing. Such event normally occurs at 6A and causes steep front transients depending on electrical system under consideration. This phenomenon is defined as current chopping.

Due to non-deterministic nature of chopping current, earlier researches have defined distinct load current chopping levels for different contact materials [33]. According to [33] mean chopping current I_{ch} is estimated by (3.1) as:

$$I_{ch}=(\omega \times i \times \alpha \times \beta)^{q} \tag{3.1}$$

Where;

$$\omega = 2 \times \pi \times f \text{ Hz} \tag{3.2}$$

$$i = \text{amplitude of power frequency current} \tag{3.3}$$

$$\alpha = 6.2 \times 10^{-16} \text{ sec} \tag{3.4}$$

$$\beta = 14.3 \tag{3.5}$$

$$q=(1-\beta)^{-1} \tag{3.6}$$

3.1.1.2 Cold gap breakdown

During the separation of VCB contacts, the withstand breakdown voltage of the contact gap changes linearly with time. This process takes finite amount of time. An arc is generated across the contact gap of the vacuum, when the transient recovery voltage of the vacuum gap surpasses the threshold voltage of the VCB. The electrical circuit is closed again as the high frequency arc is reignited across the contact gap. Thus cold gap breakdown depends on rate of rise of transient recovery voltage [33].

3.1.1.3 Voltage escalation and re-ignitions

Reignition takes place because voltage breakdown of the circuit VCB initiates a high frequency oscillatory current as the arc conducts. The oscillatory frequency is generated because of stray capacitance and stray inductance of VCB and the external circuit parameters. The high frequency current interrupts the circuit, clamping the load side voltage to a higher value. Now, transient recovery voltage across the VCB rises and goes beyond the withstand capability of the VCB, giving rise to further breakdowns. This phenomenon is called voltage escalation, as every following voltage breakdown will clamp the voltage to a higher voltage level. Voltage escalation is dependent on the natural resonating frequencies and is a function of electrical path created by the external circuit [10].

A temporary breakdown of the buildup voltage across the vacuum gap, taking place during the first quarter cycle is defined as reignition. Reignition generally takes place after the first current interruption. However, a restrike happens after a quarter cycle that takes place due to switching of capacitive circuits [60], [52].

3.1.1.4 Current quenching capability of VCB

High frequency arc generated across the contacts of the VCB has certain inertia of its own. This inertia will succumb the interruption, when the arc goes through high frequency current zero. Therefore, in a precise model of VCB, initial high frequency current zeros are not obstructed and actual arc interruption takes place after these non-interrupted current zeros have passed. The current quenching capability of VCB is a measured from first order derivative of high frequency current flowing through the arc. The arc across the vacuum gap extinguishes after a fixed number of zero current crossings have passed.

3.1.1.5 Pre-strikes

The prestrikes are observed once the vacuum gap of VCB closes from an open position. During the opening operation of a circuit VCB, reignition and restrikes are observed. The high frequency phenomenon is similar for both prestrikes and restrikes. The only difference is that escalations in voltage will not occur in prestrikes as the vacuum gap is shrinking with time [33].

3.1.1.6 Finite arc resistance

The high frequency current flows through the arc right after the cold gap breakdown. However, a reignition voltage is imposed across the gap as this arc has finite resistance. This re-ignition voltage depends on the rate at which the high frequency current rises and the impedance of external circuit [33].

3.1.1.7 Probabilistic attribute of the VCB model

The VCB high frequency phenomenon is highly probabilistic and is derived from experimental values. A sophisticated VCB model should accommodate the statistical nature of arcing time [33].

3.1.1.8 Hot gap breakdown

Hot gap voltage breakdown occurs after the arc across the contacts has extinguished. Surplus charge carriers that endure on the surface of VCB contacts reduce the length of breakdown gap. These surplus charges cause the breakdown of vacuum gap at lower voltage than expected [33].

3.1.2 Dielectric Strength Calculation

While modeling the dielectric strength of VCB, it is important to define voltage withstand capability of galvanic contacts. In the proposed VCB model, cold and hot gap breakdown cumulatively define the voltage withstand capability of VCB. VCB's contact distance derives the gap breakdown characteristic. It is assumed that, the dielectric withstand capability of VCB is linearly dependent on speed of switching operation [61]. Equation (3.7) represents the linear variation of dielectric strength:

$$V_{breakdown} = A \times (t - t_o) + B \tag{3.7}$$

The parameters A and B at different dielectric strengths are listed in Table 3-1 [2].

Table 3-1: The parameters of equation (3.7) at different dielectric strengths

Dielectric Strength	A(V/Sec)	B(V)
High	1.7E7	3.40E3
Medium	1.3E7	0.69E3
Low	0.47E6	0.69E3

Equation (3.7) represents the dielectric strength just after the contacts have separated, where the constant A represents the opening speed. The same representation can be used for both opening and closing the VCB as well as the closing time.

3.1.3 High Frequency Current Quenching Capability

Reignition occurs when the transient recovery voltage of the VCB contacts exceeds the dielectric withstand capability of the VCB. Once reignition happens, high frequency current starts flowing through the arc generated across the VCB contacts. VCB, with its current quenching ability can interrupt this high frequency current. The successful interruption of high frequency current depends on the first order derivative of high frequency current at natural zero crossing. For positive disruption of the arc current, the rate of change of current at current zero should be less than the current quenching capability of VCB [33]. The high frequency current quenching capability of a VCB is represented in equation (3.8). The current quenching capability of the VCB is a function of speed at contact opening.

$$\frac{di}{dt} = C \times (t - t_o) + D \tag{3.8}$$

The term $\frac{di}{dt}$ represents the highest current derivative that the VCB can break at the current zero crossing. The value of $\frac{di}{dt}$ is summarized in Table 3-2.

Table 3-2: The constants C and D at different current quenching capability

Current Quenching Capability	C (A/s^2)	D (A/s)
High	-3.4E11	255E6
Medium	0.32E12	155E6
Low	1E12	190E6

3.1.4 Simulation of restrike phenomena of VCB in a capacitive circuit

This section describes the phenomena of restrike in electrical circuits with capacitive loads. Restrikes pre dominantly happens in capacitive switching circuits. A single-phase test setup is created in PSCAD/EMTDC to simulate the phenomena of restrike. Figure 3.1 shows the test circuit under consideration with a capacitive load.

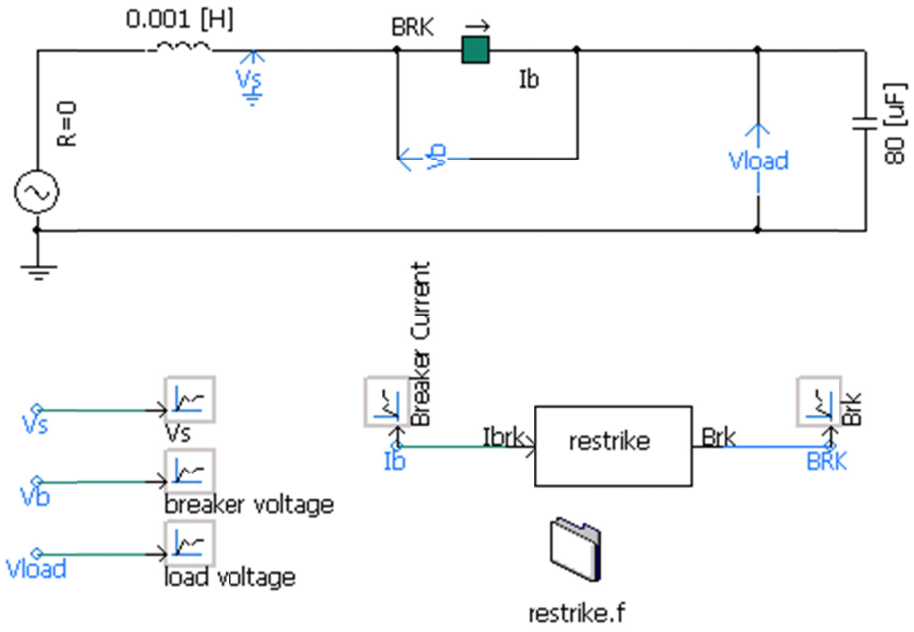

Figure 3.1: Test circuit used to simulate restrike phenomena in PSCAD/EMTDC

The electrical circuit is rated at 20 kV and is used to show the voltage escalations during capacitive current interruption. An external black box model shown in Figure 3.2 that is used to model the re-striking in this capacitive circuit controls a normal VCB model in PSCAD/EMTDC. There are following assumptions during simulating the above-mentioned phenomena:

I. The VCB can interrupt the high frequency current at the first current zero after every restrike.

II. The restrike occurs every half cycle of fundamental frequency. The restrike time is specified by the restrike component (phase angle between phase angle between the current zero and restrike).

Figure 3.3 shows the flowchat that simulates the phenomena of restrike. The program shown in the flowchart supposes that the restrike occurs every half cycle at the instant specified by the T_{strike}. When the VCB is close, there is a phase difference between current and voltage. Restrike instant decides

whether the voltage is suppressed or escalated. For a capacitive current interruption, the worst scenario is restrike at 180 degree after current zero (when T_{strike} = 1/(2*60) = 0.008333s).

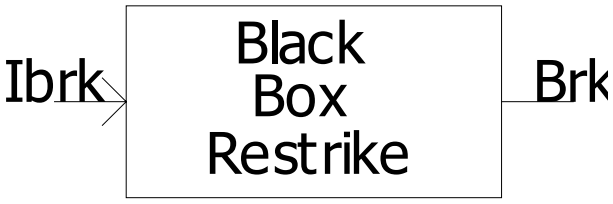

Figure 3.2: Black Box restrike module

Here flag is used to show whether the current is interrupted or not. Brk is the control signal of an ideal VCB. I_{brk} show the VCB current. T_{start} is the time to start the restrike simulation, it should not be confused with the instant of the current zero crossing or restrike. T_{strike} is the interval of the first current zero and the first restrike. Clock is the timer to determine if the restrike should occurs.

In the simulation, the restriking phenomenon starts at 0.05 seconds, and the angle between the current zero and restrike is kept 180 degrees. The following plots are presented to observe the restriking phenomena:

- Current across the VCB
- Voltage of the source
- Voltage of the source
- Voltage across the VCB

As stated earlier the restriking phenomenon starts at 0.05 seconds. The inductance of the source and load capacitance resonates during the period of restrike to create a pre-dominant frequency component, to which restrike occurs. The source inductance (L=0.001 H) and capacitance(C=80uF) produce a resonating frequency (f_1) of 558 Hz.

$$f_1 = \frac{1}{2*\pi*(L*C)} = 558.5 \text{ Hz} \quad (3.9)$$

This component of frequency can be seen as the restriking current in Figure 3.6. Impedance sweep or the frequency scan of the circuit shows that there is a huge peak at 558.5 Hz and this frequency in the current and the voltage during the period of the restrike.

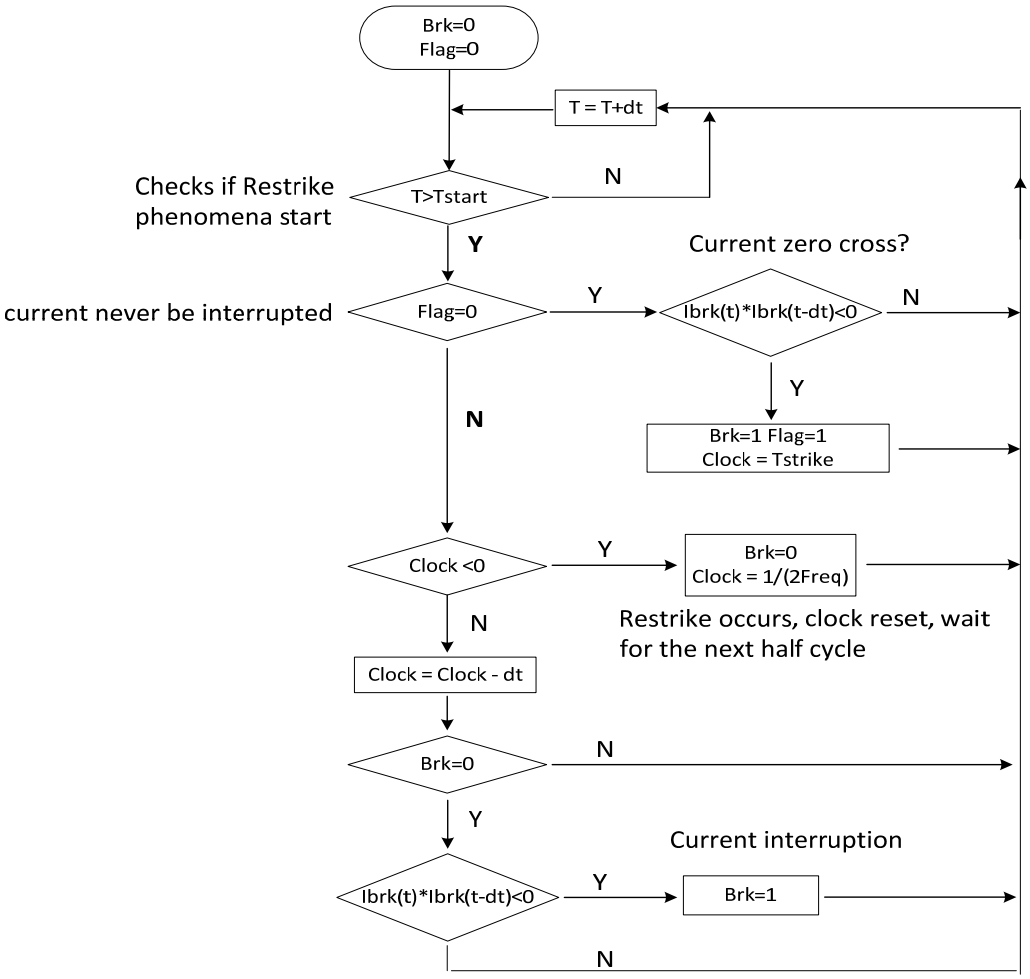

Figure 3.3: Flow chart of restrike phenomenon in PSCAD/EMTDC

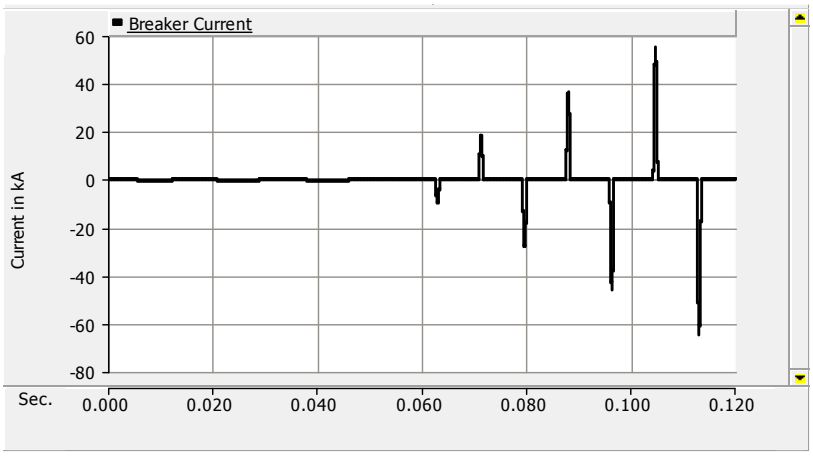

Figure 3.4 Current across the VCB during phenomenon of restrike

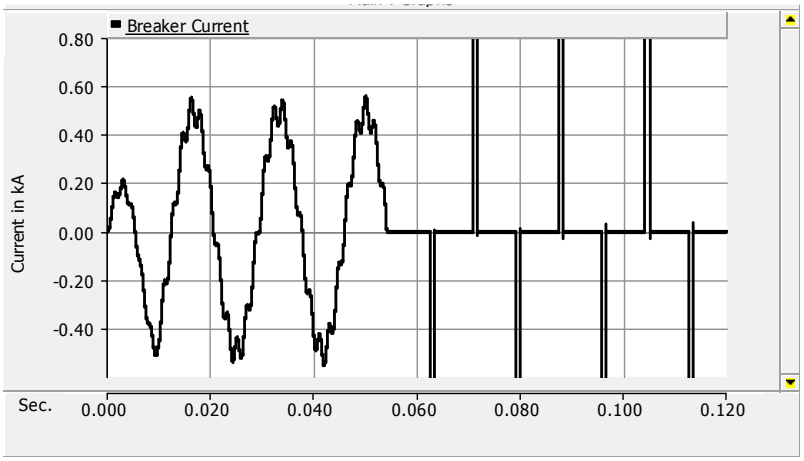

Figure 3.5: Zoomed in view of current across the VCB during phenomenon of restrike

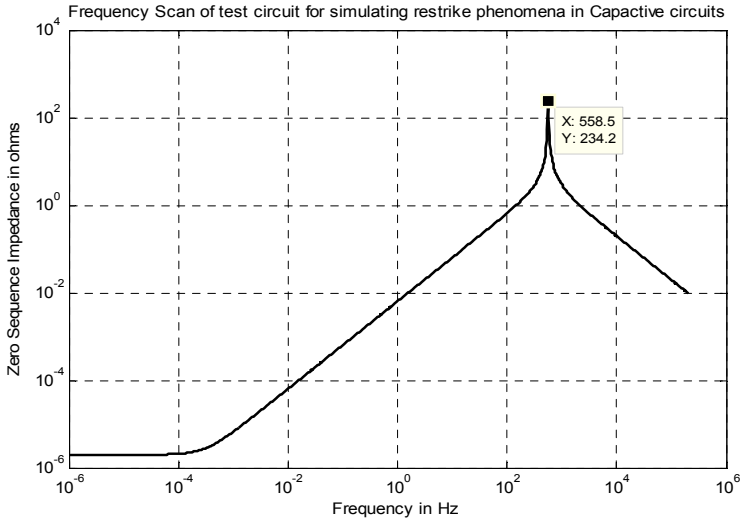

Figure 3.6: Bode plot showing impedance sweep of the test circuit during restrike mode

The load voltage, source voltage and VCB voltage experience similar overvoltages as the VCB current during the period of restrike. Figure 3.7 and 3.8 show the relationship between the load voltage and the source voltage. Source voltage gets clamped with the load voltage during the period of restrike. In a purely capacitive circuit, as the one we have in the test system, if the restrike occurs at 180^0 after current zero, the voltage escalations are 3,5,7,9...times the source voltage after every restrike.

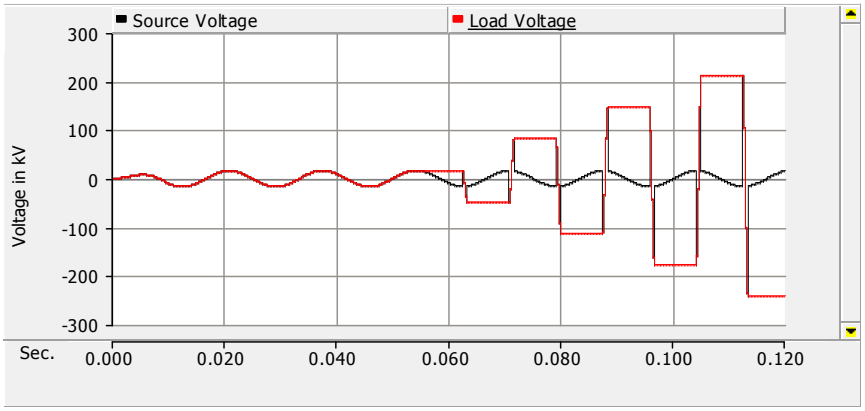

Figure 3.7: Source voltage and load voltage of the test circuit during restrike

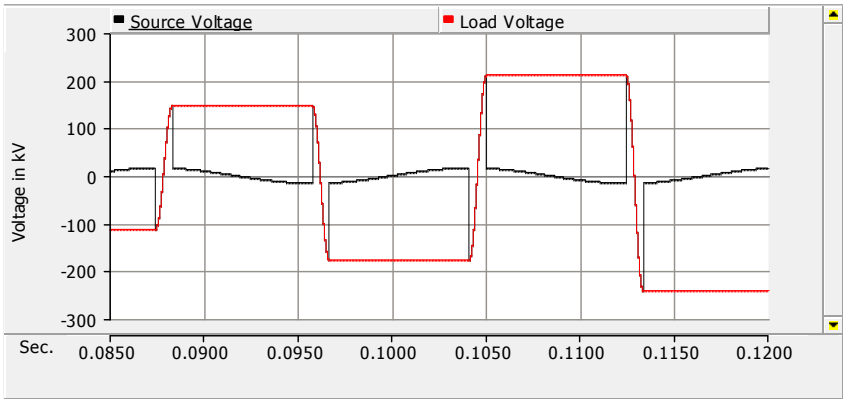

Figure 3.8: Zoomed view of source voltage and load voltage

As explained earlier, the escalating voltages are odd multiples of the nominal rated voltage. The voltage across the VCB is shown in Figure 3.9.

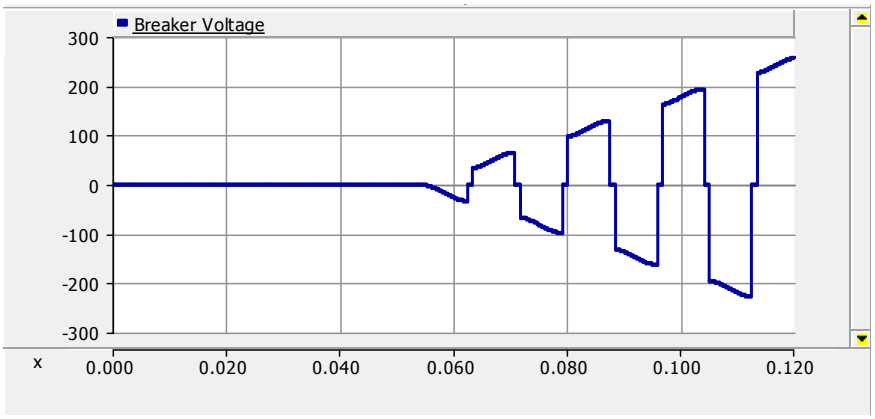

Figure 3.9: Voltage across the VCB

Figure 3.10 shows a comparison of voltages and current across the VCB, source and load during the period of restrike. During restrikes, as can be seen in Figure 3.10 the voltage across the VCB goes zero and the high frequency current flows through the VCB.

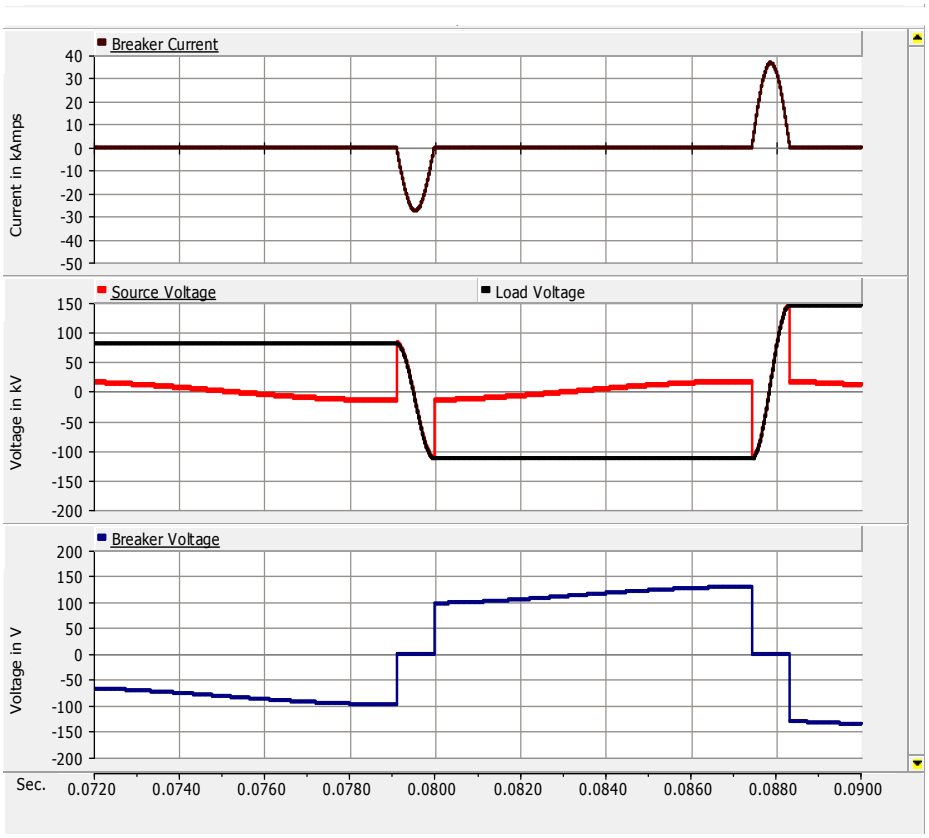

Figure 3.10: Comparison of VCB voltage, load voltage, source voltage and VCB current during restrike period

3.1.5 VCB model in PSCAD/EMTDC

3.1.5.1 Test system for simulating VCB in PSCAD/EMTDC

The test circuit for simulating the statistical and probabilistic model of VCB is shown in Figure 3.11 [62], [33]. This diagram simulates a 3.46 kV single-phase electrical system representing a transformer, which is connected to a VCB through a cable. To keep the test circuit simple the transformer and cable are represented by their equivalent R, L and C network.

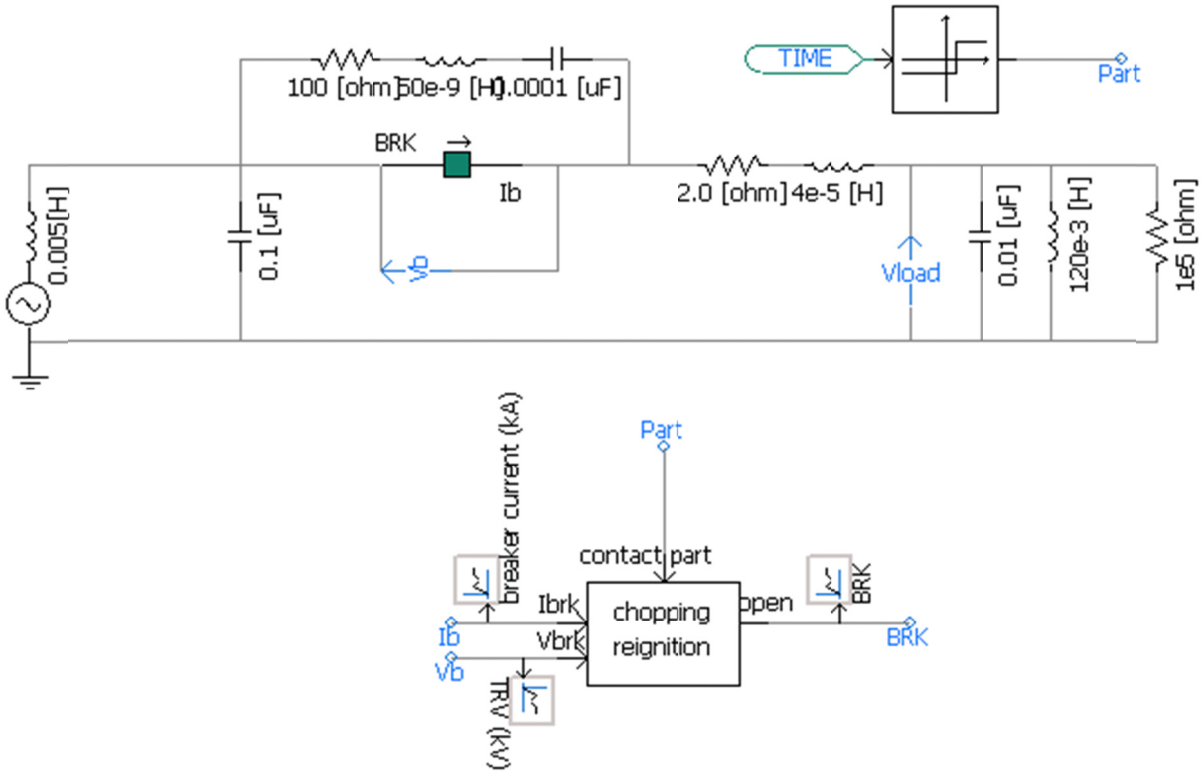

Figure 3.11: Test circuit to demonstrate the black box VCB model in PSCAD/EMTDC

The supply side connected to the vacuum VCB is represented by the L_n and C_n of the busbar and cable connection together. L_n=5mH, C_n=100 nF. R_c=2 ohm and L_c=4e-2 mH are representing the cable connected to the load. C_l=10nF is the cable capacitance and load capacitance added together. R_l=1e5 ohm and L_l=120 mH are representing the load parameters. C_s = 0.0001 µF, L_s = 50 nF and R_s = 100 µ.

It is important to determine the resonating frequencies manually, to match the resonating branches of the test circuit with the frequency sweeps obtained during the VCB operation. The power frequency component of 60 Hz is ignored, as we are concerned with high frequency components occurring during the VCB operation.

The first frequency component is the natural resonating frequency of the load. This component resonates at a frequency of 4.57 kHz. The voltage oscillations observed at this frequency are generated due to exchange of energy between load inductance and load capacitance.

$$f_{load} = \frac{1}{2*\pi*\sqrt{L_l*C_l}} = 4.57 \text{ kHz} \qquad (3.10)$$

Second frequency component is observed during the closing operation of VCB. In this case, the switching operation creates a step change in the voltage oscillations across the load terminals, as prestrikes are observed. The magnitude of the oscillating frequency is dependent on L_k and L_l. As both of these inductances are in parallel and L_l is larger of the two, L_k will govern the equivalent inductance. The capacitance seen by equivalent circuit is C_l, hence the observed resonant frequency is

$$f_l = \frac{1}{2*\pi*\sqrt{L_k*C_l}} = 250 \text{ kHz} \tag{3.11}$$

Once a step change in voltage is applied across the contact gap, a new frequency component arises during the opening operation of VCB. The resonating branch for this frequency component comprises of Ls and Lk in parallel with L_l. L_k dominates equivalent inductance of the circuit. Additionally, the equivalent capacitances comprises of C_s and C_l, which are in parallel with each other. The observed frequency component is at the frequency of f_2.

$$C_{eq} = \frac{C_s*C_l}{C_s+C_l} \tag{3.12}$$

$$f_2 = \frac{1}{2*\pi*\sqrt{L_k*C_{eq}}} = 1.8 \text{ MHz} \tag{3.13}$$

The test circuit anticipates a final resonant frequency of 50 MHz across the VCB contact terminals. This frequency is observed because of series resonance of C_s and L_s. The frequency has been eliminated from the analysis as an acutely feeble time step is required to capture this component. It is observed that the frequency component of 50 MHz damps within 2μs, which is another reason of excluding this frequency component from the analysis.

3.1.5.2 Opening operation of VCB

Under the opening condition of VCB in Figure 3.12, the resonating frequencies appearing in the voltage using impedance sweep are presented.

Since the high frequency current flowing through the arc is of interest, we need to determine the excitation frequency associated with this current. The negative peak as opposed to positive peak is observed around 250 kHz. This confirms the theoretical calculations shown in the previous section. The time step of 0.001 μsec is not feeble enough to capture 50 MHz frequency and is not seen in the frequency scan.

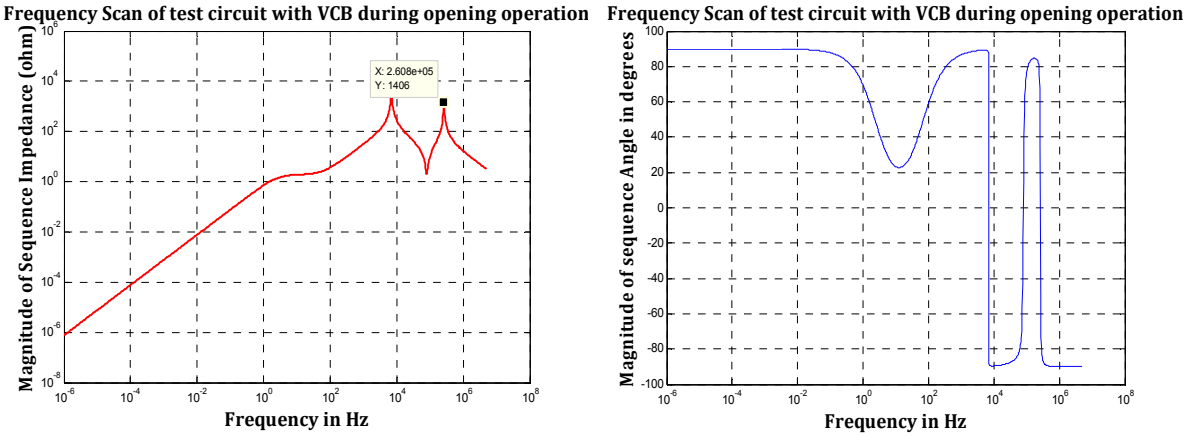

Figure 3.12: Frequency scan of VCB circuit during the opening operation

Figure 3.13 shows the opening operation of the test circuit using VCB. The opening of VCB contacts takes place at 16 ms and four reigntions are observed. The post transient oscillations take about 8ms to die and are observed across the load voltage.

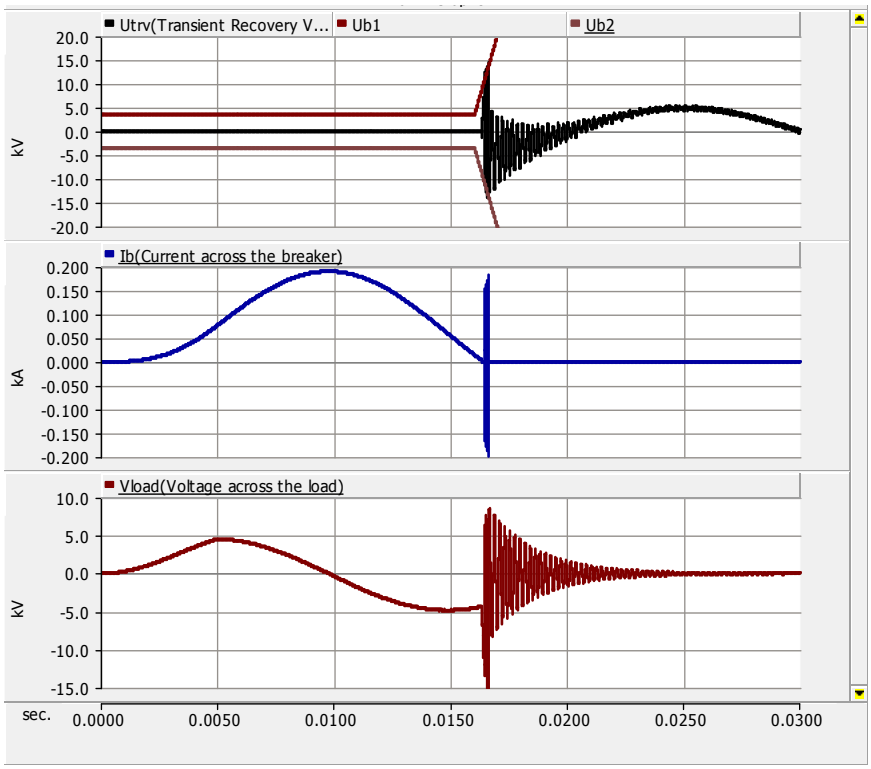

Figure 3.13: Opening operation of the test circuit during at 1.6 ms

The zoomed in view of transient recovery voltage (Utrv), during the opening of VCB contacts shows four reignitions. This phenomenon can be observed in Figure 3.14.

Figure 3.15 shows the VCB current and load voltage for the zoomed in TRV across the VCB. Figure 3.14 depicts the transient recovery voltage across the VCB (Utrv), current of the VCB (Ib), voltage across the load (Vload) and Ub1 and Ub2 show the voltage withstand capability of the VCB, as referred in equation (3.7). The physical opening of the contacts starts at 0.016 seconds. The first criteria needed for multiple reignitions is accounted by the prompt jump observed in the withstand voltage of the VCB. The separation of VCB contacts should start before the natural current zero. This phenomenon is depicted in Figure 3.14 during the initial opening across the VCB contacts.

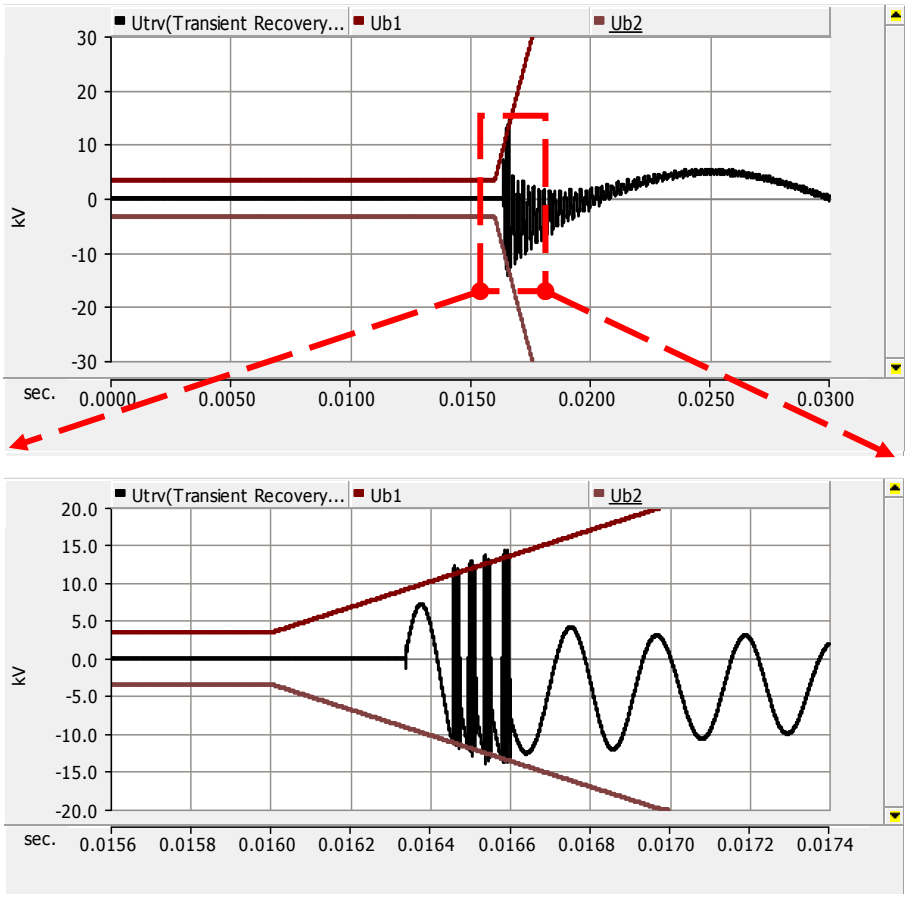

Figure 3.14: Zoomed in view of transient recovery voltage (Utrv)

The frequency components explained in the previous sections are revealed in Figure 3.15. In the switching transient study, the prime motive is to recognize high frequency components, hence a minor time step is chosen. This tiny time step eliminates power frequency component in the observed

waveforms. A time step of 0.01 µsec is required to precisely capture the high frequency components. The model is verified from the results obtained in [62], [33].

Figure 3.17 shows the zoomed view of first reignition in TRV across the VCB as elaborated in Figure 3.16, with corresponding VCB current and voltage across the load terminals. The small transient observed in the beginning of Figure 3.17, is because of the chopping current that takes place at 3 Amps. Figure 3.18 shows the chopping of the current and responsive TRV across the VCB during the current chopping.

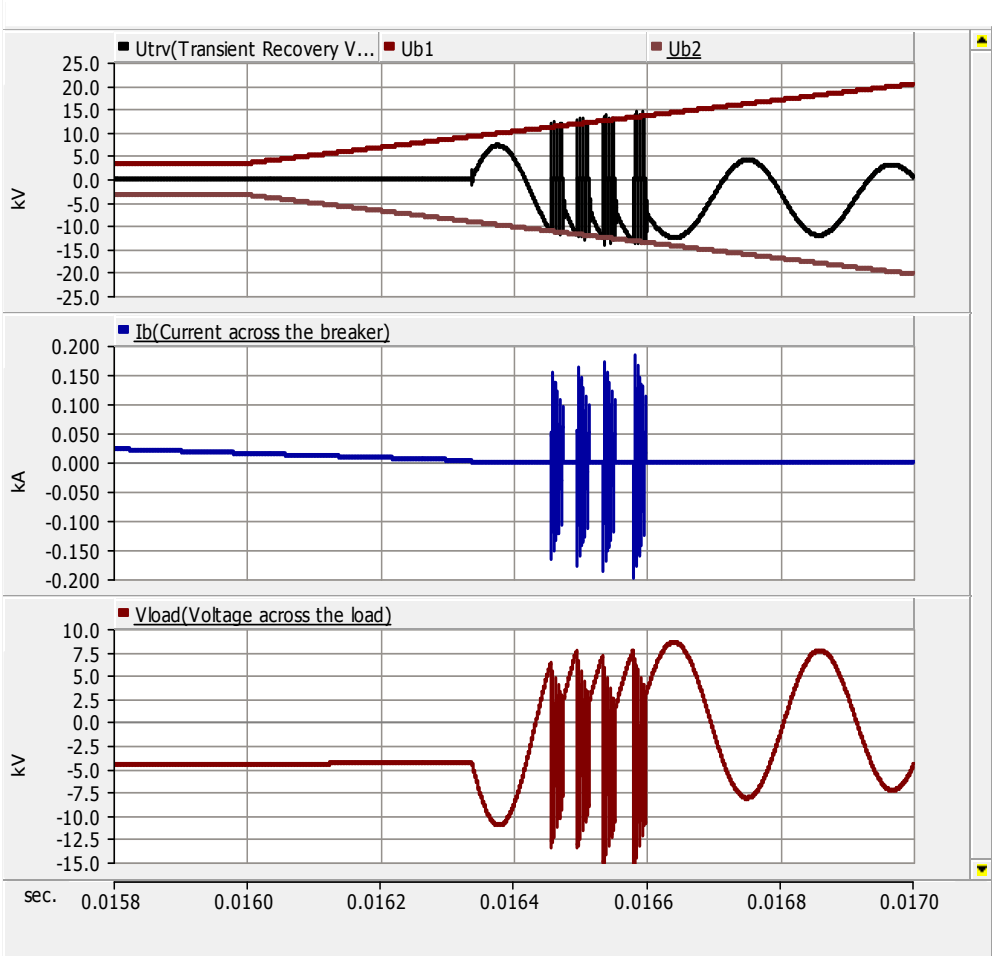

Figure 3.15: Opening operation of VCB at 1.6 ms

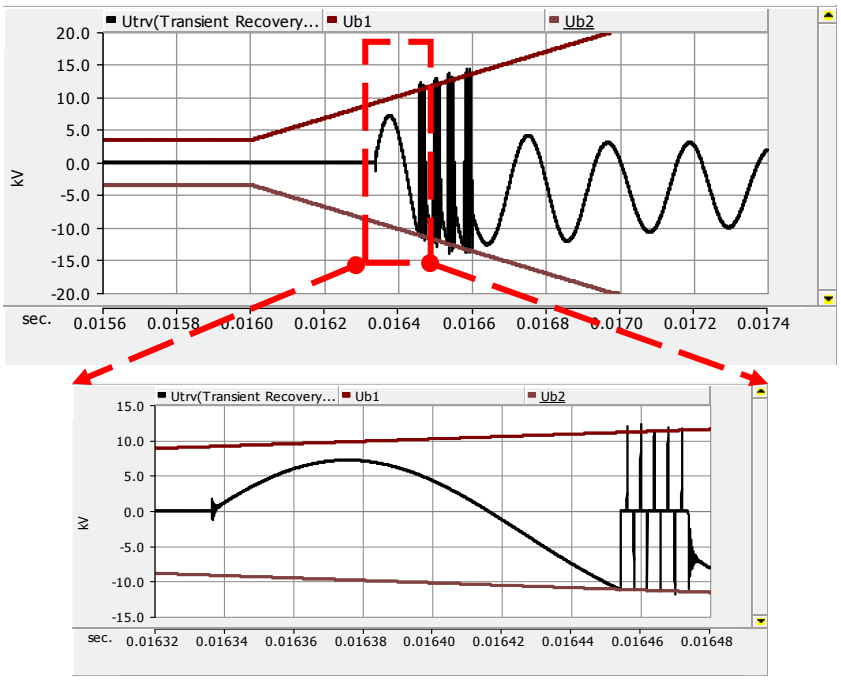

Figure 3.16: Zoomed in view of transient recovery voltage (Utrv)

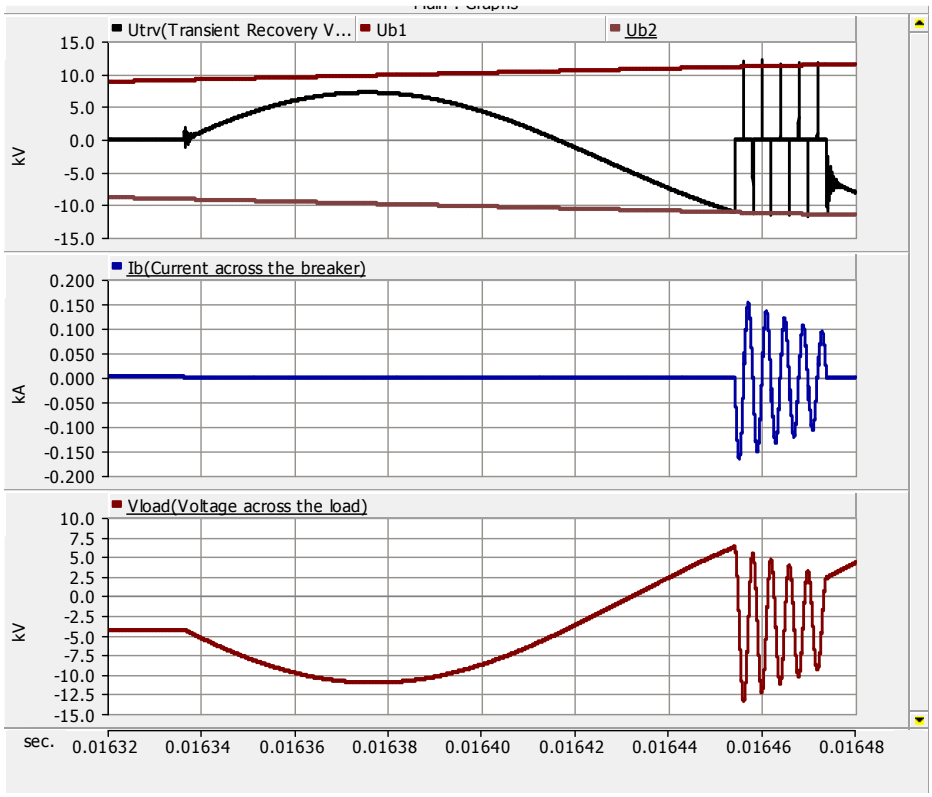

Figure 3.17: Zoomed view of first reignition

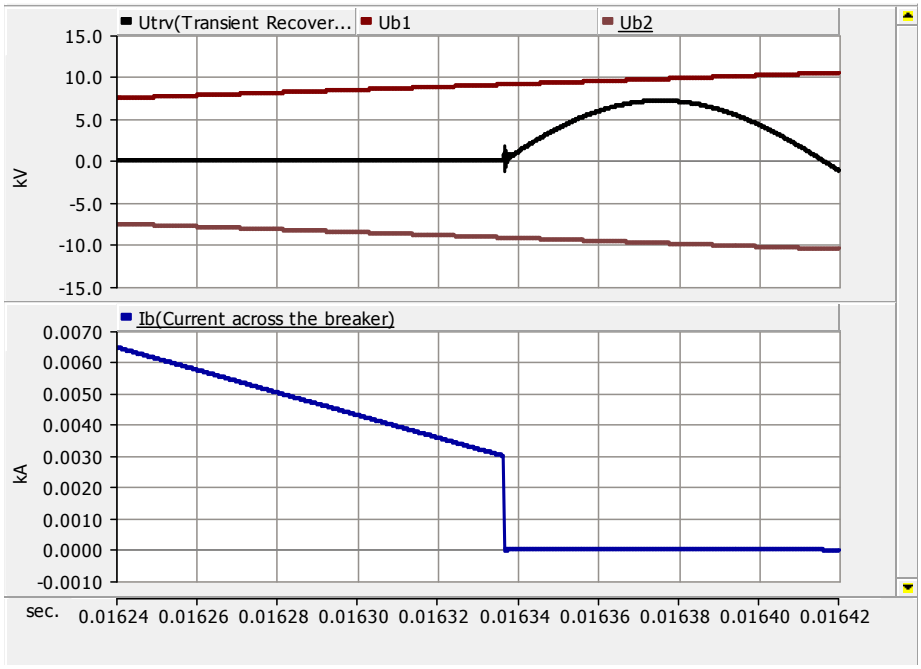

Figure 3.18: Phenomena of current chopping

Diminishing voltage spikes are observed in Figure 3.16 and Figure 3.17 (further zoomed in Figure 3.19). The frequency component that creates these spikes needs further explanation. The arc between the VCB contacts extinguishes when a fixed number of high frequency current zeros have crossed. Once the arc extinguishes, the TRV across the VCB starts to increase. The high frequency component observed at the inception of this phenomenon is 1.8 MHz. As the arc extinguishes the rate of rise of voltage is very high. The high rate of rise of voltage succumbs the 1.8 MHz component, resulting in TRV across the breaker surpassing the withstand voltage of VCB, causing subsequent breakdowns. This phenomenon is observed as narrow spikes in the voltage waveforms.

It is worth observing the phenomena of reignition. As can be seen during the start of the simulation, the voltage across the VCB is compared to the withstand capability of the VCB. As the TRV across the VCB surpasses the withstand capability, the reignition occurs. The transients stop when the TRV across the VCB is less than the voltage withstand capability of the gap, as observed in the first section of Figure 3.21.

Successful high frequency current interruption is observed in Figure 3.21, when the TRV does not exceed dielectric withstand capability of VCB. The time step chosen in this demonstration is different

from previous graphs. The final purpose of VCB is to disrupt the current that is accurately depicted in this waveform.

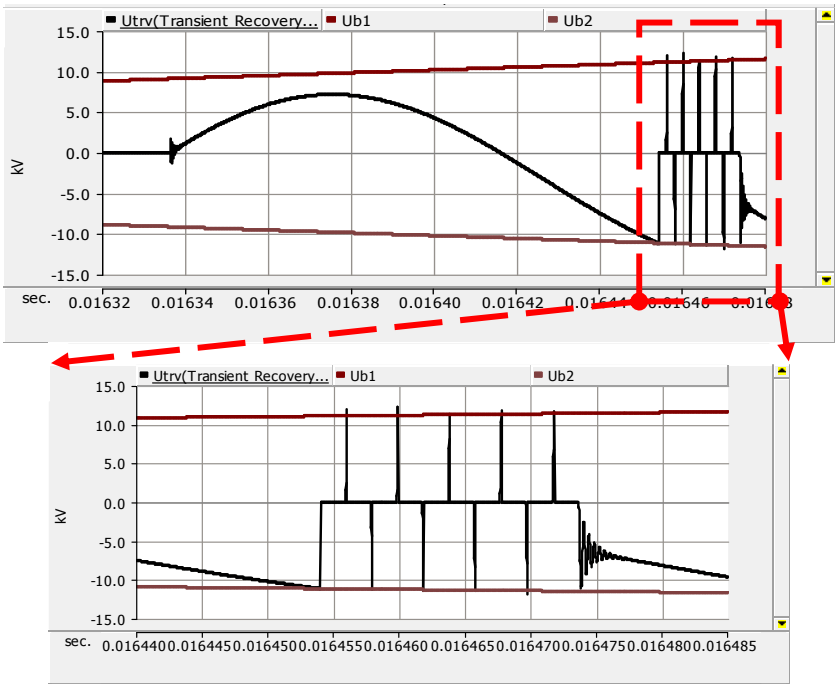

Figure 3.19: Figure depicting 1.8 MHz component

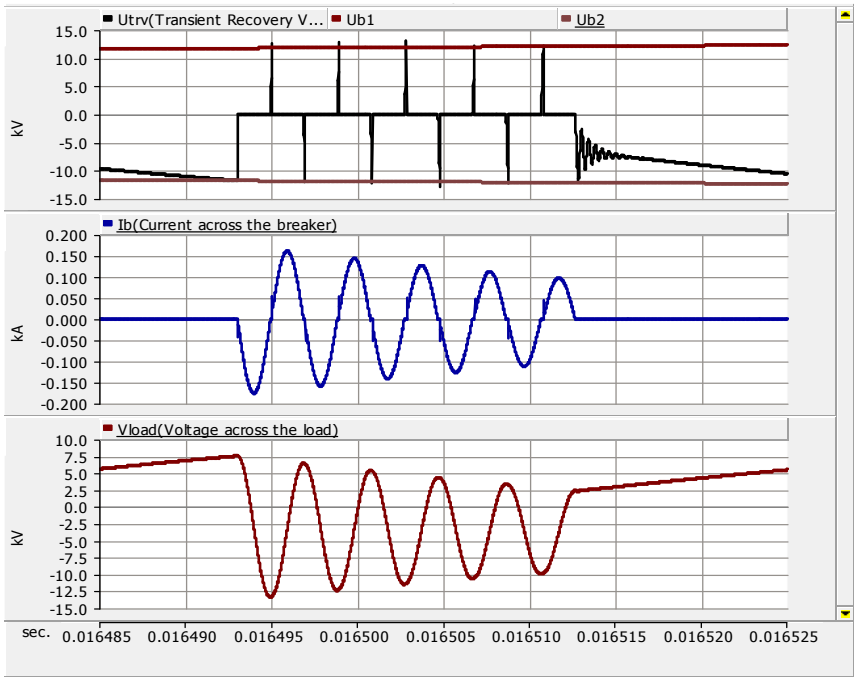

Figure 3.20: Voltage spikes during current chopping

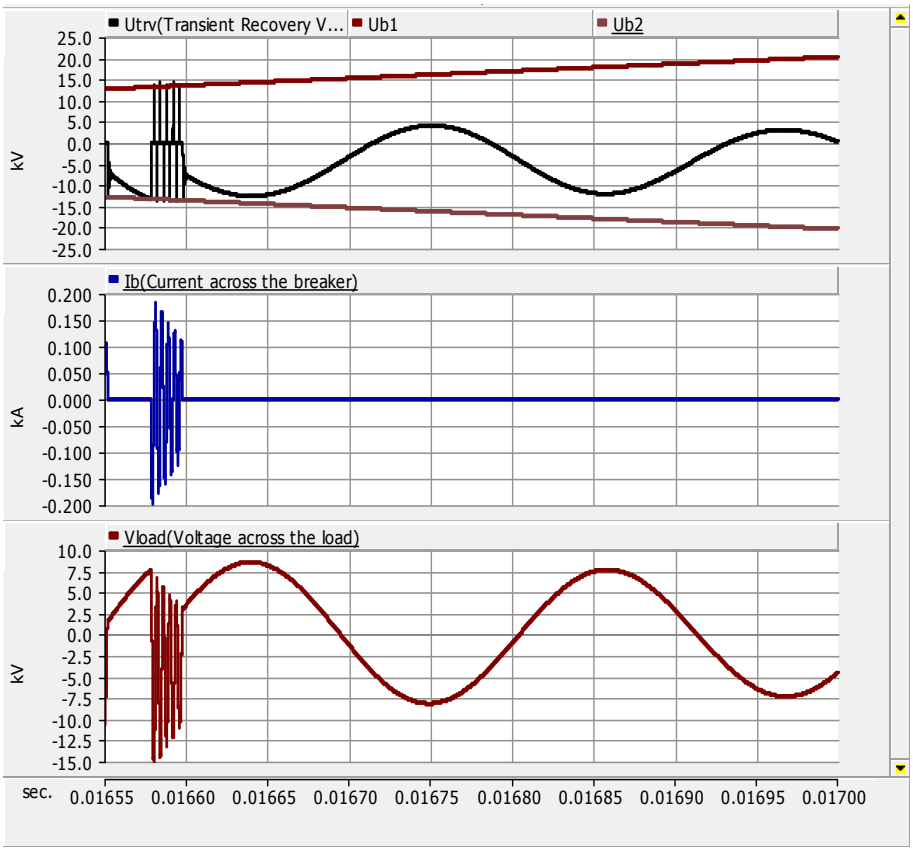

Figure 3.21: Successful Interruption of current

3.1.5.3 Closing operation of VCB

Under the closing condition of VCB in Figure 3.22, the resonating frequencies appearing in the voltage waveform are presented. The frequencies with 886 kHz and 2.6 MHz components are observed.

Previous section is dedicated to the problem of restrikes and depicts the phenomena observed during the opening operation of VCB. During the closing operation of VCB, the problem of prestrikes is observed (Figure 3.23). The amount of prestrikes depends on cold gap withstand voltage of the VCB and the speed with which contacts of VCB close. In a peculiar condition, it is observed that the high frequency arc between the galvanic contacts of VCB conducts the power frequency before contacts are physically closed. This phenomenon is dependent on the rate at which VCB contacts close.

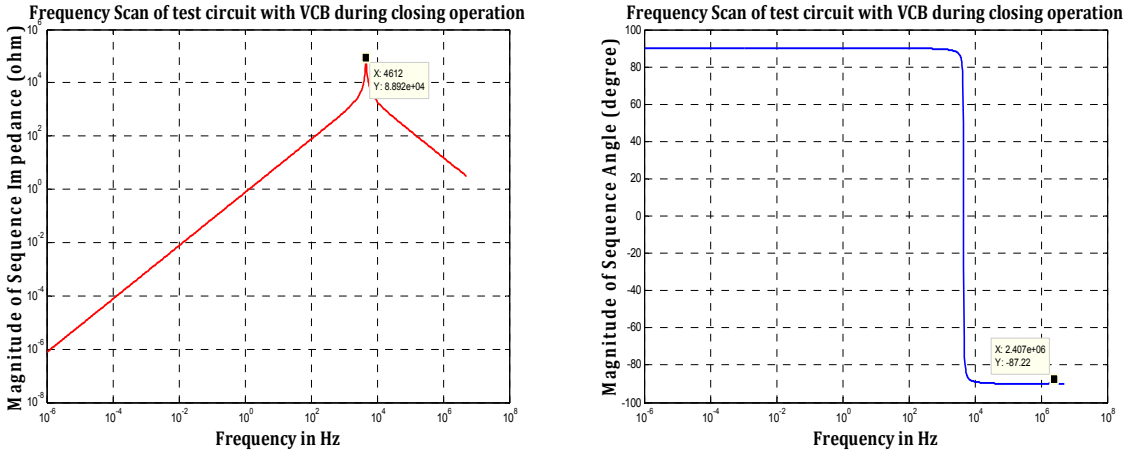

Figure 3.22: Frequency scan of VCB circuit during the closing operation

The phenomenon where current quenching capability of VCB is unable to snap the power frequency current at zero current crossing is referred as an ineffective interruption. It becomes very difficult for VCB to obstruct the current at high frequency, once the arc across the VCB contacts has attained its natural inertia. Due to inability of VCB to interrupt this current no further zero crossings are observed. Under such condition, the external circuit interrupts the arc at natural current zero. This phenomenon is observed in the three-phase system, where three different phases are involved and due to insufficient interruptions, second pole operates before the first pole and successfully succumbs the current. Even though the arc conducts for longer than expected, the high dielectric withstand capability of VCB contacts will result in no further breakdown and the high frequency arc is terminated.

Figure 3.25 shows the effect of pre-strikes. As the VCB contacts are approaching the actual closing state, the voltage between the contacts rises and cross the gradually diminishing dielectric withstands voltage of the gap. An arcing current establishes, as the gap breaks down before the actual closing state is reached. This phenomenon is attributed to hot gap breakdown characteristic of VCB's galvanic contacts. This arcing current results in first pre-strike. Subsequently, the high frequency conducting arc again establishes, depending on external electrical circuit. Second prestrikes are observed once the VCB interrupts the high frequency current at next current zero. As this process repeats numerous prestrike are observed. Resulting multiple prestrikes ensure steep front voltage transients. This phenomenon is observed in Figure 3.27.

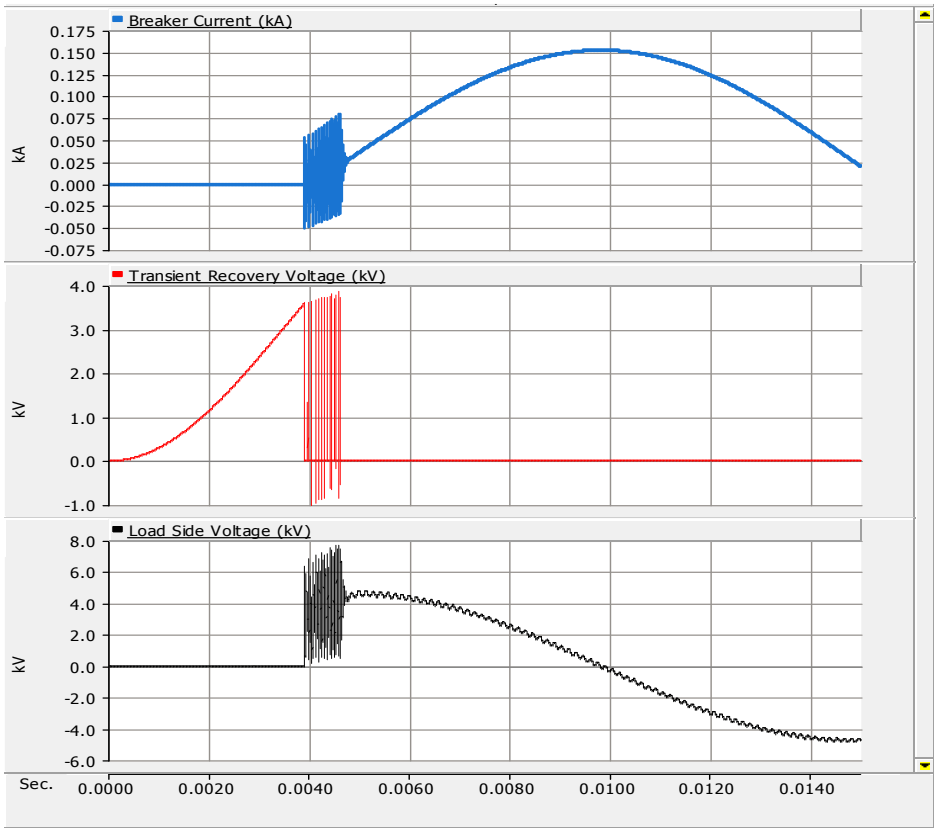

Figure 3.23: Closing operation of VCB at 4.7 ms

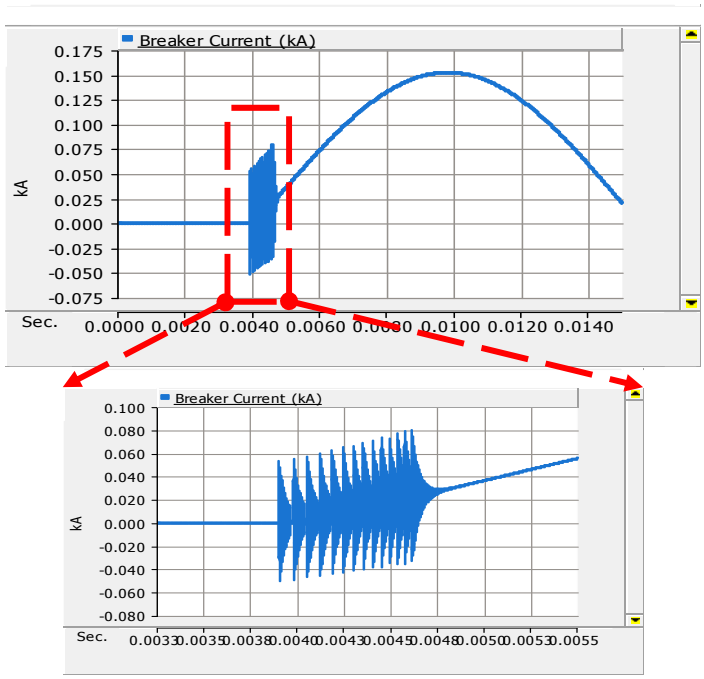

Figure 3.24: Zoomed view of breaker current

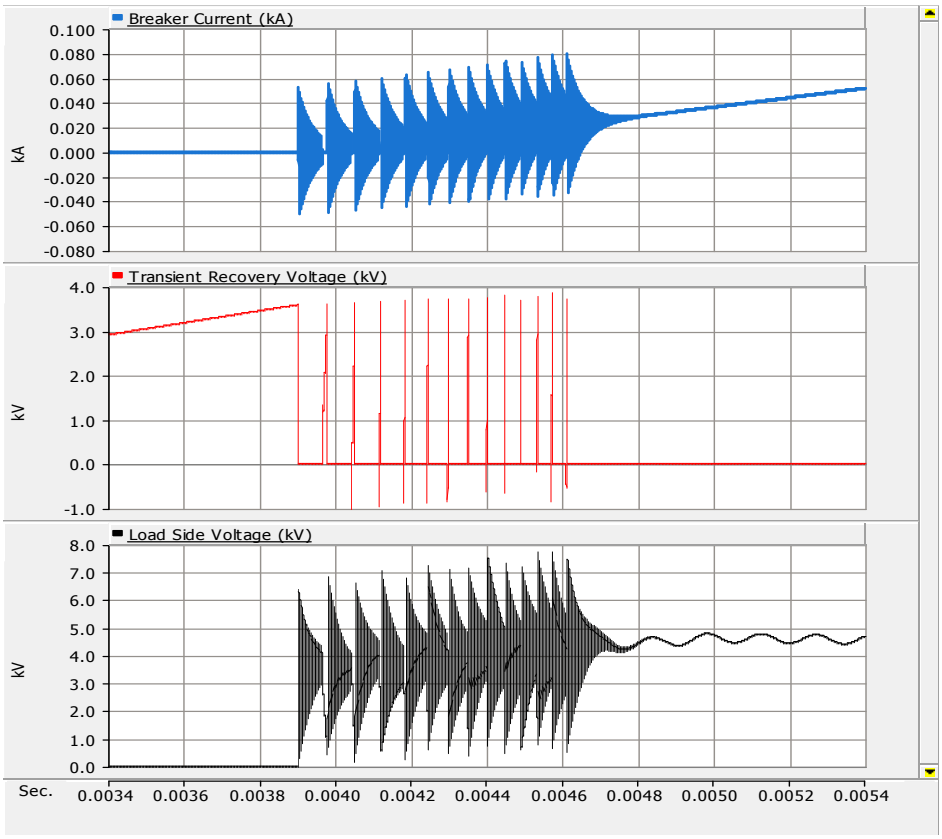

Figure 3.25: Effect of prestrikes during the closing operation of VCB

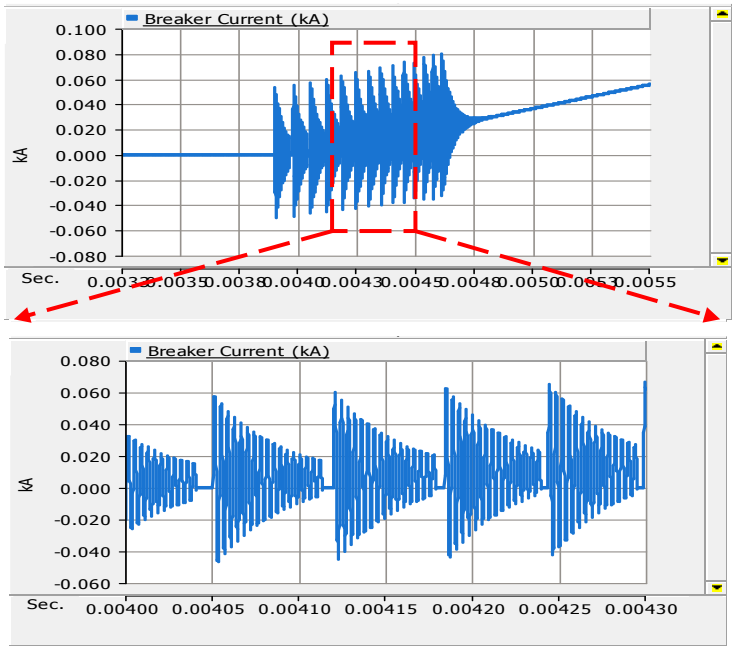

Figure 3.26: Zoomed view of breaker current

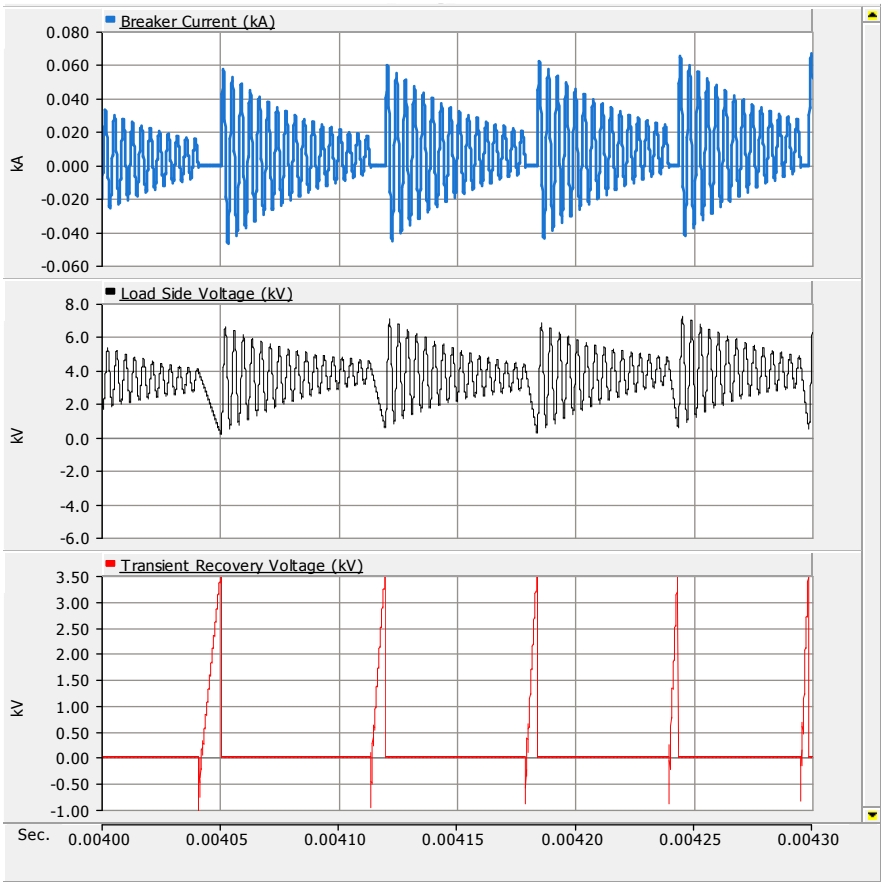

Figure 3.27: Zoomed version of Figure 3.25

3.1.5.4 VCB in a Three Phase System

The VCB used in the test bench is a three phase VCB and the user needs to analyze the effects of choosing distinct operating instant for each phase of three-phase system. Figure 3.28 depicts the electrical circuit chosen to observe the effects of three-phase VCB. The loads and electrical configuration of the three-phase circuit is similar to the single-phase test circuit chosen before.

The test case is opening the VCB at 19 ms. Each phase observe different number of reignitions. A different electrical configuration is observed by each phase of three-phase VCB because of 120^0 phase difference. As the current chopping is different at each phase, the TRV across each one of the phases will be different, creating unique number of restrikes. This phenomenon is observed in Figure 3.29 [33]. This observation corresponds to real case scenario, where each phase shows different number of restrikes or prestrikes because of unique current chopping level and virtual current chopping.

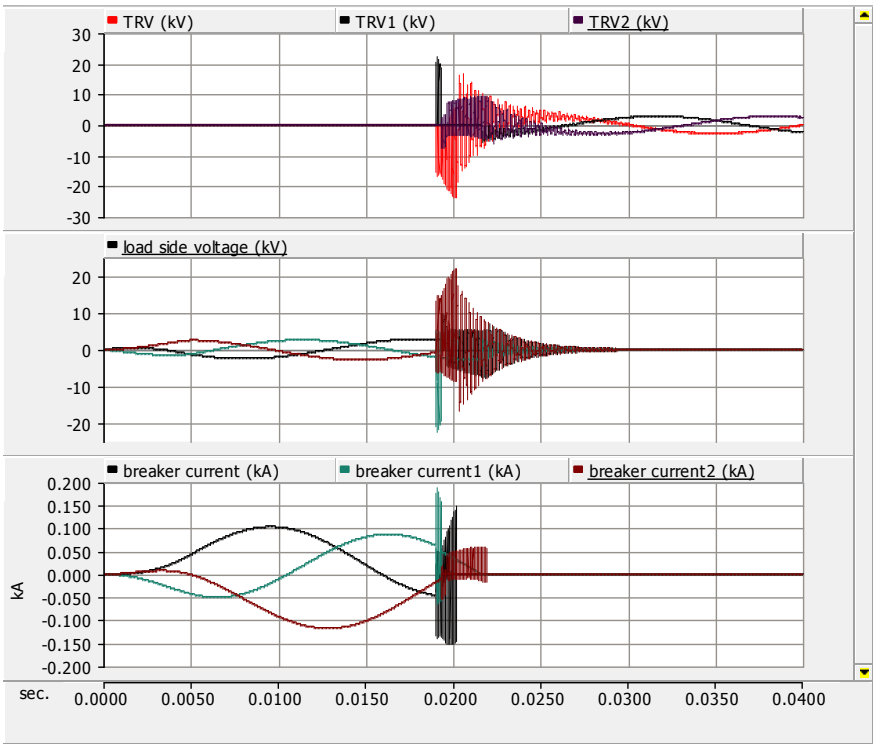

Figure 3.28: Opening of VCB at 19 ms

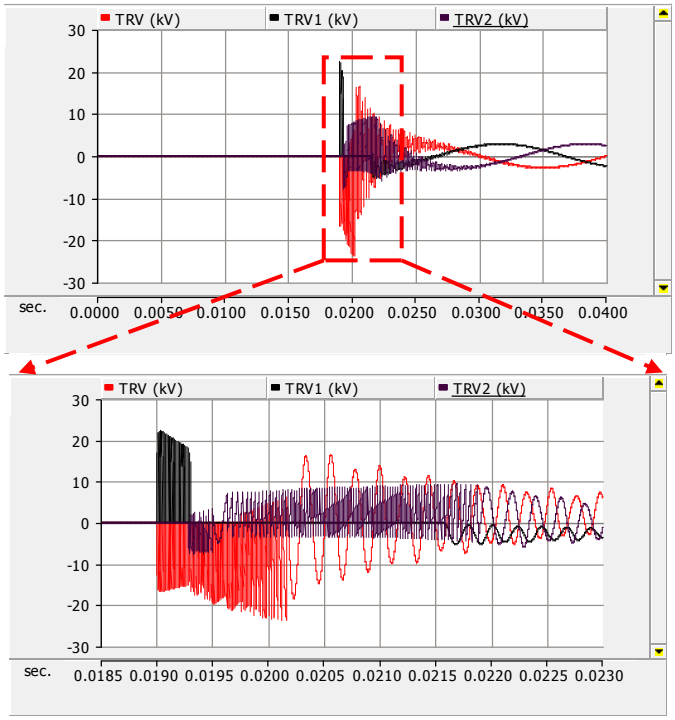

Figure 3.29: Zoomed view of TRV

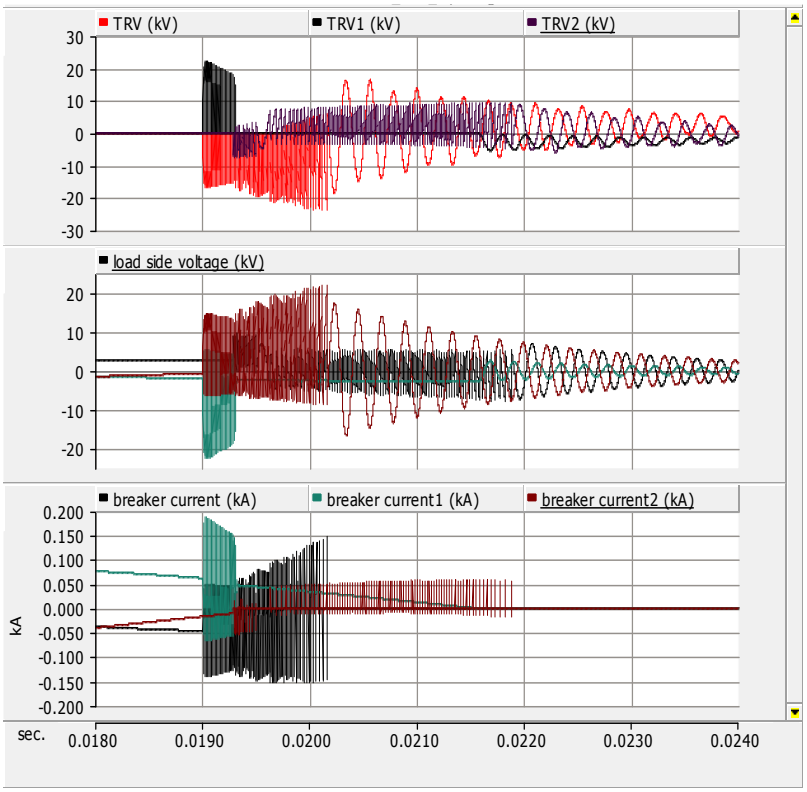

Figure 3.30: Zoomed view of Figure 3.29

3.2 Cable Modeling

This section illustrates high frequency modeling technique of a power cable in PSCAD/EMTDC. Eventual goal of the proposed cable model is to replicate high frequency behavior of the real power cable. The cable model presented here incorporates the high frequency phenomena of skin effect, reflections, electromagnetic transient propagation, speed of propagation etc. The model developed is employed to formulate a novel test bench to investigate VCB initiated high frequency transients in a wind farm.

In steady state power system studies, the power cable is represented as an equivalent RLC electrical network. Nevertheless, for switching transient studies, a frequency dependent model that incorporates the distributed parameters of the cable and is able to replicate high frequency phenomena of reflective transients, should be used.

PSCAD/EMTDC accommodates three alternatives to a power cable model:

- **Bergeron model**

Bergeron is the most basic model of the power cable. Here, cable is modelled as subsequent sections of R, L and C. This model is employed in standard power system studies, to precisely represent electrical response of a cable to an excitation frequency.

- **Frequency dependent mode model**

Mode model employs the constant transformation of internal matrices to represent the high frequency phenomena in a cable. As a major disadvantage, this model fails to replicate the cable behavior during ideal transposition of core conductors.

- **Frequency dependent phase model**

This is the most sophisticated cable model in PSCAD\EMTDC. In this model, dependency of distributed parameters is defined for a particular range of frequency. The rational transformation matrix uses frequency dependence characteristics to replicate phenomena like skin effect, reflections and EM wave propagation. This model is used in switching transient studies.

Series impedance matrix and shunt admittance matrix are the primary parameters of power cables or transmission lines. Equation (3.1) and (3.2) represent impedance and admittance matrices.

$$Z(\omega) = R(w) + j\omega L \tag{3.14}$$

$$Y(\omega) = G(w) + j\omega C \tag{3.15}$$

Where G, R, C, L are shunt conductance, series resistance, shunt capacitance and series inductance respectively. Impedance and admittance are both function of frequency.

In PSCAD/EMTDC, parameters of the cable simulated depend on the geometry and physical attributes of the specific material used in cable. Structural configuration of the proposed cable model is different from the real cable. This model does not account for the semiconductor screen of the actual cable. The cable model asserts that the core of the cable is a consistent conductor in comparison to the core conductor in actual cable, which is made up of different strands.

The cable representation on in PSCAD/EMTDC only requires the geometric parameters for the conductors, sheaths and insulators. PSCAD/EMTDC does not take into account the core stranding, inner and outer semiconductor screens and wire screen.

PSCAD/EMTDC fails to represent following features of the cable:

1) Stranding of core

2) Semiconductor layers

3) Wire screen

The presented sections are used to obtain parameters of cable required by PSCAD/EMTDC and three steps are followed to simulate cable in PSCAD/EMTDC:

1. Calculate the different layers of the cable model in PSCAD/EMTDC.
2. Specify the physical properties of the cable material used.
3. Calculate the per unit length capacitance and inductance of the cable.

3.2.1 Layers of cable model in PSCAD/EMTDC

Figure 3.31 shows the ABB XLPE cable that has been modeled in PSCAD/EMTDC. The single-phase cable has a cross section 95 mm^2 and is designed to operate at a rated voltage of 33.3 kV. As described earlier, core stranding, inner & outer semiconductor screens and wire screens are not present in the model of cable in PSCAD/EMTDC, some layers should be grouped together.

Cross-section of conductor	Diameter of conductor	Insulation thickness	Diameter over insulation	Cross-section of screen	Outer diameter of cable	Cable weight (Al-conductor)	Cable weight (Cu-conductor)	Capacitance	Charging current per phase at 50 Hz	Inductance		Surge impedance
										♣	●●●	
mm²	mm	mm	mm	mm²	mm	kg/m	kg/m	µF/km	A/km	mH/km	mH/km	Ω
240	11.2	5.5	23.8	25	32.0	1.1	1.7	0.22	0.8	0.40	0.68	26.2

Figure 3.31:ABB XLPE cable modelled in PSCAD/EMTDC

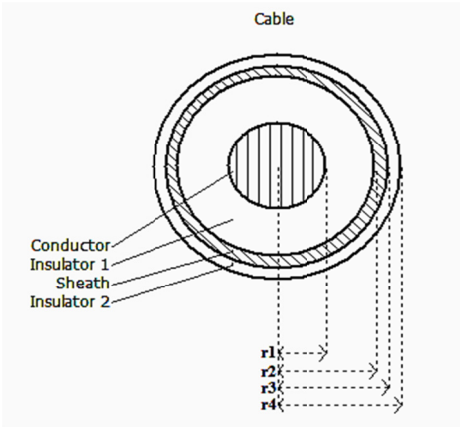

Figure 3.32: Cable specified by PSCAD/EMTDC Frequency dependent phase model

The Figure 3.32 shows four layers of cable that have to be specified while representing cable in PSCAD/EMTDC. Here, r1 represents the radius of the conductor. r2 can be obtained from the sum of

r1, main insulation thickness and outer & inner semiconductor thickness. r3 is obtained from radius r2 and radius of cross section of the screen. The outermost radius of cable is r4. Table 3-3 shows the calculations for the four different layers of cable model in PSCAD/EMTDC.

Table 3-3: Calculation depicting the four different layers of cable model in PSCAD/EMTDC

Radius	Calculation	Value
r1	$\frac{\text{Diameter of the conductor}}{2} = \frac{11.2 \text{ mm}}{2} = 5.6$ mm	5.6 mm
r2	r2 = r1 + main insulation thickness + outer & inner semiconductor screen thickness r2 = 5.6 mm + 5.5 mm + 0.5 mm + 1 mm = 12.6 mm	12. 6 mm
r3	$r3 = \sqrt{(A_s/\pi)^1 + {r_2}^2}$ where A_s is the area of cross section of screen	13.26 mm
r4	$\frac{\text{Outer diameter of the cable}}{2} = \frac{32 \text{ mm}}{2} = 16$ mm	16 mm

3.2.2 Physical properties of the cable materials used

The cable model not only requires the thickness of layers but also the physical properties of the material of the layers. The approximated values used in the cable model in PSCAD/EMTDC are given in the Table 3-4.

Table 3-4: Properties of the cable material

Cable material properties		
Resistivity [Ω.m]	Copper	1.7×10^{-8}
	Aluminum	2.82×10^{-8}
	Lead	1.9×10^{-7}
Relative Permittivity	XLPE	2.3
Permittivity [F\m]	Vacuum	8.854×10^{-12}

3.2.3 Matching the capacitance and inductance of the cable

Calculation of per unit inductance and capacitance of the cable is presented the Table 3-5.

Table 3-5: Matching the inductance and capacitance of the cable

Capacitance	$C_{per\_unit} = \frac{2 \times \pi \times \varepsilon_o \times \varepsilon_r}{\ln\left(\frac{R_{outerinsulation}}{R_{innerinsulation}}\right)} = \frac{2\pi \times 8.854 \times 10^{-12} \times 2.3}{\ln\ (12.6/5.6)} = 217.56$ pF/m	(3.16)
Inductance	$L_{per\_unit} = \frac{1}{2\pi} \times \mu_0 \times \mu_r \times \log_e(R_{outerinsulation}/R_{innerinsulation}) = 160.5$ nH/m	(3.17)
Surge Impedance	$Z_0 = \sqrt{\frac{L}{C}} = 27.14\ \Omega$	(3.18)
Wave travelling speed	$v = \frac{1}{\sqrt{LC}} = 179.3$ m/µsec	(3.19)

The four parameters presented above have been matched to the actual cable. Capacitance, Inductance, surge impedance and wave travelling speed calculated are the within the 10% error range. The expression that describes the inductance in (eq. 3.17) does not take into account the self-inductance of the conductor, as this term is negligible at higher frequencies. This is because the skin effect confines the current to external surface of the conductor. At high frequencies, the inductance has a lower value, which is translated into lower characteristic impedance and a higher speed of propagation.

3.3 Modeling of WTSU Transformer

Several resonance points due to inductive and capacitive effects from the windings, tank and core characterize the high-frequency behavior of transformers. Overvoltage studies like switching transient overvoltage study, resonant and transfer overvoltage study should incorporate the frequency dependent behavior of the transformer. This section of the chapter outlines a procedure for development of a high frequency black box model of an actual transformer, for the suggested overvoltage studies. Specific modeling procedures used to obtain this model are presented in the following sections.

This black box model is valid for a frequency range of 20 Hz to 20 MHz. The proposed model incorporates the experimentally determined frequency dependent admittance matrix. The measured admittance matrix is first approximated by means of rational function approximation and then fitted via a vector fitting algorithm. Vector fitting is used to approximate the rational function of measured admittance matrix, in form of partial fractions [63]. Finally, an experimentally calculated rational function is formulated that is realized into a network of electrical entities (RLC) for time domain simulations. The time domain simulations are carried out in PSCAD/EMTDC.

Specific measurements are carried along the transformer terminals to obtain the frequency dependent admittance matrix. This admittance matrix characterizes low and high frequency behavior of the transformer. The modeling procedure approximates the transformer's time invariant response as a frequency dependent black box. Each block of the admittance matrix is a specific current-voltage ratio. Obtaining all admittance values generates a 6*6 admittance matrix for the three phase transformer. Vectorial curve fitting is then used to approximate the deduced admittance matrix for rational function approximation.

3.3.1 Overview of Modeling Procedure

The three-phase transformer is considered an N-terminal device, as shown in Figure 3.33. The voltage and currents are expressed in equation (3.20). Here Y(s) represents the admittance matrix and I(s) and V(s) represent the current and the voltage vectors, respectively. Expanded vector formulation, voltage and current vectors follow in equation (3.21).

$$I(s) = Y(s) * V(s) \tag{3.20}$$

$$\begin{bmatrix} I_1 \\ I_2 \\ I_3 \\ I_4 \\ I_5 \\ I_6 \end{bmatrix} = \begin{bmatrix} Y_{11} & Y_{12} & Y_{13} & Y_{14} & Y_{15} & Y_{16} \\ Y_{21} & Y_{22} & Y_{23} & Y_{24} & Y_{25} & Y_{26} \\ Y_{31} & Y_{32} & Y_{33} & Y_{34} & Y_{35} & Y_{36} \\ Y_{41} & Y_{42} & Y_{43} & Y_{44} & Y_{45} & Y_{46} \\ Y_{51} & Y_{52} & Y_{53} & Y_{54} & Y_{55} & Y_{56} \\ Y_{61} & Y_{62} & Y_{63} & Y_{64} & Y_{65} & Y_{66} \end{bmatrix} \begin{bmatrix} V_1 \\ V_2 \\ V_3 \\ V_4 \\ V_5 \\ V_6 \end{bmatrix} \tag{3.21}$$

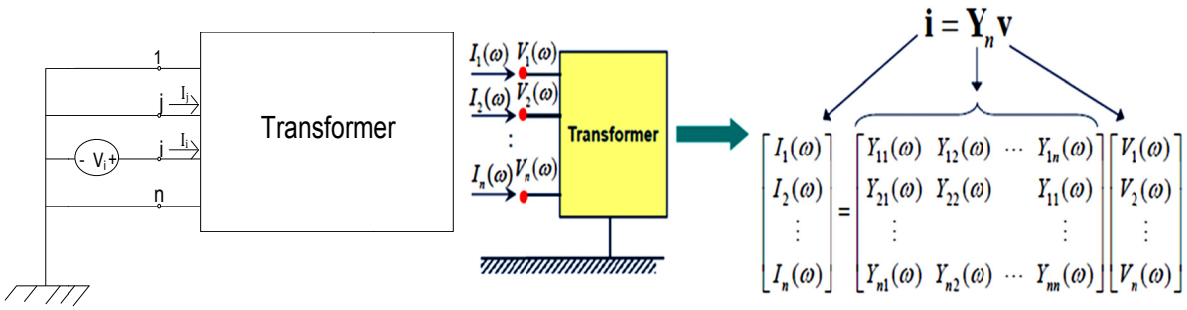

Figure 3.33: N-Terminal transformer model

As can be seen in Figure 3.33, applying a voltage of $V_i$and zero voltage to the remaining terminals produces an i^{th} column of Y(s), where Y_{ji} can be determined by finding the ratio between I_j to V_i. Similarly, the other five columns can be determined for the three-phase wind turbine step-up transformer. Figure 3.34 shows the measurement of admittances on the low and high voltage sides of the WTSU transformer.

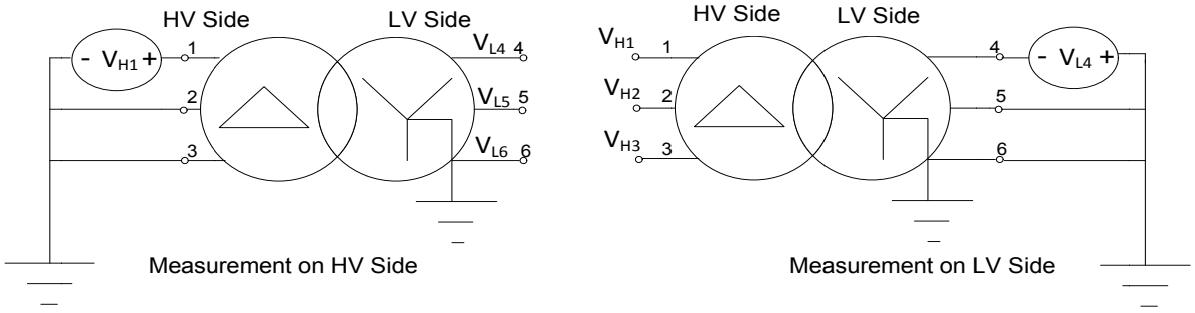

Figure 3.34: Admittance matrix measurements on the HV and LV side of the transformer

As shown in Figure 3.35 the admittance matrix measurements were performed on a WTSU Transformer that is to be commissioned in a wind farm.

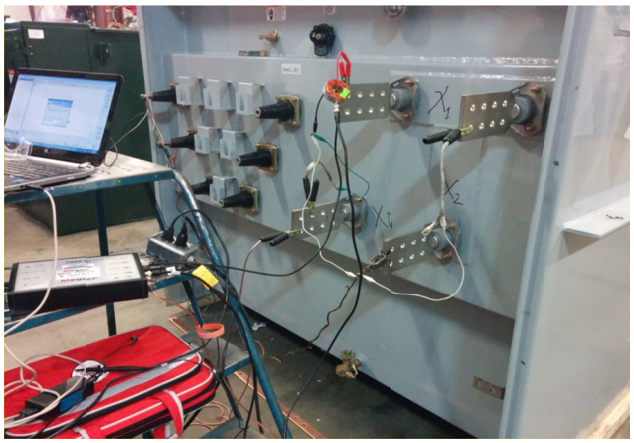

Figure 3.35: Actual WTSU Transformer simulated in PSCAD/EMTDC

Once the admittance matrix is obtained through the measurement and the high frequency black box model of the transformer is realized in PSCAD/EMTDC through vector fitting and rational function approximation, the realized model is validated by comparing the measured and calculated voltage transfer functions. Figure 3.36 shows the complete high frequency black box modeling procedure of WTSU transformer.

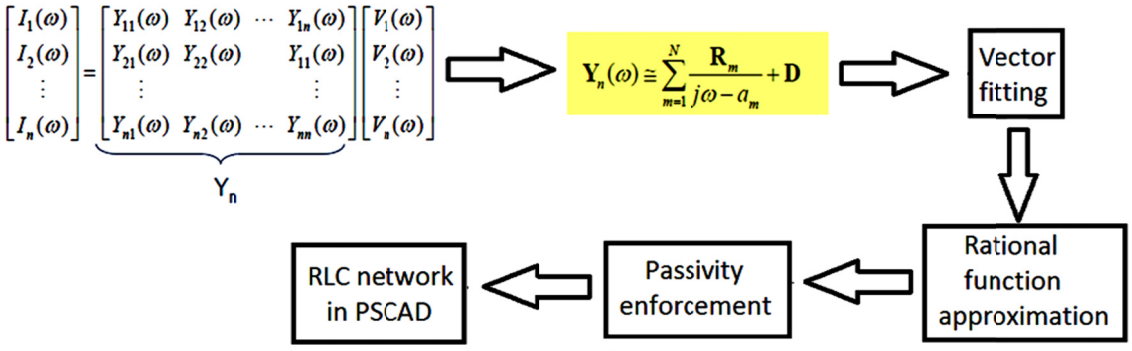

Figure 3.36: Complete high frequency black box modeling technique of the WTSU transformer

The following sections describe each step of WTSU transformer modeling procedure in details.

3.3.2 Rational approximation of frequency response by vector fitting

This section outlines rational function approximation of admittance matrix via vector fitting. The rational function approximation technique used in this method consistently approximates the measured admittance matrix in a broad frequency range. The presented technique is valid for approximation of more than one frequency response. This method is based on Santhana-Koernr iteration. The applicability of this method is highly accepted for realizing transformer's responses.

Equation 3.22 shows the approximation of order N by fitting a given set of frequency dependent data to a ratio of polynomials.

$$f(s) = \frac{a_0 + a_1 s + a_2 s^2 + a_3 s^3 + ----a_N s^N}{b_0 + b_1 s + b_2 s^2 + b_3 s^3 + ----b_N s^N} \quad (3.22)$$

In order to convert a nonlinear equation to a linear one, either side of equation should be multiplied with the denominator. The equation considered here is of type Ax=b and the coefficients are unknown. However, this technique generates an asymmetrically calibrated and non-conditioned mathematical problem, as distinct powers of s are multiplied with columns of A. Therefore, this technique is valid and applicable only for low order approximations. A sturdier linearization technique is desired by rational function approximation algorithm. Prior research studies and fitting

algorithms clearly suggest that vector fitting algorithm is effective for modeling transformer responses. Vector fitting extracts the approximated rational function from the measured raw data in form of additive partial fractions. This is accomplished by compensating initial set of poles with an augmented set of poles, through an iterative pole relocation method. The iterative pole relocation method uses least square approximation algorithm to approximate the higher order responses [64]. The initial poles should be chosen to complement the augmented problem and must be logarithmically distributed over frequency range of interest. As the passive nature is more dominant during higher frequency range, the initial poles should be complex conjugate pairs instead of real quantities.

Equation 3.23 demonstrates rational function approximation that is considered to demonstrate the vector fitting method.

$$f(s) = \sum_{n=1}^{N}\left(\frac{c_n}{s-a_n}\right) + d + s.e \tag{3.23}$$

Here f(s) represents a matrix of numerous responses as frequency dependent transfer function. Residues and poles are represented by c_n and a_n, respectively. Both residues and poles are complex conjugate pairs and their passivity should be kept in check, while approximating the higher order responses. The aim of this section, is to represent the function f(s) in terms of the variables on the right hand side. For this purpose, the unknowns of f(s) should be calculated. Once the unknowns are computed, f(s) can be easily approximated in the frequency range of interest. Hence, the problem should be linearized as one of the unknowns a_n, is in the denominator. Vector fitting algorithm linearizes the problem of higher order rational functions by identifying the poles and residues separately.

A close observation of equation (3.29) shows that zeros of $\sigma_{fitted}(s)$ are similar to the poles of f(s). Hence, the problem of realizing poles of fitted f(s) can be tackled by obtaining zeroes of linear equation (3.24).

$$\sigma(s) = \sum_{n=1}^{N}\left(\frac{\check{c}_n}{s-\bar{a}_n}\right) + d + s.e \tag{3.24}$$

The augmented problem thus produced can be rewritten as follows:

$$\begin{bmatrix} f(s)\sigma(s) \\ \sigma(s) \end{bmatrix} = \begin{bmatrix} \sum_{n=1}^{N}\left(\frac{c_n}{s-\bar{a}_n}\right) + d + s.e \\ \sum_{n=1}^{N}\left(\frac{\check{c}_n}{s-\bar{a}_n}\right) + 1 \end{bmatrix} \tag{3.25}$$

To linearize the rational function obtained in equation 3.25, the second row of equation 3.25 is multiplied by f(s) giving equation 3.26.

$$\sum_{n=1}^{N}\left(\frac{c_n}{s-\bar{a}_n}\right) + d + s.e = \left[\sum_{n=1}^{N}\left(\frac{\check{c}_n}{s-\bar{a}_n}\right) + 1\right] f(s) \tag{3.26}$$

$$(\sigma f)_{fitted}(s) = \sigma_{fitted}(s) \times f(s) \tag{3.27}$$

Equation 3.27 is a linear problem of the type Ax=b in the frequency range of interest with certain unknowns in the solution vector x.

From equation 3.27, we have

$$f(s) = \frac{(\sigma f)_{fitted}(s)}{\sigma_{fitted}(s)} \tag{3.28}$$

Both numerator and denominator of equation (3.28) have the same poles. The ratio in equation (3.28) can be rewritten as single fraction instead of sum of partial fractions, as shown in equation 3.29.

$$f(s) = e\,\frac{\prod_{n=1}^{N+1}(s-z_n)}{\prod_{n=1}^{N}(s-\check{z}_n)} \tag{3.29}$$

A close observation of equation (3.29) shows that zeros of $\sigma_{fitted}(s)$ are similar to the poles of f(s). Hence, the problem of realizing poles of fitted f(s) can be tackled by obtaining zeroes of linear equation (3.24).

Now, to precisely fit the approximated rational function, residues of the function f(s) should be recognized. In order to linearize this problem and solve the residues by substituting the unknowns c_n, d and e, the zeroes of $\sigma_{fitted}(s)$ presented above are used in the original problem (3.24) as new poles. Approximation of rational function is completed by recognizing residues and poles of function f(s). The next step is fitting the approximated rational function via vector fitting algorithm. To understand the vector fitting algorithm and its formulation, the reader is referred to [64].

3.3.3 Passivity enforcement on the fitted admittance matrix

The intention of the previous section is to obtain a rational function approximation of frequency dependent admittance matrix via vector fitting algorithm. Once an approximated rational function of admittance matrix is obtained, an equivalent RLC network of transformer is realized in PSCAD/EMTDC. The time domain RLC network thus obtained is passively linear time invariant.

During the transient simulations this model should behave passively in nature. Furthermore, for a particular input voltage, the developed model should only absorb real power.

Due to the non-passive nature, transient simulations incorporating user defined modules obtained via rational function approximation may result in instability. It has been observed that a user defined model that is already tested and verified for stability and passivity, can still exhibit non passivity once the model interacts with adjacent power system components during time domain simulations. Hence, the equivalent RLC network of transformer should be checked for passivity compliance within the frequency range of interest. Once the non-passive nature is identified, it should be removed. The method of extracting the non-passive behavior is defined as passivity enforcement.

Passivity across the rationally fitted admittance matrix is checked by analyzing the real part of admittance. For the admittance to be passive, the real part and corresponding Eigen values should be positive definite. If found non passive, the network is enforced to a correction so that a positive definite network can be realized. To minimize the fitting error caused due to variation of actual data, a lower order correction is chosen. It is observed that non passivity can be kept in check by getting an accurate measurement of admittance matrix. The passivity criterion using positive definite determination is elaborated below [65].

The equation (3.30) defined an admittance matrix in the frequency range of interest

$$I=Y\ v \tag{3.30}$$

Here I and v represent currents and voltages. The real power observed by the system is

$$P=\mathrm{Re}\ \{v^{*}Y\ v\} =\mathrm{Re}\ \{v^{*}(G+jB)v\}= \mathrm{Re}\ \{v^{*}Gv\} \tag{3.31}$$

A close observation of (3.31) shows that; if the eigen values of G are kept positive definite then the real power will always remain positive. Here '*' refers to transpose and should not be confused with multiplication. For detailed understanding of passivity enforcement, the reader is referred to [30].

3.3.4 Time domain implementation after passivity enforcement

The elementary concept to create a high frequency transformer model, is to obtain an equivalent RLC network of transformer terminal response in form of admittance matrix within a particular frequency range. The final step of complete transformer modeling is predicting the equivalent RLC network. The equivalent electrical network is generated from the rational approximation of fitted admittance matrix.

The expression Y shown in equation 3.32 is approximated rational function of the measured admittance matrix on transformer terminals using vector fitting algorithm. The fitted admittance matrix in form of a rational function is given in equation 3.32.

$$Y_{fitted}(s)_{ij} = \sum_{m=1}^{N} \frac{r_{mij}}{s - a_m} + d_{ij} + s.e_{ij} \quad (3.32)$$

Equation 3.33 depicts the branches from nodes of realized electrical network to the ground:

$$y_{ii} = \sum_{j=1}^{n} Y_{fitting}(s)_{ij} \quad (3.33)$$

Electrical branches between different nodes are given by:

$$y_{jj} = -Y_{fitting}(s)_{ij} \quad (3.34)$$

Here n depicts the size of the matrix. As it is a three phase transformer the value of n is 6. For the purpose of illustrating the time domain implementation, consider a single branch of the RLC network derived from complex and real poles:

$$y(s) = \frac{r_1}{s - a_1} + \frac{r_2}{s - a_2} + \text{---} + \frac{\dot{r}_1 - j\bar{r}_1}{s - (\hat{a}_1 - j\grave{a}_1)} + \frac{\dot{r}_1 - j\bar{r}_1}{s - (\hat{a}_1 + j\grave{a}_1)} + \frac{\dot{r}_2 - j\bar{r}_2}{s - (\hat{a}_2 - j\grave{a}_2)} + \frac{\dot{r}_2 - j\bar{r}_2}{s - (\hat{a}_2 + j\grave{a}_2)} + \text{---} + d + s.e \quad (3.35)$$

Figure 3.37 shows an electrical network of parallel branches derived from evaluation of equation 3.35.

where,

$$R_o = \frac{1}{a}\ ;\ C_o = e\ ; \quad (3.36)$$

RL circuit represents the real pole as;

$$L_r = \frac{1}{r}\ ;\ R_r = -\left(\frac{a}{r}\right) \quad (3.37)$$

The complex conjugate pair is given by RLCG network:

$$L_c = \frac{1}{2r}\ ;\ R_c = 2L_c\,(L_c(\dot{r}_1\hat{a}_1 + \bar{r}_2\grave{a}_2) - \hat{a}_1) \quad (3.38)$$

$$C_c = \frac{1}{L_c(\hat{a}_1 + \grave{a}_1 + 2R_c(\dot{r}\grave{a} + \bar{r}\hat{a}))}\ ;\ G_c = -2L_cG_c(\bar{r}\hat{a} + \dot{r}\grave{a}) \quad (3.39)$$

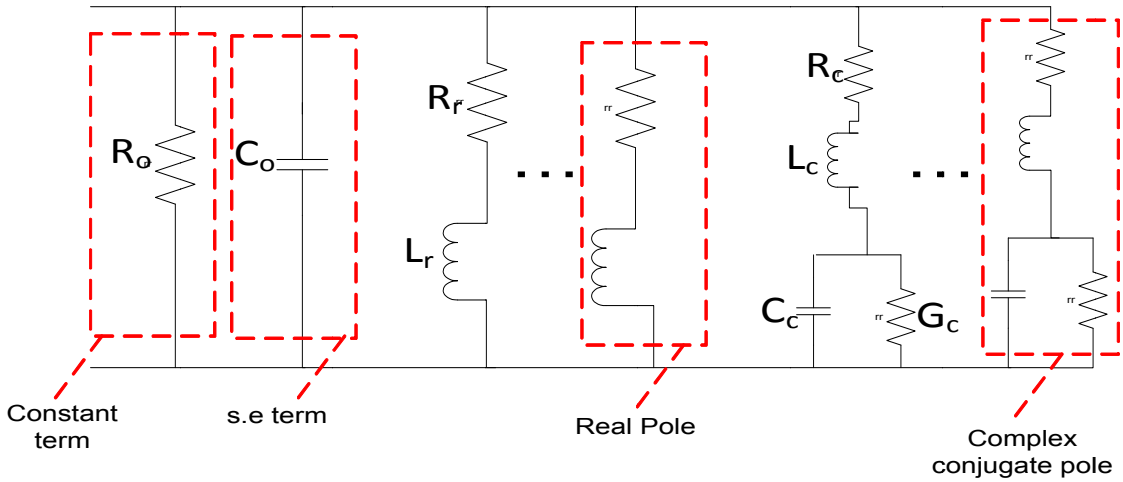

Figure 3.37: Network realization of admittance matrix in PSCAD/EMTDC

3.3.5 Final WTSU Transformer model in PSCAD/EMTDC

The measurement of admittance matrix for WTSU transformer is done by using a network analyzer with in a frequency range of 20 Hz to 20 MHz. Figure 3.38 shows the measurement setup configured to measure Y_{31} of the admittance matrix.

The experimental setup configured, uses the network analyzer, current probe, cables and WTSU transformer to measure 36 admittance blocks and 9 voltage transfer functions. Measurement of current is done with a sensitive current probe. The transformer terminals are excited by connecting the cables from the output terminal of network analyzer to the transformer terminals. The transformer terminals are connected to the input port of the network analyzer to measure current and voltage, subsequently, generating corresponding admittance values.

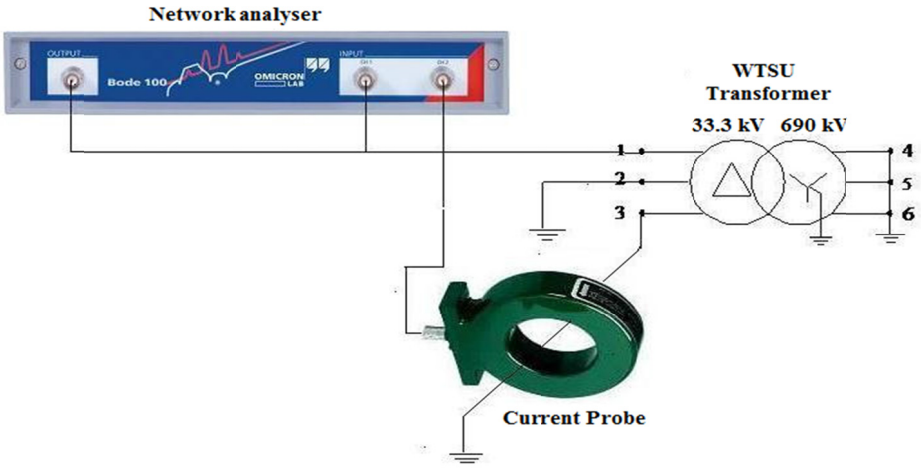

Figure 3.38: Experimental setup to measure Y31 of the admittance matrix

Figure 3.39 depicts the high frequency response of transformer terminals in form of admittance matrix. These characteristics are obtained via direct frequency sweep measurements with sampling window of 1201 points. Passivity enforcement over the raw data accounts for the inaccuracies due to noise and other factors. The authenticity of measured admittance matrix is validated by 6 set of identical measurements.

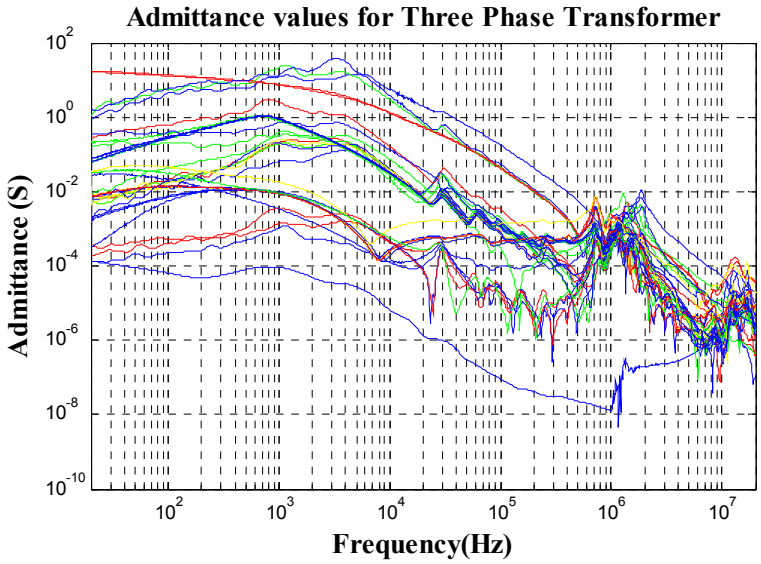

Figure 3.39: Terminal response of transformer in the form of an admittance matrix

Frequency dependent network equivalent (FDNE) model is used to simulate WTSU Transformer in PSCAD/EMTDC. FDNE creates a multi-port, frequency-dependent network equivalent from given characteristics, such as impedance or admittance values in a wide frequency range. The admittance data given as a function of frequency is approximated using rational functions and vector fitting technique. Once the parameters are expressed as rational functions, an electromagnetic transient-type, frequency-dependent network equivalent is constructed, consisting of admittances and current sources. Following parameters are to be chosen to simulate the frequency dependent equivalent model of WTSU Transformer:

- Maximum fitting error
- Maximum order of fitting
- Steady state frequency
- Weighting factor from minimum to steady state frequency
- Weighting factor of steady state frequency

- Weighting factor of steady state frequency to maximum frequency

Figure 3.40 and Figure 3.41 show the magnitude and phase of each admittance block in the admittance matrix. An order of 23 is chosen for approximation of the rational function. The iterative loop runs 6 times and passivity enforcement over 1201 points generate an equivalent RLC time domain network. The frequency range of interest is 20 Hz to 20 MHz. The low frequency segment around 600 kHz exhibit a near perfect fit, however, a very high resolution approximation is not observed at high frequencies.

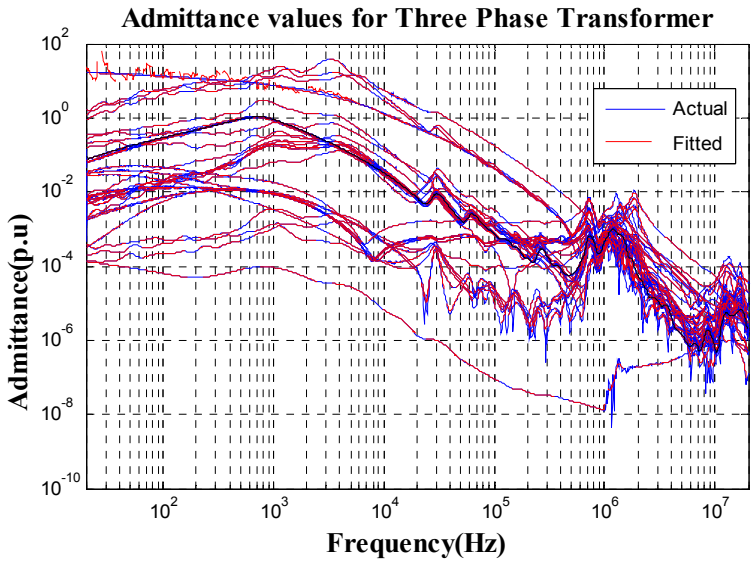

Figure 3.40: Measured and calculated values of admittance matrix of the transformer

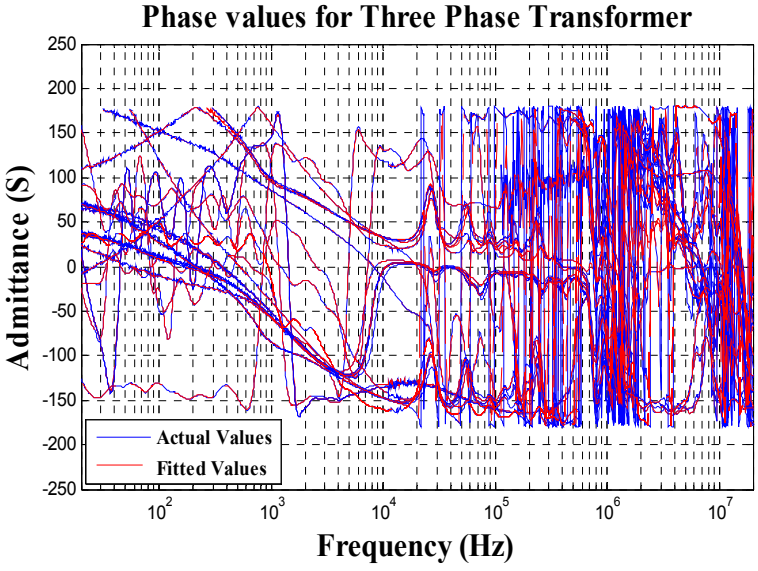

Figure 3.41: Measured and calculated values of phases of admittance matrix of the transformer

A congruently perfect fitting is obtained if the highest order of approximation is chosen. However, this is not possible in practical applications. A higher order of approximation results in large element size which in turn needs a sophisticated computational setup. The modeling technique presented in this thesis, uses the order of approximation of N=23. This approximation order facilitates an acceptable fitting and the rms error in the realized model in 1.3563%.

3.4 Summary

This chapter presented the high frequency modeling procedures of VCB, cable, and WTSU Transformers. To simulate VCB model in PSCAD/EMTDC, a user defined black box model is considered. A control strategy based VCB model cannot be used for simulating high frequency transients, as it does not take into account mutual interaction of power system components. Considering all high frequency parameters and statistical nature of arcing phenomenon, a high frequency user defined black box model of VCB is created in PSCAD/EMTDC. The developed VCB model is validated through a single-phase test circuit.

There are three models available for cables in PSCAD/EMTDC. For analyzing high frequency switching transients the frequency dependent (phase) model should be used in PSCAD/EMTDC. The cable model in PSCAD/EMTDC does not account for all the layer of a real cable therefore a cable model is developed that can represent the high frequency phenomena of the real cable to the best possible extent.

A high frequency black box model of WTSU transformer, within a frequency range of 20 Hz to 20 MHz is simulated in PSCAD/EMTDC. Black box model of actual transformer is developed because the transformer terminal models available in literature are only valid for 0Hz - 250 kHz frequency range.

These high frequency models are used to create a type IV wind farm (chapter 4) that serves as the test bench for carrying out VCB initiated high frequency transient study on WTSU transformer of a type IV wind farm.

Chapter 4

VCB initiated switching transient analysis on Type IV Wind Farm

In this chapter, a test bench (type IV wind farm) using the user defined high frequency black box models of VCB, cable and WTSU transformer is outlined. Four different cases are defined where switching transients generated due to opening and closing operation of VCB on low voltage side and high voltage side of WTSU transformer are investigated. The VCB initiated switching transient study is done in PSCAD/EMTDC.

4.1 Test Bench Layout

The test bench under consideration is a type-IV wind farm that is synchronized with the grid. Figure 4.1 shows the schematic of wind farm that has been designed in PSCAD/EMTDC.

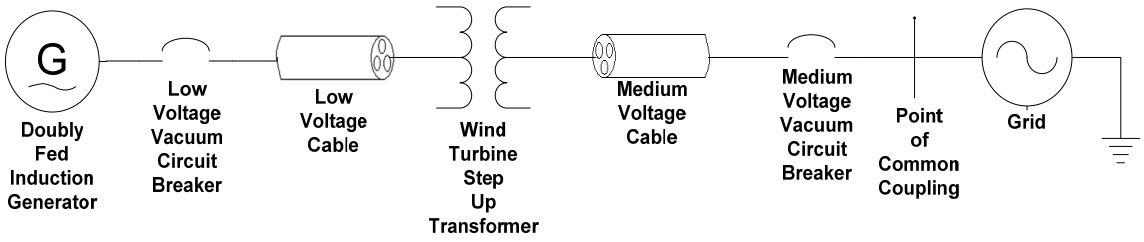

Figure 4.1: Type IV wind turbine synchronized with the grid

The electrical system shown in Figure 4.1 is a single wind turbine generator synchronized with the grid. As, the focus of this study is to investigate switching transients generated from the adjacent VCBs of WTSU transformer, there are certain assumptions made during the development of this test bench, are listed below:

- The generation system is an approximated model of DFIG.
- There is no significant impact of stator and rotor side converters on the magnitude of switching transient overvoltages imposed on WTSU transformer. Hence, generic and approximated stator and rotor converter models are used.
- High frequency harmonic filters are not included in the test setup.
- SVCs and STATCOMs do not affect the magnitude of switching transient overvoltages and are not included in the test bench.

For the switching transient study, the saturation characteristics of WTSU transformer must be included. During the energization of transformer, heavy inrush current that flows contains low frequency harmonics. A voltage magnification can take place if the resonance frequency matches the natural frequency of the grid. Such saturation characteristic contributes to the high transient overvoltages when the inrush current of transformer is interrupted. The high frequency model of WTSU transformer used in this study includes the transformer saturation characteristic.

The following sections describe the components of test bench.

4.1.1 Generation System: Doubly fed induction generator

As the test bench replicates the type IV wind farm, the generation system is an approximated DFIG model. The DFIG model (Figure 4.2) is a strongly coupled system including induction generator, power converters and non-linear multi-variable feedback controller. Back to back frequency converter with pitch control of rotor enables variable speed operation, which results in generation of large amount of power. In the DIFG model, the rotor of the generator is fed with variable voltage and frequency while fixed frequency electrical power is extracted from the stator. Back to back converters in the form of generator converter and grid converter are used in the model. The grid side converter's main function is to control the voltage of the DC bus bar. Generator converter controls the magnetization and torque currents. These converters require two-stage power conversion that allows the bidirectional power flow. A generic control algorithm is used to control the overall DFIG system. Large dc link capacitors are used to synchronize AC-DC-AC converter system.

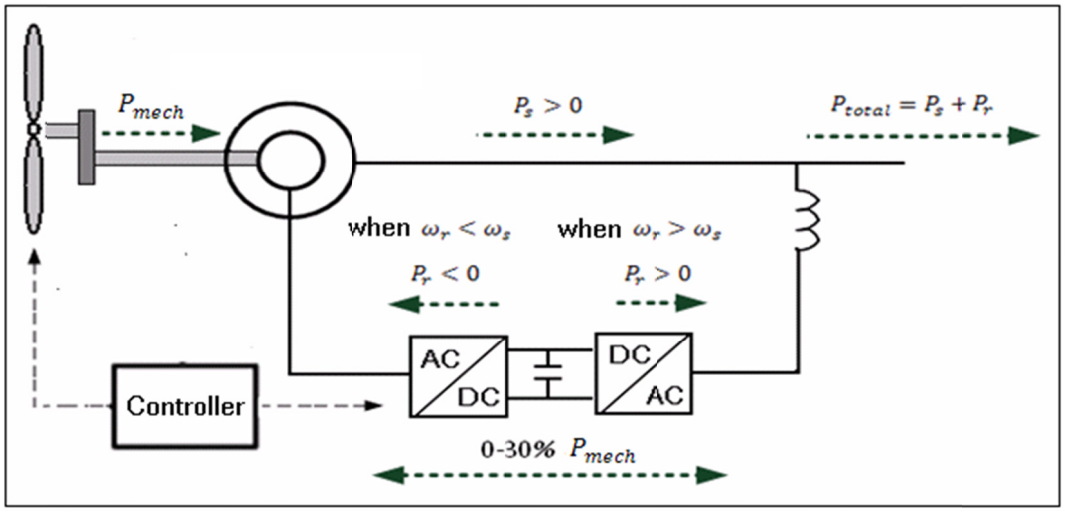

Figure 4.2: DFIG model

This DFIG design has the power converters built with two, three phase self-commutated back to back PWM converters. The DC bus voltage regulation is taken care of by the intermediate capacitor link. The dq frame representation of DFIG is given by following equations.

Equations for stator side of DIFG:

$$\lambda_{ds} = -L_s t_{ds} + L_r t_{dr} \quad (4.1)$$

$$\lambda_{qs} = -L_s t_{qs} + L_r t_{qr} \quad (4.2)$$

$$V_{ds} = -R_s i_{ds} - w_s \lambda_{qs} + \frac{d\lambda_{ds}}{dt} \quad (4.3)$$

$$V_{dq} = -R_s i_{qs} - w_s \lambda_{ds} + \frac{d\lambda_{qs}}{dt} \quad (4.4)$$

Equations for rotor side of DIFG:

$$V_{dr} = R_r i_{dr} - sw_s \lambda_{dr} + \frac{d\lambda_{dr}}{dt} \quad (4.5)$$

$$V_{qr} = R_r i_{qr} - sw_s \lambda_{qr} + \frac{d\lambda_{qr}}{dt} \quad (4.6)$$

Electrical output from the DFIG is given by:

$$P_s = \frac{3}{2} (V_{ds} i_{ds} + V_{qs} i_{qs}) \quad (4.7)$$

$$P_r = \frac{3}{2} (V_{dr} i_{dr} + V_{qr} i_{qr}) \quad (4.8)$$

As, there is no power flow analysis or reactive power studies involved in this research, the reactive power calculations and controllers for the generator and grid side converters are not elaborated in detail. To understand the control strategies for the controllers in detail follow the reference [66].

4.1.2 Vacuum Circuit Breaker

High frequency black box modeling of VCB has been discussed in previous chapter. In the test bench, the black box model of VCB is fed with physical parameters defined in chapter 3 for high and low voltage connections.

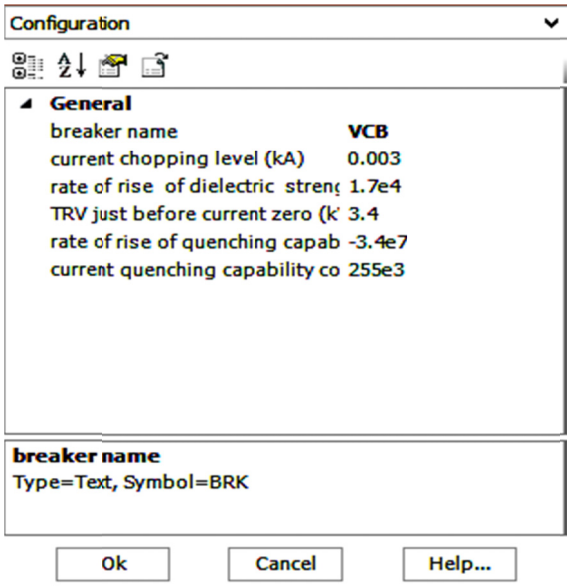

Figure 4.3: Configuration of black box VCB in PSCAD/EMTDC

As observed in Figure 4.3 the following five parameters are the basis to define a black box VCB model in PSCAD/EMTDC for different voltage levels:

- Chopping current
- Rate of rise of dielectric strength
- Transient recovery voltage just before current zero
- Rate of rise of quenching capability
- Current quenching capability of the breaker

Table 4-1 outlines the parameters chosen for high and low voltage VCBs in the test bench.

Table 4-1: Properties of VCB used in the test bench

Type of VCB	Current chopping (kA)	Rate of rise of dielectric strength (kV/sec)	Transient recovery voltage (kV)	Rate of rise of current quenching capability (kA/sec^2)	Current quenching capability (kA/sec)
Medium Voltage	5A	1.7e4	33.3	-3.4e7	255e3
Low Voltage	5A	0.47e3	0.69	1e8	190e3

4.1.3 Cable

The cables used in the test bench are ABB XLPE single core cables. The length of low voltage cable is 110 mm and medium voltage side is 180 mm. Cable modeling discussed in chapter 3, defined particular entities that are attributed to cable model in PSCAD/EMTDC, in order to get high frequency effects of real cable. Figure 4.4 shows all the physical parameters needed by the cable model in PSCAD/EMTDC.

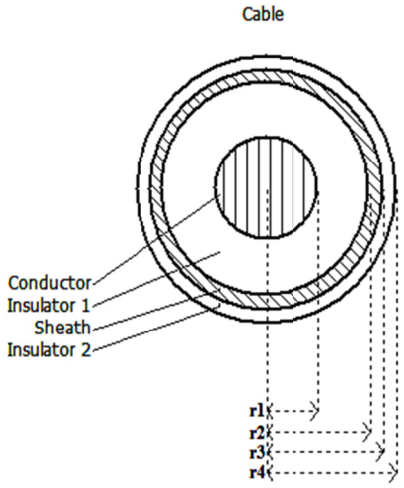

Figure 4.4: Parameters of cable model in PSCAD/EMTDC

The entities of cable model in PSCAD\EMTDC are as follows:

- Radius of each layer of cable model
- Resistivity
- Relative permittivity
- Permittivity
- Capacitance
- Inductance
- Surge impedance
- Wave travelling speed

Table 4-2 specifies all the cable parameters used in the cable model of the test bench.

Table 4-2: Cable model specifications

Radius (mm)				Resistivity (Ω.m)	Relative Permittivity	Permittivity (F/m)	Capacitance (pF/m)	Inductance (nH/m)	Wave Travelling Speed (m/µsec)
r1	r2	r3	r4						
5.6	12.6	13.6	16	2.82×10^{-8}	2.3	8.854×10^{-12}	217.54	160.5	179.3

4.1.4 WTSU Transformer

The transformer of the test bench is a 2.65 MVA, 690 V/33.3 kV WTSU transformer. As explained in the previous chapter, a high frequency black box model of WTSU transformer is developed using frequency dependent network equivalent (FDNE) in PSCAD/EMTDC.

The FDNE (Figure 4.5) represents the frequency dependent effects of transformer through rational function approximation based models. The input to FDNE module is the transformer's port behavior admittance matrix as a function of frequency. For the purpose of time domain simulations, the model uses pole-residue form. Table 4-3 specifies the parameters used in the WTSU transformer model of the test bench. Following curve fitting options are available in FDNE module:

- Total number of ports
- Maximum fitting error
- Maximum order of fitting
- Weighting factor for minimum to steady state frequency
- Weighting factor for steady state frequency
- Weighting factor for steady state to maximum frequency

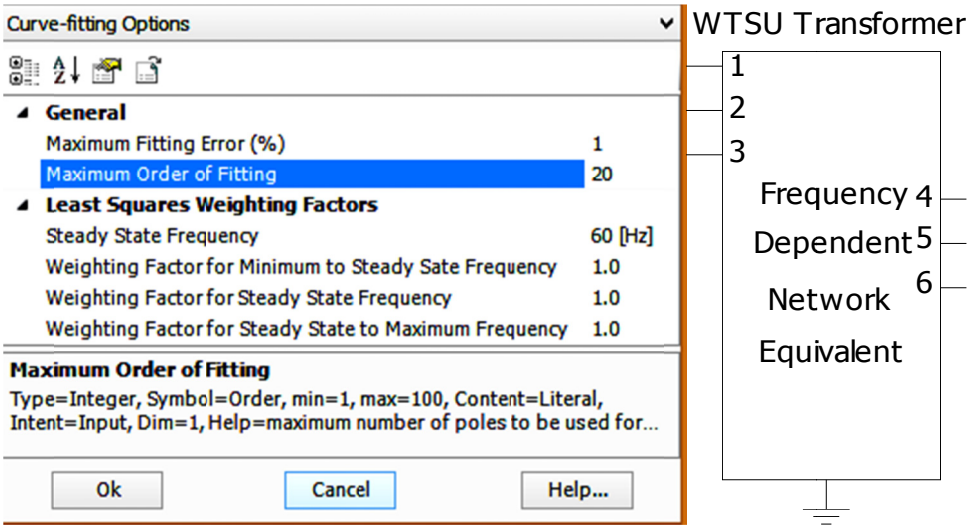

Figure 4.5: FDNE module and curve fitting options

Table 4-3: WTSU transformer parameters for FDNE module in PSCAD/EMTDC

Total number of ports	Maximum fitting error	Maximum order of fitting	Weighting factor for minimum to steady state frequency	Weighting factor for steady state frequency	Weighting factor for steady state to maximum frequency
3	0.01%	23	1	1	1

4.1.5 Collection grid

The collector grid in the test bench is modeled as a three phase voltage source behind impedance, together representing the grid in PSCAD/EMTDC, as shown in the Figure 4.6. The grid impedance also known as the short circuit impedance is equal to 0.68 + j6.78 Ω (4.9).

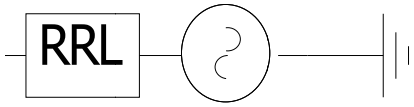

Figure 4.6: Collection grid used in the test bench

The value of the impedance represents the strength of the utility grid. A smaller value of the impedance indicates a stronger grid. Therefore, the grid is weaker if it has a low short-circuit current. The short-circuit current is often used in many cases to describe the strength of the grid. Theoretically, the strongest grid would occur if the short-circuit impedance is equal to zero and short-

circuit current would be infinite. P_{base} and V_{base} selected for the shown collector grid is 100 MW and 33 kV respectively.

4.2 Tools for classifying the switching transients

The case studies subsequently presented in this chapter investigate following aspects of the switching transients observed on the terminals of WTSU transformer:

- Loading condition of the transformer
- Peak voltage
- Peak breaker current
- Maximum rate of change of voltage
- Frequency of oscillations
- Number of reignitions

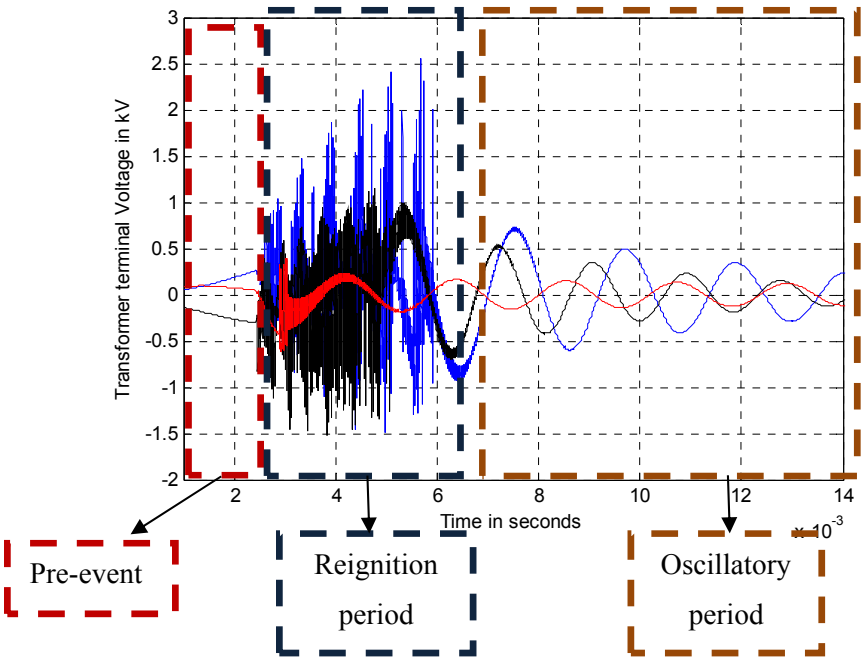

Figure 4.7: An example depicting different time regimes of transient waveform

The quantitative comparison of all the test cases will consider if the reignitions have occurred and investigate the performance of the VCB once it has attained fully open or closed status. It is also

determined if the response of VCB (once an open or closed status is obtained) is oscillatory or not. Figure 4.7 depicts different time regimes of a transient waveform.

There are four different frequency dependent behaviors that are observed in the VCB initiated switching transients. First is the post transient voltage oscillation. This phenomenon of oscillatory transients is observed once the transient period is over and switch is totally closed or open. The electrical system resonates at one of the natural frequencies during these voltage oscillations. Second phenomenon is re-strike which takes place at a frequency that is excited by the multiple reignitions during the transient period. Third phenomenon is breakdown across the contact gap of the VCB. The breakdown oscillations occur when the transient recovery voltage across the contact gap exceeds the breakdown capability of the contact gap. The fourth and final phenomenon is cable reflections. The frequency at which the cable reflections occur depends on the speed of propagation of the electromagnetic waves in a particular cable and the length of the cable. Typical value for the propagation speed of waves in cables is 200 m/μs but this value is different for each cable.

4.3 VCB initiated switching transient test cases

The following scenarios are carried out to analyze transient overvoltages in the proposed test bench:

- VCB opening and closing on LV side of the WTSU transformer under no-load
- VCB opening and closing on the LV side of the WTSU transformer under inductively load
- VCB opening and closing on the HV side of the WTSU transformer under no-load
- VCB opening and closing on the HV side of the WTSU transformer under inductively load

For all cases, the breaker operating time has been adjusted to match with the corresponding points on the voltage waveform. The peak voltage and maximum rate of change of voltage are determined from the time domain voltage waveform during restrike or prestrike periods. The frequency of oscillations is determined by calculating the number of peaks from the start of oscillatory response (approximately from 9 ms for this particular example as shown in Figure 4.7).

4.4 Elaboration of the test cases

This section of the chapter discusses the proposed test case scenarios.

4.4.1 Case I: VCB opening on LV side of WTSU transformer under no load

This simulation case shows the high frequency switching transients observed on the LV side of the WTSU transformer during the opening operation of VCB. The selection of simulation time step is very important for the transient simulations. It is observed that the simulation will not run if the chosen time step is higher than 0.13 µsec.

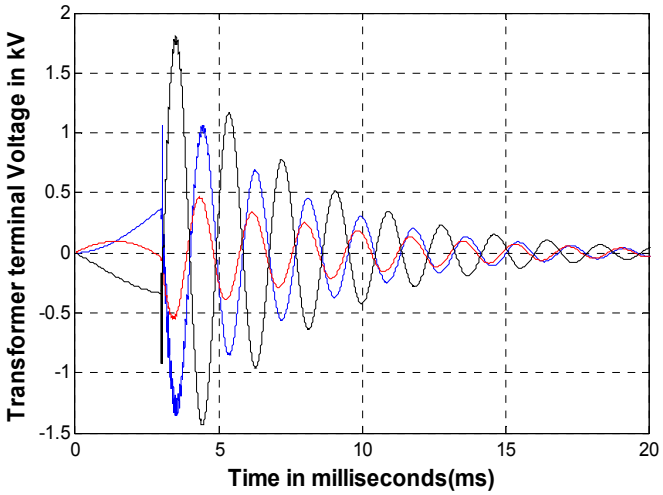

Figure 4.8: Voltage waveform on LV side of WTSU transformer (not loaded)

The opening of the VCB takes place at 3 ms (Figure 4.8). No reignitions are observed, as the voltage build up in form of transient recovery voltage across the breaker is not enough to exceed the voltage withstand characteristics of the breaker.

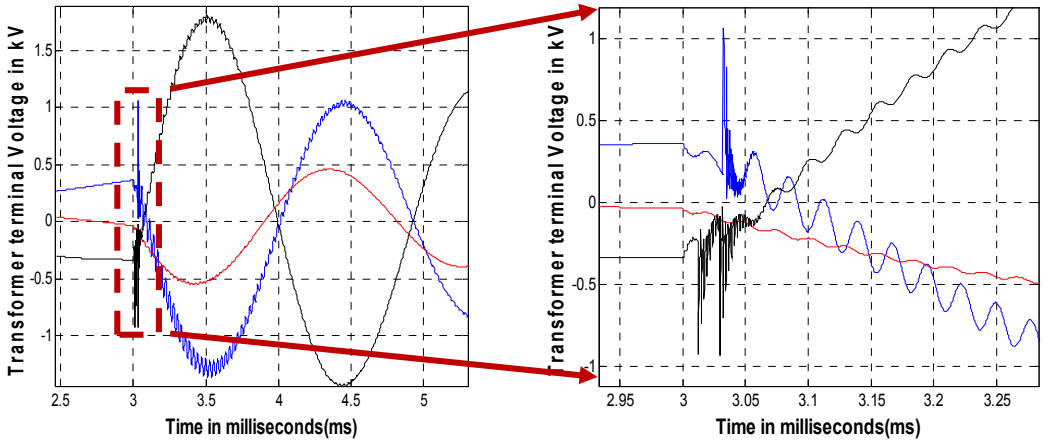

Figure 4.9: Zoomed in view of voltage waveform at WTSU transformer LV terminal

Figure 4.9 shows the spikes observed during the period when the high frequency current tries to establish an arc across the separating terminals of the VCB. As the voltage build up is not enough to the support the arc and allow the high frequency current to flow, the current is eventually quenched by the current quenching capability of the breaker. The synchronous oscillations observed in the post transient waveform is because of the inductance of the generation system and the capacitance of the LV cable. The post transient oscillations last for 18 ms. A close observation of the transient voltage waveform suggests that there are no spikes observed in phase B (Red) during the transient period. This phenomenon is attributed to the fact that there is no chopping current associated with the phase B and the opening of the contacts for phase B takes at the natural current zero. Phase B exhibits zero voltage build up during the transient period as no current is interrupted. Table 4-4 presents the quantitative comparison of this case.

Table 4-4: Quantitative comparison of test case I

Transformer loading	Peak voltage (pu)	Peak breaker current (kA)	Maximum rate of change of voltage (kV/µsec)	Frequency of oscillations (kHz)	Number of reignitions
No load	1.4	0.07	----	0.59	----

4.4.2 Case II: VCB opening on LV side of WTSU transformer under an inductive load

This scenario investigates transients on LV side of an inductively loaded WTSU transformer. The transformer is loaded with 0.1Ω of inductive load. The value of the inductive load has been chosen in accordance to IEEE Std. 57.142 and switching transient study analysis presented in [54] [55]. The time step for this simulation scenario is kept 0.001 µsec, because of the high frequency steep front reflective transients in transient phase of the voltage waveform. The reflections were observed in the transient period during the reignitions when the time step is not appropriately chosen. The simulation stopped abruptly when the time step is less than the 0.013 µsec because the compiler of PSCAD/EMTDC is not able to calculate the distributed parameters of cable and transformer model involved in the test bench.

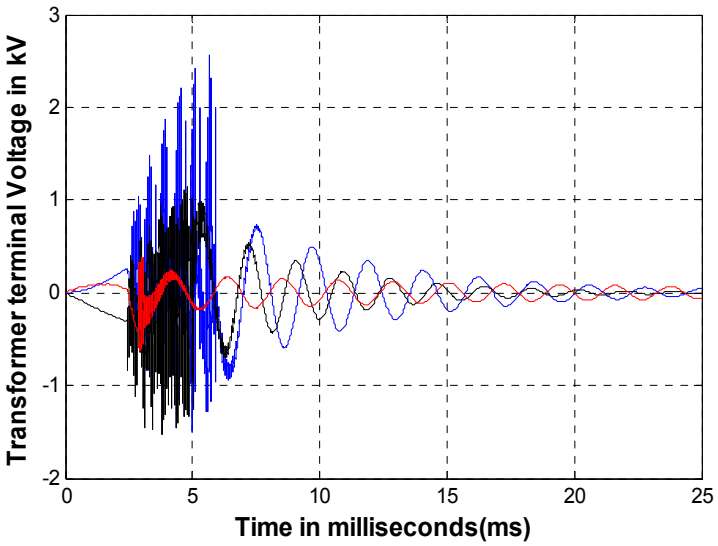

Figure 4.10: Voltage waveform on LV side of WTSU transformer (loaded)

The phenomenon of opening VCB contacts starts at 2.5 ms (Figure 4.10). The major observation in the scenario is that phase B (Red) exhibits only 5 reignitions. As mentioned earlier, the chopping current in phase B is less as compared to the other two phases. Phase A and phase C exhibit 59 and 73 reignitions, respectively. The voltage oscillations die out in 19 ms.

The transient period lasts for 3.5 ms (Figure 4.10). The number of reignitions and the voltage build up across the VCB contacts are fairly similar for phase A and phase C. Figure 4.11 shows the high frequency reflective transients observed during the transient period. The highest frequency observed during the transient period is 12.6 MHz. Table 4-5 presents the quantitative comparison of this case.

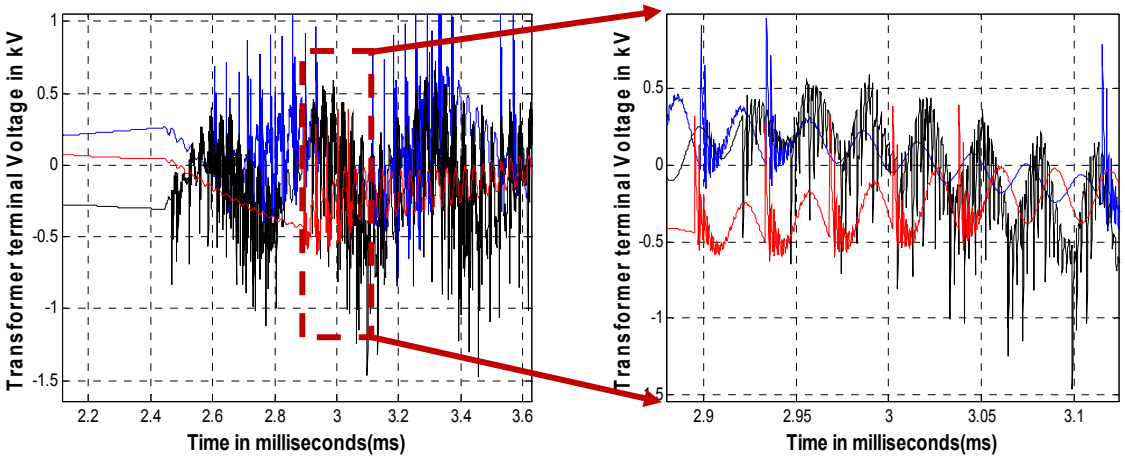

Figure 4.11: Zoomed in view of voltage waveform at WTSU transformer LV terminal

Table 4-5: Quantitative comparison of test case II

Transformer loading	Peak voltage (pu)	Peak breaker current (kA)	Maximum rate of change of voltage (kV/µsec)	Frequency of oscillations (kHz)	Number of reignitions
Inductive	3.5	0.09	7.5	0.47	73

4.4.3 Case III: VCB closing on LV side of WTSU transformer under no load

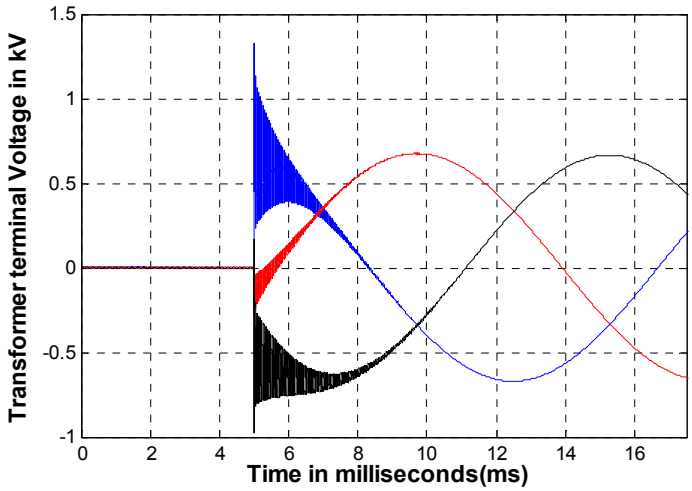

Figure 4.12: Voltage waveform on LV side of WTSU transformer (not loaded, closing)

With the closing operation of VCB, arises the problem of prestrikes. The case of closing the VCB on LV side of WTSU transformer shows occurrence of no prestrikes. In comparison to the opening operation under no load, closing operation exhibits high frequency voltage oscillations. The closing operation of VCB takes place at 5 ms. Table 4-6 presents the quantitative comparison of this case.

Table 4-6: Quantitative comparison of test case III

Transformer loading	Peak voltage (pu)	Peak breaker current (kA)	Maximum rate of change of voltage (kV/µsec)	Frequency of oscillations (kHz)	Number of reignitions
No load	1.72	0.12	-	22.1	-

4.4.4 Case IV: VCB closing on LV side of WTSU transformer under inductive load

The problem of prestrike gets pronounced during the inductive loading scenario of WTSU transformer. During the closing operation of VCB on LV side of WTSU transformer, prestrikes are observed in each phase of voltage waveform. This phenomenon is observed in Figure 4.13. The number of prestrike is different for each phase, as the rate of rise of voltage at the instant of first prestrike is different in each phase. The closing of vacuum circuit breaker takes place at 5.5 ms. Highest number of reignitions is observed in phase B with 71 reignitions (Table 4-7). Phase A observed 39 and phase C observed 21 reignitions, respectively. With regard to the oscillatory period, which starts the post transient period, the oscillating frequency is 21 kHz. The oscillations die out in 3 ms.

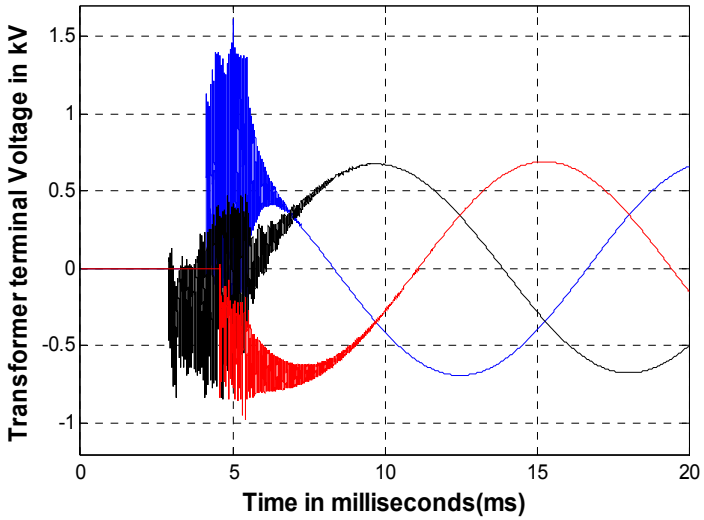

Figure 4.13: Voltage waveform on LV side of WTSU transformer (loaded, closing)

The post transient voltage oscillations are dependent on the natural frequency of the electrical circuit. Once the closing of VCB contacts takes place the configuration of the electrical system changes. Hence, the post transient voltage oscillations observed during the opening and closing operation of VCB are different.

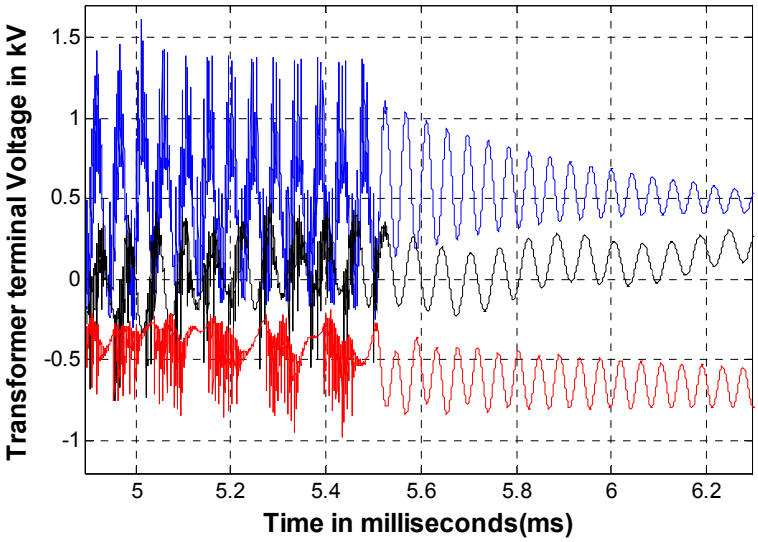

Figure 4.14: Post transient voltage oscillations for case IV

Table 4-7: Quantitative comparison of test case IV

Transformer loading	Peak voltage (pu)	Peak breaker current (kA)	Maximum rate of change of voltage (kV/µsec)	Frequency of oscillations (kHz)	Number of reignitions
Inductive	2.1	0.09	1.1	20.3	71

4.4.5 Case V: VCB opening on HV side of WTSU transformer under no load

In contrast to case I, the opening operation on HV side of WTSU transformer shows some restrikes. The rate of rise of voltage build up is 2.3 kV/µsec (Table 4-8), which does not exceed the withstand capability of the contact gap for more than 4 times. The opening of vacuum circuit breaker takes place at 1.5 ms. Highest number of reignitions is observed in phase B with 4 reignitions. Phase A observed 2 and phase C observed 3 reignitions, respectively. The post transient voltage oscillations die out in 6.5 ms.

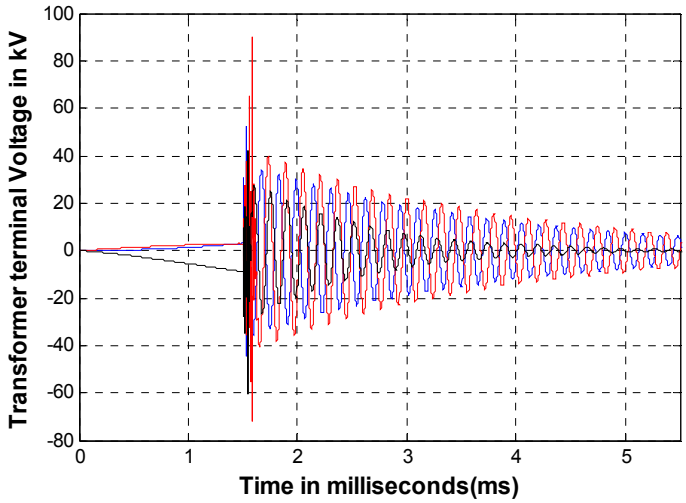

Figure 4.15: Voltage waveform on HV side of WTSU transformer (not loaded)

As observed in the previous cases, chopping current is very low in one of the phases. Phase A (black) with only two reignitions shows least magnitude of TRV (Figure 4.16).

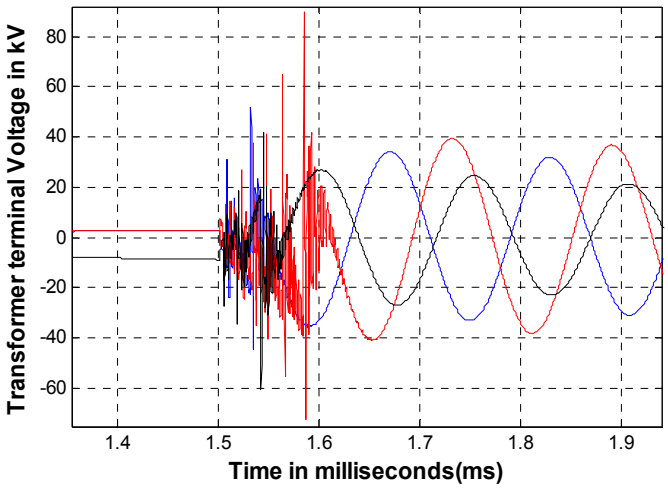

Figure 4.16: Zoomed view of voltage waveform for case V

Table 4-8: Quantitative comparison of test case IV

Transformer loading	Peak voltage (pu)	Peak breaker current (kA)	Maximum rate of change of voltage (kV/µsec)	Frequency of oscillations (kHz)	Number of reignitions
No load	2.9	0.09	2.3	0.66	4

4.4.6 Case VI: VCB opening on HV side of WTSU transformer under inductive load

This scenario exhibits the highest peak voltage and maximum rate of rise of voltage for the voltage waveforms observed at the WTSU transformer terminals. Figure 4.17 depicts all the three phases exhibiting reignitions. The instant of VCB contact opening is 1.5 ms. The post transient voltage oscillations die out in 4.5 ms. Phase C (black), observed the highest voltage peaks, because the magnitude of recovery voltage across the contact gaps of the VCB is higher for phase C in comparison to other two phases. Table 4-9 presents the quantitative comparison of this case. Highest number of reignitions is observed in phase B with 74 reignitions. Phase A observed 56 and phase C observed 62 reignitions, respectively.

Table 4-9: Quantitative comparison of test case VI

Transformer loading	Peak voltage (pu)	Peak breaker current (kA)	Maximum rate of change of voltage (kV/µsec)	Frequency of oscillations (kHz)	Number of reignitions
Inductive	3.03	0.73	28	0.56	74

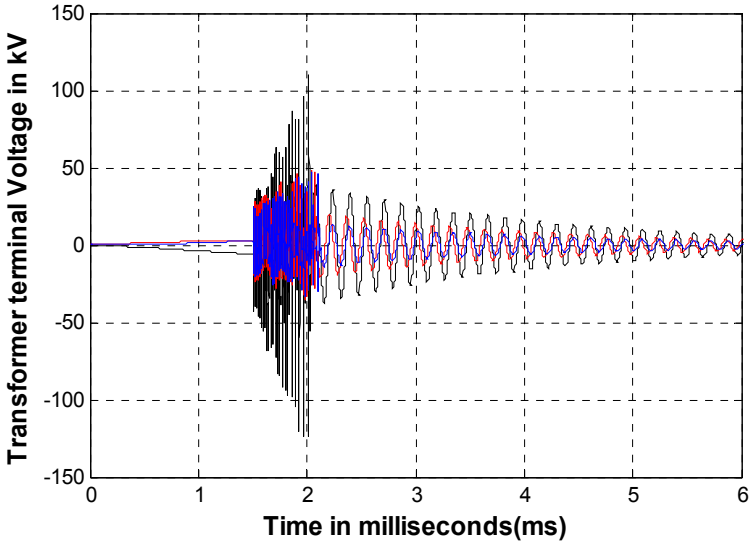

Figure 4.17: Voltage waveform for case VI

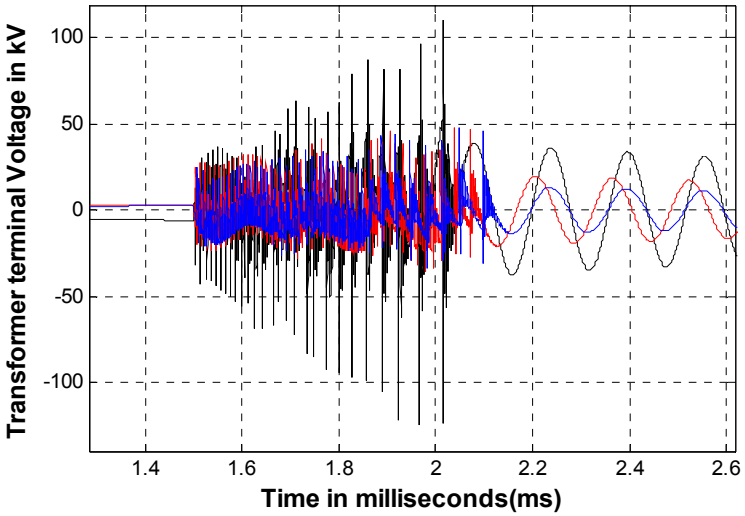

Figure 4.18: Zoomed view depicting transient period for case VI voltage waveform

4.4.7 Case VII: VCB closing on HV side of WTSU transformer under no load

The results obtained for this case are similar to case III, where similar switching scenario is carried on LV side. There is no reignition observed during the transient phase (Table 4-10). The frequency of the post transient oscillations is similar to case III, as is the equivalent circuit after closing of VCB terminals.

Closing of the VCB contacts start at 5 ms, resulting in voltage oscillations of 22 kHz, which die out in 2 ms.

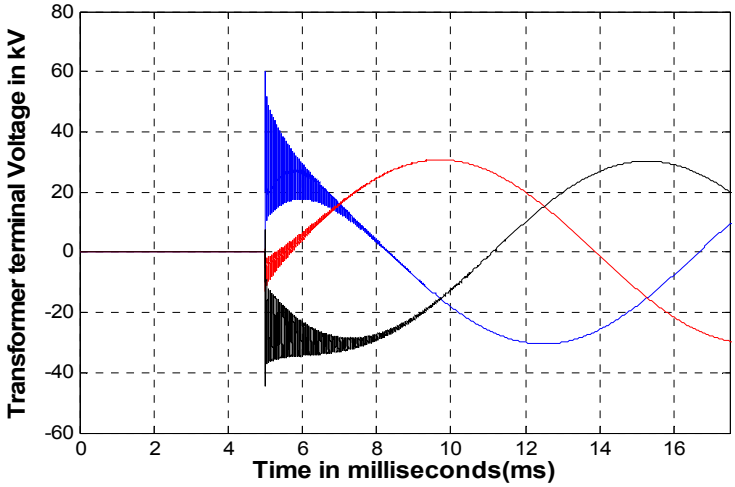

Figure 4.19: Voltage waveform on HV side of WTSU transformer (not loaded, closing)

Table 4-10: Quantitative comparison of test case VII

Transformer loading	Peak voltage (pu)	Peak breaker current (kA)	Maximum rate of change of voltage (kV/µsec)	Frequency of oscillations (kHz)	Number of reignitions
No load	1.8	0.17	----	22	----

4.4.8 Case VIII: VCB closing on HV side of WTSU transformer under inductive load

High frequency steep front reflective transients are observed during VCB closing on HV side of WTSU transformer under 0.1Ω inductive load. Simulation results (Figure 4.20) for this condition show reignitions in all the three phases. The closing of vacuum circuit breaker takes place at 2.45 ms. It is interesting to note that phase B (red) shows higher number of reignitions than the other two phases (Figure 4.21). However, the magnitude of transient overvoltages is less in comparison to the other two phases. Lower magnitude of TRV across phase B is governed by low chopping current in phase B. Higher number of reignitions is observed because the stray inductance of the phase B resonates with the impedance (capacitive part) of the collector grid, giving rise to higher number of reignitions.

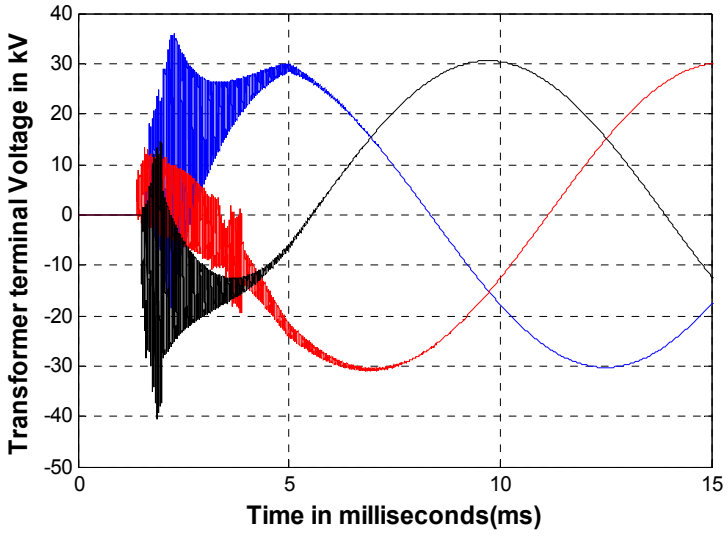

Figure 4.20: Voltage waveform across WTSU transformer terminals for case VIII

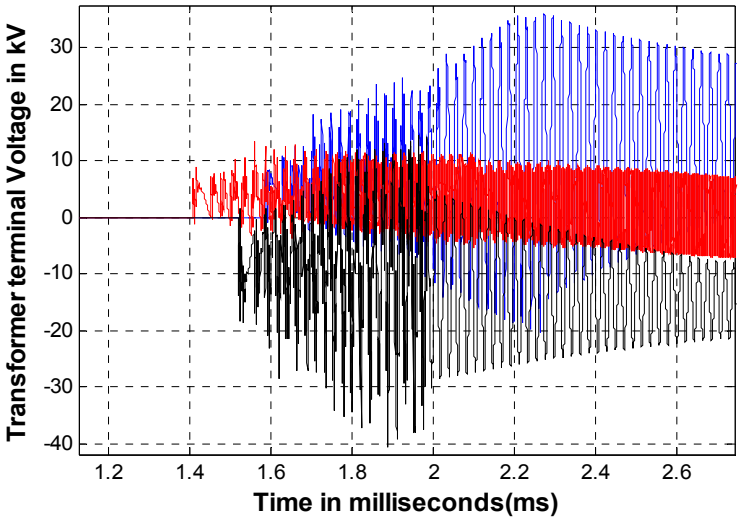

Figure 4.21: Zoomed in voltage waveform depicting transient period

Table 4-11: Quantitative comparison of test case VIII

Transformer loading	Peak voltage (pu)	Peak breaker current (kA)	Maximum rate of change of voltage (kV/µsec)	Frequency of oscillations (kHz)	Number of reignitions
Inductive	1.1	0.49	5.5	24	64

4.5 Summary

A test bench is proposed using user defined black box high frequency power system modules to investigate VCB initiated transients. Six different attributes of voltage waveforms across the WTSU transformer are used to investigate the transient behavior in eight different cases carried out on the proposed test bench.

Chapter 5
Discussion

Voltage waveforms obtained from the VCB switching transient studies in Chapter 4 are used to investigate the behavior of transients to which WTSU transformers are exposed under certain loading conditions. Comparisons are made with earlier research work to highlight the relative differences and contributions of the proposed work. The earlier research work includes switching transient studies on different models of transformers and generic VCB models.

5.1 Investigation of VCB initiated transients on WTSU transformers

In this study, a new test bench is proposed to investigate VCB initiated high frequency transients experienced at low and high voltage sides of WTSU transformers. The switching transient studies carried out on the test bench elucidate the nature of the switching transients to which WTSU transformers are exposed. Table 5-1 presents the quantitative comparison results for 8 cases that contribute to the investigative transient study.

Table 5-1: Quantitative Comparison Results of Switching Transient Study

Case No.	Peak Voltage (pu)	Peak Breaker Current (kA)	Maximum Rate of Voltage Change (kV/µsec)	Frequency of Oscillations (kHz)	Number of Reignitions
I	1.4	0.07	----	0.59	----
II	3.5	0.09	7.5	0.47	73
III	1.72	0.12	-	22.1	-
IV	2.1	0.09	1.1	20.3	71
V	2.9	0.09	2.3	0.66	4
VI	3.03	0.73	28	0.56	74
VII	1.8	0.17	----	22	----
VIII	1.1	0.49	5.5	24	64

During the transient period, five of the test cases exhibited reignitions in all three phases. As expected, the cases with an inductively loaded WTSU transformer exhibited more severe switching scenarios than did those with unloaded transformers. From these results, we can see that the TRV across the VCB contacts is highly dependent on the configuration of external electrical circuits and

the magnitude of the chopping current. Since the magnitude of the chopping current here is different for each phase, the linear time-dependent VCB voltage withstand capability and unusual TRVs along each phase resulted in a different number of reignitions.

Compared to the opening operation, the closing operation of VCBs gave rise to much higher post-transient frequency oscillations. The equivalent impedance of wind farm changes resulted in different post-transient oscillations after the switching operation of VCBs. This phenomenon can be seen in cases VI and VIII. In contrast to the frequency of 0.56 kHz exhibited during the opening of the VCB on an inductively loaded WTSU transformer (case VI), the closing of the VCB (case VIII) exhibited a post-transient oscillation frequency of 21 kHz.

The transient overvoltages observed in cases involving inductive load show a higher number of reignitions because of the higher rate of voltage build-up. Furthermore, current that is quenched after each reignition is different in loaded and unloaded transformers. This difference is evident in cases V and VI, where the switching of unloaded and inductively loaded WTSU transformers is presented. In both cases, the first reignition occurred at a peak voltage of 1.2 pu. After every reignition, the current quenching capability of the breaker attempted to quench the high frequency current at the next zero crossing, thereby resulting in fast-rising voltages across the VCB contacts. The interruption of high frequency inductive current resulted in high TRV and caused 74 reignitions, as indicated in case VI. In contrast, case V exhibited only 4 reignitions with no load current quenching.

Case VI, which shows the opening of a VCB on the HV side of a WTSU transformer under inductive load, is recognized as the most onerous switching scenario. The voltage waveform captured on the HV side of the WTSU transformer during the opening of the adjacent VCB under inductive load depicts the highest rate of voltage rise during the transient period and also exhibits the maximum peak voltage (Figure 5.1). Furthermore, the maximum number of reignitions is observed in this case.

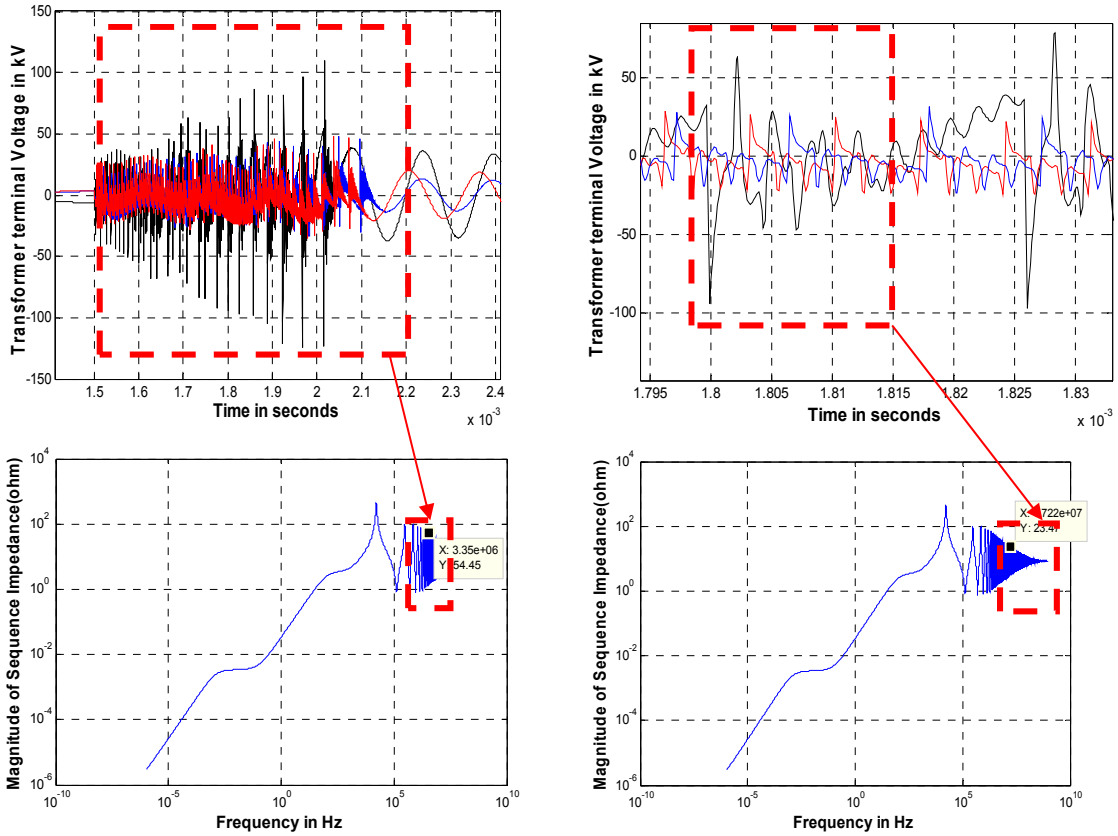

Figure 5.1: Frequencies corresponding to different regimes of the transient period for case VI

5.2 Comparison of proposed VCB model with existing VCB model

The VCB model used in the proposed switching transient study incorporates the stochastic and statistical nature of the vacuum arc. The VCB models available in previous research work do not take into account the statistical nature of arcing time. The study by Gopal and Gajjar [67] provides a guide that describes the dynamic modeling of VCB in PSCAD/EMTDC. Although the model presented in this paper simulates the physical phenomena of VCB, the statistical nature of arcing time is not taken into account. Their model has the following two limitations compared to the model presented in this work:

- It does not replicate the exact behaviour of prestrikes during the closing operations of VCB.
- It does not describe the modeling strategy for a three-phase VCB, where the coordination between three different phases is required to exactly replicate the real case switching scenario.

Figure 5.2 depicts the TRV and current waveforms in Gopal and Gajjar's paper. As we can see, once prestrikes occur, there is no post-transient voltage oscillation, which defies the real-time physical phenomenon of VCB. Once the transient period is over, the high frequency arc still conducts the power frequency current, which is finally quenched at the next current zero. This limitation exists in Gopal and Gajjar's VCB model because it does not incorporate hot and cold gap breakdown phenomena, which results in varied behavior of arcing time.

Once the transient period is over; the VCB contacts are either fully open or fully closed. The ideal behavior of VCB is presented in Figure 3.13 (the model presented in this thesis), where the VCB contacts are fully opened once the transient period takes place in the form of reignitions.

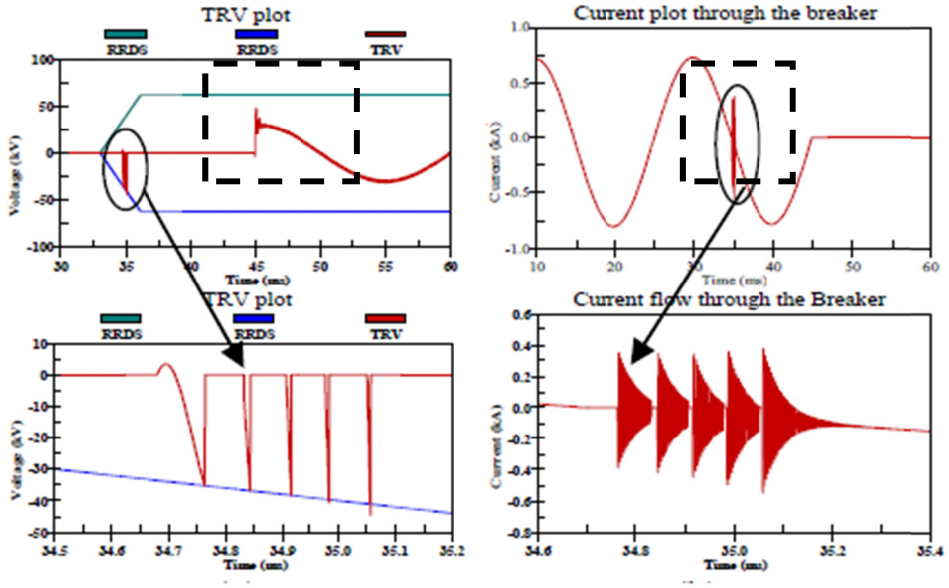

Figure 5.2: TRV and current of VCB [67]

The VCB model presented in this thesis incorporate following phenomena to exhibit the statistical nature of arcing time:

- Successful interruption only takes place at high arcing times.
- The current is not interrupted at low arcing times.
- There are no reigntions at high arcing times.
- Reigntions only take place at low arcing times.
- Prestrikes take place only at high closing times.
- No prestrikes should be observed at low arcing times.

5.3 Comparison of results with switching transient analysis using power frequency transformer model

In this section, a comparison is drawn between the presented work using high frequency transformer model and previous research work that uses transformer model valid for power frequency.

Mireanue [33] presented switching transient study of a wind farm. This switching transient study uses power frequency transformer model and π- model representation of the cable. One of the voltage waveforms captured at the transformer terminals at the wind farm (Mireanue's thesis) is presented in Figure 5.3.

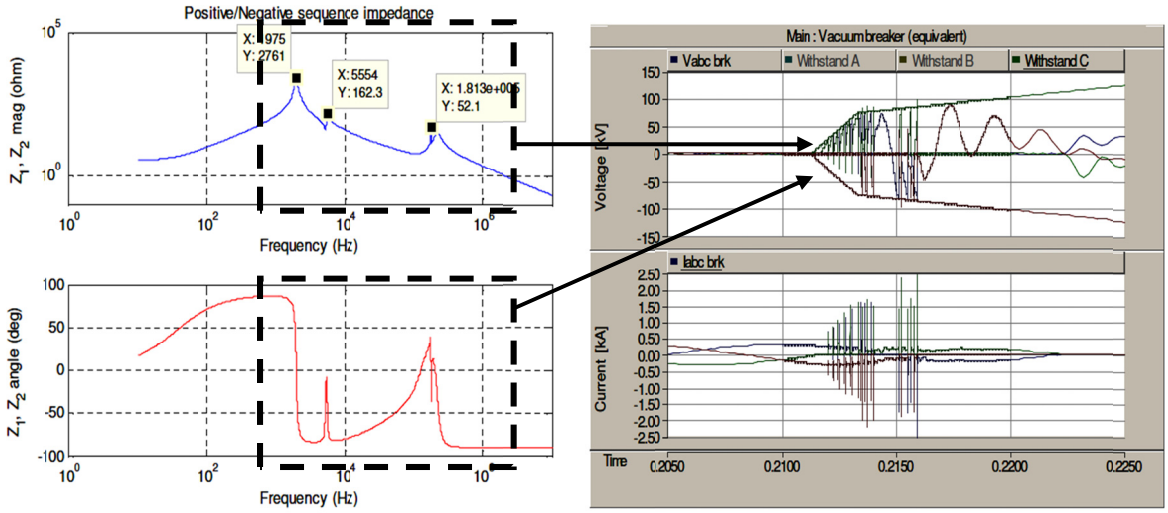

Figure 5.3: Voltage waveform at a transformer terminal in Mireanue's wind farm system [33]

Table 5-2: Comparison of Similar Test Cases from Mireaneu [33] and Current Work

Work	Test Case	Maximum Frequency Content	Reflective Transients	Observation of Voltage Oscillations	Transformer Model	Cable Model	Generation System
Mireaneu [33]	Opening of VCB on HV side of transformer	181 kHz	Not observed	Limited and fade away in two cycles	UMEC (Power frequency transformer model)	Π-model	Voltage source
Current Work	Opening of VCB on HV side of transformer	5MHz - 25 MHz	Observed	Observed	High frequency black box model of original transformer	Phase-dependent frequency model	Doubly-fed induction generator

It is observed that the high frequency effect of switching transients in the wind farm is not captured because the transformer and cable models did not take into account high frequency phenomena. The scenario shown in Figure 5.3 isolates one feeder of a simplified wind farm system. The highest frequency component observed is 181 kHz and reflective transients are not observed.

In the proposed test bench, use of a frequency-dependent cable model and a high frequency transformer model facilitate the observation of high frequency reflective transients.

Figure 4.18 shows a similar switching scenario (case VI) in the proposed wind farm test bench. The highest frequency components are observed within a range of 5 MHz - 25 MHz because of the mutual interaction of power system components, which are seen at high frequencies. The frequency component predominant in reflective transients is 14.75 MHz.

The comparison drawn from the observation of the two similar test cases is shown in Table 5-2. The table illustrates that high frequency cable and transformer models are required to investigate the frequency-dependent behavior of switching transients.

5.4 Problem of initial voltage spike and synchronized three-phase VCB model

Choosing a synchronized three-phase VCB model and observing the initial voltage spike are two subjects that have not been dealt in the literature. The study by Shipp [68] uses a desynchronized three-phase VCB model, which does not adequately represent the initial voltage spike needed for reignition.

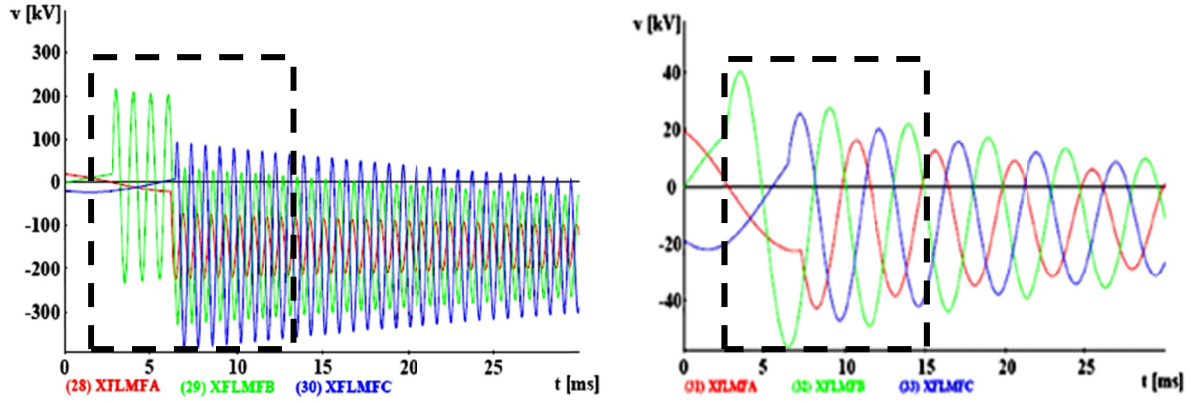

Figure 5.4: Overvoltage during de-energization of LMF transformer by the vacuum breaker [68]

Figure 5.4 shows the three-phase voltage across the LMF transformer [68]. Firstly, we can see that the opening of VCB contacts is different for each phase. This defies the real-time physical

phenomena of the VCB contact gap opening, as the switching of the VCB contacts for all three phases takes place at the same time. A distinct opening regime for each VCB phase is highlighted in Figure 5.4, which shows that the three-phase VCB is not well coordinated.

Secondly, zero build-up voltage is observed during the contact gap opening, even though the contact opening starts before the zero crossing. This accounts for the phenomenon of no reignition. The transient recovery voltage across the VCB contacts is not included in Shipp's VCB model.

The two physical phenomena mentioned above have been dealt in the VCB model and switching transient analysis presented in this thesis. The three-phase VCB model incorporates a control strategy that synchronizes the three-phase VCB operation for the three distinct poles. The VCB model includes the dielectric characteristics of the vacuum and recovery voltage of the breaker to account for the initial build-up of voltage during the transient period (Figure 4.9). Both of these attributes of the VCB model are discussed in Chapter 3.

5.5 WTSU Transformer model Validation

The WTSU transformer model is validated by comparing the voltage ratio (voltage transfer functions) measured directly on the transformer terminals (as shown in Figure 5.5 and Figure 5.6) with the calculated and simulated voltage ratios of the WTSU transformer model in PSCAD/EMTDC. The voltage ratios calculated were obtained from the measured admittances as discussed in section 3.3.5 of chapter 3.

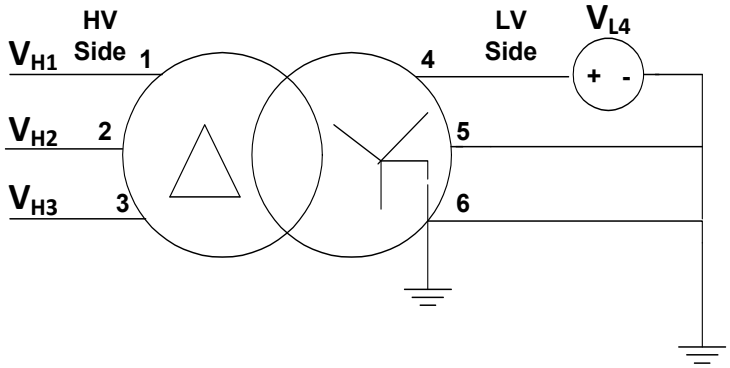

$$V_{HL}\,(V_{HL14}=\frac{V_{H1}}{V_{L4}}\,;\,V_{HL24}=\frac{V_{H2}}{V_{L4}}\,;\,V_{HL34}=\frac{V_{H3}}{V_{L4}}\,)$$

Figure 5.5: Voltage ratios from high voltage side to low voltage side

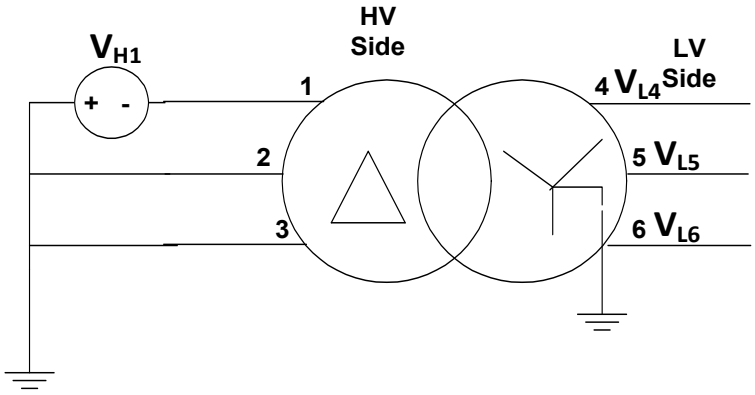

$$V_{LH}\,(V_{LH41}=\frac{V_{L4}}{V_{H1}}\,;\,V_{LH51}=\frac{V_{L5}}{V_{H1}}\,;\,V_{LH61}=\frac{V_{L6}}{V_{H1}}\,)$$

Figure 5.6: Voltage ratios from high voltage to low voltage side

To validate the transformer model, six different voltage ratios were measured (equation 5.1) on the transformer terminals and were compared with the calculated voltage ratios.

$$V_{14}=\frac{V_{H1}}{V_{L4}}\,;\,V_{41}=\frac{V_{L4}}{V_{H1}}\,;V_{36}=\frac{V_{H3}}{V_{L6}}\,;\,V_{63}=\frac{V_{L6}}{V_{H3}}\,;\,V_{52}=\frac{V_{L5}}{V_{H2}}\,;\,V_{25}=\frac{V_{H2}}{V_{L5}} \tag{5.1}$$

The PSCAD/EMTDC WTSU transformer model is obtained by admittance matrix measurements with 1201 frequency points. The order of rational function approximation used via vector fitting is 23. Figure 5.7 compares the calculated voltage ratios with the corresponding simulated and measured voltage ratios. It is observed that simulated voltage ratios reciprocate with the transfer characteristics of measured voltage ratios. The small error observed in the low voltage segment is because of the distinct zero sequence components of admittance values at low frequencies. Furthermore, Figure 5.7 shows that the simulated voltage ratios are in agreement with the calculated voltage ratios. As the final transformer model is generated from the rational approximation of admittance matrix but not from the real admittance matrix, a small deviation is observed between the simulated and calculated admittances. This deviation between simulated and calculated voltage ratios accounts for the fitting error observed in Figure 5.7. The WTSU transformer model is validated through the method of comparison of measured, calculated and simulated voltage ratios.

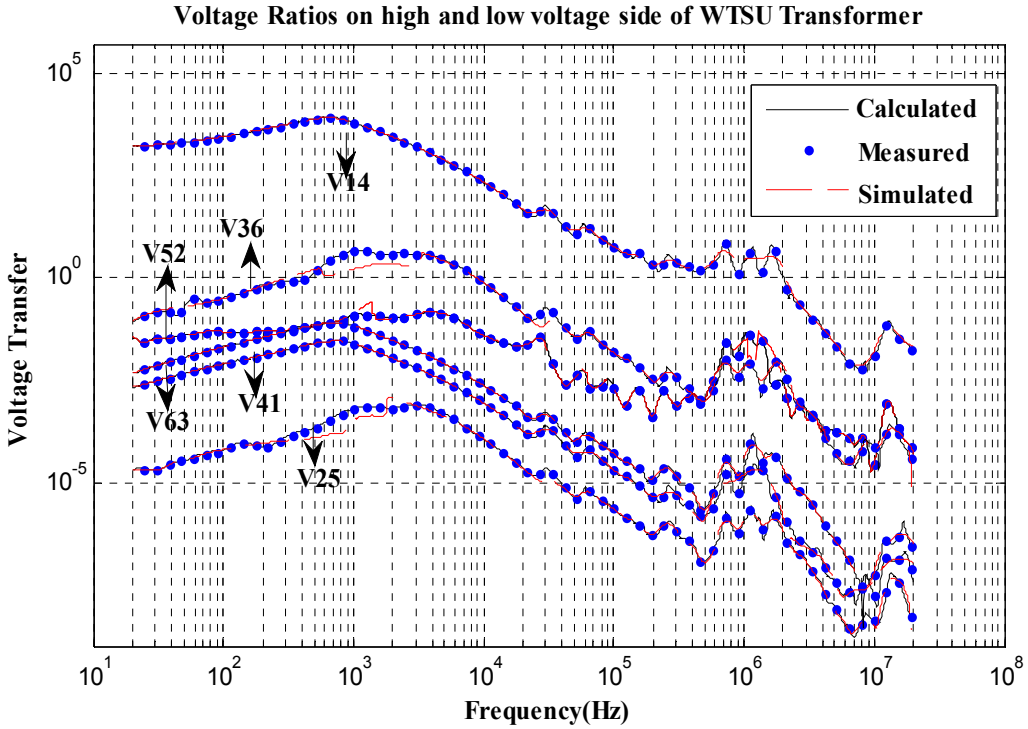

Figure 5.7: Comparison of voltage ratios for measured, calculated and simulated values

5.6 Summary

A quantitative comparison of a VCB initiated switching transient analysis considering eight switching scenarios inferred that a VCB opening on the HV side of a WTSU transformer under inductive load (case VI) resulted in the most severe switching scenario. A detailed comparison of the proposed models with previously published research work showed the need for incorporating the physical attributes and high frequency phenomena of specific power system components during a switching transient study. The chapter concludes with the validation of the WTSU transformer model through voltage transfer function matching technique.

Chapter 6
Conclusions and Future Work

6.1 Conclusions

The objective of this research study was to identify and develop high frequency black box models of VCB, cable and WTSU transformer, alongwith conducting a VCB initiated switching transient study on Type IV wind farm test bench.

The opening chapter reviewed wind technology and its development in Ontario's grid. It also discussed typical configuration of wind farm generators and problems associated with WTSU transformers. An overview of high frequency transients in wind farms and cable systems was presented in the literature review section. Following this, modeling procedures of high frequency model of VCB, frequency dependent phase model of cable and rational function approximation model of an actual WTSU transformer were discussed. A single phase test circuit was established to realize the statistical nature of arcing time and physical phenomena of VCB. The WTSU transformer model was validated through voltage transfer function matching technique. Later these high frequency models were used to formulate a test bench for investigating VCB initiated switching transients on WTSU transformer. Lastly, the results of switching transient study were used to predict the behavior of transient overvoltages experienced by WTSU transformers and identify the most severe switching scenario. Based on the results of this work, the following conclusions can be drawn:

- Internal overvoltages generated within the transformer due to switching transients, cannot be computed using the PSCAD/EMTDC model. PSCAD/EMTDC generates an equivalent real time RLC model of transformer, which is different from a detailed internal winding model of transformer.
- A VCB model that is able to simulate physical phenomena of vacuum gap and statistical nature of arcing time with an ability of accurately representing overvoltages on the power system components it interacts with is essential for switching transient analysis.
- User defined black box models that can efficiently represent the frequency dependent behaviour of cable and transformer, are necessary to capture the high frequency response of electrical system to switching operations initiated by VCBs.

- Of the eight test cases conducted during the switching transient study, opening of VCB on HV side of WTSU transformer under inductive load is recognised as more severe switching transient scenario.
- Higher post transient frequency oscillations are observed during closing operation VCB instead of opening operation.
- In comparison to no load currents, interruption of high frequency inductive currents results in higher magnitude of TRV (transient recovery voltage) leading to higher number of reignitions.

6.2 Future Work

This work can be extended to address a number of distinct challenges. This section highlights some of the important points.

6.2.1 Simulation and investigation of VCB initiated transients on whole wind farm

The test bench presented in this thesis comprises of single wind turbine synchronized with the grid. Simulating whole wind farm as a test bench and analyzing effect of different wind farm configuration on switching transients are important. Observation of variation in switching transients with addition of multiple wind turbines to the proposed test bench is further required.

6.2.2 High frequency DFIG model studies

An advanced high frequency DFIG model will represent the switching transient more accurately. Until now, inclusion of stator filter and grid inverter filter to existing DFIG model represents the high frequency DFIG model. A discrete model representing frequency dependent characteristics of DFIG is required to be developed and employed for switching transient studies.

6.2.3 High frequency harmonics in the wind farm

The focus of this research study was to investigate VCB initiated switching transients hence the proposed test bench does not account for the high frequency harmonics generated from the converters in the wind farm. As listed in chapter 1, high frequency harmonics from converters is identified as a potential cause of WTSU transformer failures. This signifies the need of investigating converter initiated high frequency harmonics in the wind farm. Incorporating sophisticated rotor and stator converter controls with high frequency harmonic filters in the proposed test bench will facilitate the

analysis of high frequency harmonics experienced by WTSU transformer along with VCB initiated switching transients.

6.2.4 Measurement setup for admittance matrix of transformer

The measurement of admittance matrix across the transformer terminals is a very time consuming process because the connections are made every time a single element of admittance matrix or voltage ratio is measured. During the WTSU transformer modeling procedure, 36 admittance elements and 9 voltage ratios were measured. In total 45 different connections were made, which was a time consuming process. Also, background noise signals were observed while measuring the voltage ratios. De-noising these unwanted signals increases the computational time of transformer model. An adaptive measurement setup dedicated to measure the admittance matrix and voltage ratio, which allow easy reconnection and de-noising will provide an alternative to an otherwise time consuming procedure of transformer modeling.

Bibliography

[1] http://en.wikipedia.org/wiki/Wind_power_in_Canada.

[2] http://canwea.ca/wind-energy/ontario/

[3] http://www.windontario.ca/

[4] http://www.ieso.ca/Pages/Power-Data/Supply.aspx

[5] http://canwea.ca/wind-energy/ontario/

[6] G. Jose and R. Chacko, "A review on wind turbine transformers," in *Emerging Research Areas: Magnetics, Machines and Drives (AICERA/iCMMD), 2014 Annual International Conference on*, 2014, pp. 1-7.

[7] T. R. Ayodele, A. A. Jimoh, J. L. Munda, and J. T. Agee, "Impact of variation of wind speed in a wind integrated power system," in *Advances in Energy Engineering (ICAEE), 2010 International Conference on*, 2010, pp. 110-114.

[8] http://www.vatransformer.com/padmounttransformer.aspx. *Addressing premature failures of pad mounted transformers*.doc

[9] Badrzadeh, B.; Hogdahl, M.; Isabegovic, E., "Transients in wind power plants - part I: Modeling methodology and validation," in *Industry Applications Society Annual Meeting (IAS), 2011 IEEE*, vol., no., pp.1-11, 9-13 Oct. 2011.

[10] Boyle, G. (2012). *Energy systems and sustainability: Power for a sustainable future* (2nd Ed.). Oxford; New York: Oxford University Press, in association with the Open University.

[11] https://www.planning.org/research/wind/pdf/pas566.pdf

[12] http://energy.gov/science-innovation/energy-sources

[13] D. Yao and R. G. Harley, "Present and future trends in wind turbine generator designs," in *Power Electronics and Machines in Wind Applications, 2009. PEMWA 2009. IEEE*, 2009, pp. 1-6.

[14] H. Ohsaki, L. Queval, and Y. Terao, "Design and characteristic analysis of 10 MW class superconducting wind turbine generators with different types of stator and rotor configurations," in *Clean Electrical Power (ICCEP), 2013 International Conference on*, 2013, pp. 395-398.

[15] D. F. Howard, J. Restrepo, T. Smith, M. Starke, J. Dang, and R. G. Harley, "Calculation of fault current contribution of Type I wind turbine-generators," in *Power and Energy Society General Meeting, 2011 IEEE*, 2011, pp. 1-7.

[16] M. Chaudhary, S. M. Brahma, and S. J. Ranade, "Circuit breaker selection in a wind farm with Type-2 wind turbine generators," in *Power and Energy Society General Meeting (PES), 2013 IEEE*, 2013, pp. 1-5.

[17] T. M. Masaud and P. K. Sen, "Modeling and control of doubly fed induction generator for wind power," in *North American Power Symposium (NAPS), 2011*, 2011, pp. 1-8.

[18] D. N. Hussein, M. Matar, and R. Iravani, "A Type-4 Wind Power Plant Equivalent Model for the Analysis of Electromagnetic Transients in Power Systems," *Power Systems, IEEE Transactions on,* vol. 28, pp. 3096-3104, 2013.

[19] M. Chaudhary, S. M. Brahma, and S. J. Ranade, "Interpreting the short circuit behavior of Type 4 wind turbine generator," in *T&D Conference and Exposition, 2014 IEEE PES*, 2014, pp. 1-5.

[20] B. Franken, H. Breder, M. Dahlgren, and E. K. Nielsen, "Collection grid topologies for off-shore wind parks," in *Electricity Distribution, 2005. CIRED 2005. 18th International Conference and Exhibition on*, 2005, pp. 1-5.

[21] http://www.windsystemsmag.com/

[22] http://www.vonroll.com/en/von-roll-transformers.html

[23] http://www.vatransformer.com/padmounttransformer.aspx. *Addressing premature failures of pad mounted transformers*.doc

[24] K. J. Cornick and T. R. Thompson, "Steep-fronted switching voltage transients and their distribution in motor windings. Part 1: System measurements of steep-fronted switching voltage transients," *Electric Power Applications, IEE Proceedings B,* vol. 129, pp. 45-55, 1982.

[25] P. I. Vukelja, R. M. Naumov, G. V. Drobnjak, and J. D. Mrvic, "Experimental investigations of overvoltages in 6 kV station service cable networks of thermal power plants," in *Electrical Insulation, 1996., Conference Record of the 1996 IEEE International Symposium on*, 1996, pp. 620-623 vol.2.

[26] E. M. Hope, T. A. Bellei, and M. Reyes, "Wind turbine generator step-up transformer failure investigation," in *Transmission and Distribution Conference and Exposition (T&D), 2012 IEEE PES*, 2012, pp. 1-7.

[27] A. Greenwood,"Electrical Transients in Power Systems", 2nd Edition, Wiley- Interscience.

[28] D. Chapman, "The Cost of Poor Power Quality", Power Quality Application Guide, Section 2.1, Copper Development Association of UK, November 2001.

[29] T. Van Craenenbroeck, J. De Ceuster, J. P. Marly, H. De Herdt, B. Brouwers, and D. Van Dommelen, "Experimental and numerical analysis of fast transient phenomena in distribution transformers," in *Power Engineering Society Winter Meeting, 2000. IEEE*, 2000, pp. 2193-2198 vol.3.

[30] Compel: The International Journal for Computation and Mathematics in Electrical and Electronic Engineering. (1982).

[31] M. Popov and L. van der Sluis, "Improved calculations for no-load transformer switching surges," *Power Delivery, IEEE Transactions on,* vol. 16, pp. 401-408, 2001.

[32] A. Daniel and S. Gebre, "Analysis of transients in wind parks: modeling of system components and experimental verification," *MSc in Electric Power Engineering, Chalmers University of Technology, Göteborg, Sweden,* 2008.

[33] D. MIREANU, "Transient Overvoltages in Cable Systems", MSc in Electric Power Engineering, CHALMERS UNIVERSITY OF TECHNOLOGY, Sweden, 2007.

[34] Patel, D.; Varma, R.K.; Seethapathy, R.; Dang, M., "Impact of wind turbine generators on network resonance and harmonic distortion," in *Electrical and Computer Engineering (CCECE), 2010 23rd Canadian Conference on* , vol., no., pp.1-6, 2-5 May 2010.

[35] Kosmac, J.; Zunko, P., "A statistical vacuum circuit breaker model for simulation of transient overvoltages," in *Power Delivery, IEEE Transactions on* , vol.10, no.1, pp.294-300, Jan 1995.

[36] Heyn, D.; Lindmayer, M.; Wilkening, E.-D., "Effect of contact material on the extinction of vacuum arcs under line frequency and high frequency conditions," in *Components, Hybrids, and Manufacturing Technology, IEEE Transactions on* , vol.14, no.1, pp.65-70, Mar 1991.

[37] Liu Xin; Zhang Nailu; Guo Chaoyang; He Li, "Research on arc stability control system for vacuum arc remelting furnace based on fuzzy-PID," in *Electronics, Computer and Applications, 2014 IEEE Workshop on* , vol., no., pp.23-26, 8-9 May 2014.

[38] Alilzadeh, Saeed; Shabani, A.; Zanjani, M., "New design for electromagnetic actuator of the VCB and simulation of its static and dynamic behavior," in *Power and Energy Conference, 2008. PECon 2008. IEEE 2nd International*, vol., no., pp.1383-1386, 1-3 Dec. 2008.

[39] Popov, M.; Acha, E., "Overvoltages due to switching off an unloaded transformer with a vacuum circuit breaker," in *Power Delivery, IEEE Transactions on*, vol.14, no.4, pp.1317-1326, Oct 1999.

[40] Helmer, J.; Lindmayer, M., "Mathematical modeling of the high frequency behavior of vacuum interrupters and comparison with measured transients in power systems," in *Discharges and Electrical Insulation in Vacuum, 1996. Proceedings. ISDEIV, XVIIth International Symposium on* , vol.1, no., pp.323-331 vol.1, 21-26 Jul 1996.

[41] Popov, "Switching three phase distribution transformer with a Vacuum Circuit Breaker", PhD Dissertation, Electrical Department, Delft University of Technology, Delft, Switzerland, 2002.

[42] Oussalah, N.; Zebboudj, Y.; Boggs, S.A., "Partial Discharge Pulse Propagation in Shielded Power Cable and Implications for Detection Sensitivity," in *Electrical Insulation Magazine, IEEE* , vol.23, no.6, pp.5-10, Nov.-Dec. 2007.

[43] Mugala, G.; Eriksson, R.; Gafvert, U., "High frequency characterization of the semi-conducting screens of medium voltage XLPE cables," in *Electrical Insulation and Dielectric Phenomena, 2002 Annual Report Conference on* , vol., no., pp.887-890, 2002.

[44] Bamji, S.S.; Kaufhold, M.; Bulinski, A.T., "Electroluminescence technique to evaluate the effect of impulse tests on high voltage cables," in *Dielectrics and Electrical Insulation, IEEE Transactions on*, vol.5, no.2, pp.204-210, Apr 1998.

[45] T. ABDULAHOVIÂ, "Analysis of High-Frequency Electrical Transients in Offshore Wind Parks", PhD Dissertation, Division of Electric Power Engineering, CHALMERS UNIVERSITY OF TECHNOLOGY, Goteborg, Sweden, 2011.

[46] Abdulahovic, T.; Thiringer, T., "Voltage Stress in a Transformer Winding During Very Fast Transients Caused by Breaker Closing Event," in *Power Delivery, IEEE Transactions on* , vol.29, no.4, pp.1946-1954, Aug. 2014

[47] Reza, Muhamad; Breder, Henrik; Liljestrand, Lars; Abdulahovic, Tarik; Thiringer, Torbjorn; Sannino, Ambra, "Experimental investigations of switching transients in a wind collection grid scale model in a cable system laboratory," in *Electricity Distribution - Part 2, 2009. CIRED 2009. The 20th International Conference and Exhibition on*, vol., no., pp.1-13, 8-11 June 2009.

[48] Abdulahovic, T.; Thiringer, T., "Transformers internal voltage stress during current interruption for different wind turbine layouts," in *Power Electronics and Applications (EPE), 2013 15th European Conference on* , vol., no., pp.1-10, 2-6 Sept. 2013.

[49] Eichenberg, J.P.; Hennenfent, H.; Liljestrand, L., "Multiple re-strikes phenomenon when using vacuum circuit breakers to start refiner motors," in *Pulp and Paper Industry Technical Conference, 1998. Conference Record of 1998 Annual*, vol., no., pp.266-273, 21-26 June 1998.

[50] Gibbs, J.D.; Koch, D.; Malkin, P.; Cornick, K.J., "Investigations of prestriking and current chopping in medium voltage SF_6 rotating arc and vacuum switchgear," in *Power Delivery, IEEE Transactions on*, vol.4, no.1, pp.308-316, Jan 1989.

[51] Greenwood, A.; Glinkowski, M., "Voltage escalation in vacuum switching operations," in *Power Delivery, IEEE Transactions on* , vol.3, no.4, pp.1698-1706, Oct 1988.

[52] Lee, T.H.; Greenwood, Allan; Crouch, D.W.; Titus, C.H., "Development of Power Vacuum Interrupters," in *Power Apparatus and Systems, Part III. Transactions of the American Institute of Electrical Engineers*, vol.81, no.3, pp.629-636, April 1962.

[53] Gibbs, J.D.; Koch, D.; Malkin, P.; Cornick, K.J., "Comparison of performance of switching technologies on E Cigre motor simulation circuit," in *Power Delivery, IEEE Transactions on* , vol.4, no.3, pp.1745-1750, Jul 1989.

[54] Ihara, S.; Panek, J.; Tuohy, E.J., "Chopping of Transformer Magnetizing Currents Part II: Three-Phase Transformers," in *Power Apparatus and Systems, IEEE Transactions on* , vol.PAS-102, no.5, pp.1106-1114, May 1983.

[55] Itoh, T.; Murai, Y.; Ohkura, T.; Takami, T., "Voltage Escalation in the Switching of the Motor Control Circuit by the Vacuum Contactor," in *Power Apparatus and Systems, IEEE Transactions on* , vol.PAS-91, no.5, pp.1897-1903, Sept. 1972.

[56] Moore, A.H.; Blalock, T.J., "Extensive field measurements support new approach to protection of arc furnace transformers against switching transients," in *Power Apparatus and Systems, IEEE Transactions on* , vol.94, no.2, pp.473-481, Mar 1975.

[57] FrÃhlich, K., "Experimental Investigation of Low-Current Vacuum Arc Instabilities," in *Plasma Science, IEEE Transactions on* , vol.8, no.4, pp.319-325, Dec. 1980.

[58] Tuohy, E.J.; Panek, J., "Chopping of Transformer Magnetizing Currents Part I: Single Phase Transformers," in *Power Apparatus and Systems, IEEE Transactions on*, vol.PAS-97, no.1, pp.261-268, Jan. 1978.

[59] Badrzadeh, B.; Zamastil, M.H.; Singh, N.K.; Breder, Henrik; Srivastava, K.; Reza, M., "Transients in Wind Power Plants—Part II: Case Studies," in *Industry Applications, IEEE Transactions on* , vol.48, no.5, pp.1628-1638, Sept.-Oct. 2012.

[60] Reza, Muhamad; Breder, Henrik; Liljestrand, Lars; Sannino, Ambra; Abdulahovic, Tarik; Thiringer, Torbjorn, "An experimental investigation of switching transients in a wind-collection grid scale model in a cable system laboratory," in *Electricity Distribution - Part 1, 2009. CIRED 2009. 20th International Conference and Exhibition on* , vol., no., pp.1-4, 8-11 June 2009

[61] Glinkowski, M.T.; Gutierrez, M.R.; Braun, D., "Voltage escalation and reignition behavior of vacuum generator circuit breakers during load shedding," in *Power Delivery, IEEE Transactions on* , vol.12, no.1, pp.219-226, Jan 1997.

[62] Helmer, J.; Lindmayer, M., "Mathematical modeling of the high frequency behavior of vacuum interrupters and comparison with measured transients in power systems," in*Discharges and Electrical Insulation in Vacuum, 1996. Proceedings. ISDEIV., XVIIth International Symposium on* , vol.1, no., pp.323-331 vol.1, 21-26 Jul 1996.

[63] Gustavsen, B.; Heitz, C., "Fast realization of the modal vector fitting method for rational modeling with accurate representation of small eigenvalues," in *Power & Energy Society General Meeting, 2009. PES '09. IEEE*, vol., no., pp.1-1, 26-30 July 2009.

[64] Cipparrone, F.A.M.; Gustavsen, B.; Semlyen, A.; Feijoo, A.; Cidras, J., "Discussion of "Enforcing passivity for admittance matrices approximated by rational functions"," in *Power Systems, IEEE Transactions on* , vol.16, no.4, pp.954-955, Nov. 2001.

[65] Grivet-Talocia, S.; Ubolli, A., "Passivity Enforcement With Relative Error Control," in *Microwave Theory and Techniques, IEEE Transactions on* , vol.55, no.11, pp.2374-2383, Nov. 2007.

[66] Li, G.H.; Zhang, B.H.; Hao, Z.G.; Wang, J.; Bo, Z.Q.; Writer, D.; Yip, T., "Modeling of DFIG based wind generator and transient characteristics analysis," in *Environment and Electrical Engineering (EEEIC), 2011 10th International Conference on* , vol., no., pp.1-4, 8-11 May 2011.

[67] Kondala Rao, B.; Gajjar, G., "Development and application of vacuum circuit breaker model in electromagnetic transient simulation," in *Power India Conference, 2006 IEEE* , vol., no., pp.7, 2006.

[68] Shipp, D.D.; Dionise, T.J.; Lorch, V.; MacFarlane, W.G., "Vacuum Circuit Breaker Transients During Switching of an LMF Transformer," in *Industry Applications, IEEE Transactions on* , vol.48, no.1, pp.37-44, Jan.-Feb. 2012.

[69] Gustavsen, B., "Study of Transformer Resonant Overvoltages Caused by Cable-Transformer High-Frequency Interaction," in *Power Delivery, IEEE Transactions on* , vol.25, no.2, pp.770-779, April 2010.